OPTIMIZATION OF RF DISCHARGES FOR EXCITATION OF CO_2 LASERS

by

SARDAR MOHAMMAD AYUB DURRANI, M.Sc.

Thesis submitted for the degree of Doctor of Philosophy

at Heriot-Watt University

Optoelectronics and Laser Engineering

Department of Physics

July 1988

PAGE NUMBERING AS ORIGINAL

NOTE

The calculations in Table 9.1 and 9.2 are based on values of current that were deduced from the power and voltage measurements assuming current and voltage to be in phase. The currents plotted in figures 9.7 and 9.8 are observed values using the technique described in Chapter 3. This technique has been found to overestimate the currents by about one order of magnitude. This is due to the fact that the displacement current in the ceramic side walls, see figure 9.1b, was overlooked.

Concerning the excited state densities tabulated in Table 9.2 we see a monotonic decline in N^* with increasing pressure. If, however allowance is made for the higher diffusive loss of excited states to the wall at low presures and the larger striations zone at low pressures, the effective excited state concentration would be expected to pass through a maximum at the middle pressures of arround 25-30 Torr. This would give a maximum in N^* under the conditions where laser output power is also a maximum as indicated in figure 9.10. The plot of N^* in figure 9.10 whilst giving the expected trend is not quantitatively accurate as it was based on the erroneous current measurements mentioned above.

TO MY DEAR MOTHER AND FATHER

Without their prayers for my success

I would not have been able to complete

the work presented in this thesis

CONTENTS

ACKNOWLEDGEMENTS

The research work detailed in this thesis would not have been possible without the help of many people and it is with pleasure that I am able to express my appreciation here.

I am especially grateful to Professor D.R. Hall who, as my supervisor, gave me the opportunity to undertake this research and whose guidance and confidence in my work did much to sustain my motivation during the last three years. I am also thankful to him for financially supporting my visit to CLEO (Conference on Lasers and Electro-optics).

I am extremely indebted for the invaluable collaboration of my friend and colleague Dr P.H. Vidaud de Plaud, without whom much of this research would have been impossible.

My thanks also go to my other colleagues Dr H.J. Baker, Dr K.M. Abramski, Dr P.E. Jackson, G.N. Pearson, A.N. Rashed, A.D. Colley and Miss A. Duncan and our group Chief Technician Mr S. Haughey for their helpful discussions.

I am grateful to the assistance from all technical staff members of the Applied Physics Department, Hull University, where I spent the first two years of my research. In particular Mr E. Farr and T. Cherry. I am also thankful to members of the technical staff of the Physics Department here, especially Mr P. Heron and Mr M. Stewart.

My thanks go to Miss J.A. Slator at the University of Hull for the typing of my

first year progress report.

I am also extremely thankful to Mrs B.D. Barlow-Young for her excellent typing of this thesis.

I am grateful to the Ministry of Education Government of Pakistan for their financial support and Baluchistan University for granting me study leave from my post.

It is my special pleasure to record here my deepest thanks to my parents who have throughout my education, through their efforts and sacrifices, given me the opportunity to follow my chosen career and whose support throughout has made hopes become a reality.

Finally, but by no means least, I thank my wife Bano, for her understanding, moral support and love which sustained me greatly over the last three years.

ABSTRACT

The purpose of the work presented here was to investigate experimentally and theoretically RF discharges at intermediate pressure with particular reference to the RF discharge used in CO_2 gas lasers. The range of parameters covered is approximately as follows:- pressure from 5 to 200 torr, frequency 9 to 80 MHz and electrode separation 4 to 20 mm. The discharges studied were all of the capacitative type employing the following gases:- nitrogen, helium, xenon and the CO_2 laser mixture $3He:1CO_2:1N_2$ with and without xenon.

Measurements have been made of the current and voltage and the time resolved and time averaged visible emission of alpha and gamma type RF capacitative discharges in N_2. A time dependent theoretical model is proposed for alpha-type discharges that yields electron energy and density, internal potentials, discharge current and power dissipation given the measured parameters of RF voltage, electrode separation, gas pressure and RF frequency. The model predicts considerable energy dissipation in the near electrode sheaths and elucidates the increasing stability of alpha discharges for higher input powers as the RF frequency is raised. Measurements have also been made on the stability region and spectroscopy of alpha and gamma RF discharges in CO_2 gas laser mixtures. Measurements were then extended to the stability region of pulsed CO_2 lasers and the formation time of striations close to the electrode boundary in N_2.

The scaling of CW CO_2 laser output power has also been studied as a function of discharge cross-section, gas pressure and RF frequency. Discharge cross-sections in the range 4-10 mm, which at wavelengths of 10 microns allows free space gaussian propagation within the discharge, have been studied in the pressure and frequency range, 10 to 70 torr and 25 to 88 MHz respectively.

Measurements of discharge voltage and currents are used with a theoretical model of capacitative RF discharges to determine the averaged electron energy ϵ in the gain zone region of the discharge. It is found that for optimum power output the RF frequency falls with increasing cross section, and that for each electrode separation studied, the value of p and f which optimise laser power correspond to discharge conditions where the calculated concentrations of CO_2 molecules in the upper laser level (00^01) pass through a maximum.

PUBLISHED WORK

[1] P. Vidaud, S.M.A. Durrani and D.R. Hall, "Alpha and Gamma RF Discharges in N_2 at Intermediate Pressures", Paper DB7, presented at 39th Annual Gaseous Electronics Conference, Wisconsin, October (1986).

[2] S.M.A. Durrani, P. Vidaud and D.R. Hall, "Discharge Geometry and Frequency Scaling in RF Excited CO_2 Lasers", Paper 20, presented at the Eighth National Quantum Electronics Conference, St. Andrews, September (1987).

[3] P. Vidaud, S.M.A. Durrani and D.R. Hall, "Alpha and Gamma RF Discharges in N_2 at Intermediate Pressures", J.Phys.D. Vol.21, 57 (1988).

[4] S.M.A. Durrani, P. Vidaud and D.R. Hall, "Optimization of Gain Zone Reduced Fields in RF Excited CO_2 Lasers", Paper THT4, presented at (CLEO) Conference on Lasers and Electro-optics, Anaheim, California, April (1988).

[5] P. Vidaud, S.M.A. Durrani and D.R. Hall, "Parameter Scaling in Diffusion Cooled RF Discharge Excited CO_2 Lasers", Submitted to IEEE J.Quantum Electron, April (1988).

CHAPTER 1

INTRODUCTION

1.1 BACKGROUND AND LITERATURE SURVEY ON INTERMEDIATE PRESSURE RF DISCHARGES

Interest in the study of processes occurring in radio-frequency (RF) discharges has increased significantly in the last decade. This interest has been prompted by the broad application of RF discharges in science and technology. Plasma chemistry [1] and laser engineering [2], are the primary fields of modern technology where the application of RF discharges has already made a significant contribution and promises to guarantee further technological progress. For the full potential of RF discharges to be realised, it is necessary to know how such discharges are generated and how they function. What differentiates RF discharges from DC discharges? How must the readily variable parameters such as external voltage, RF frequency, gas pressure and composition be selected to obtain the best plasma for the application? Until physicists are able to produce reliable theoretical models at an atomic and moleculer level, the engineers who use RF discharges will continue to rely on laborious trial and error. This thesis is primarily concerned with the experimental study and theoretical modeling of the particular type of RF discharge used in CO_2 lasers.

Historically, RF discharges attracted the attention of physicists long before any of their practical applications in technology were discovered. Some of the first experiments were performed by Tesla, Thomson and Wiedmann [3-5] at the end of the nineteenth century. In the late 1920s the first studies on RF discharges appeared, including those of Wood [6]. Since then, their unusual properties, as

well as their extraordinary colours and forms, have been a constant fascination to researchers the world over.

The variety and forms of RF discharges is significantly greater than that of DC discharges. This is because with RF discharges their is an additional parameter, the RF frequency f. Moreover, there exists the option of electrodeless excitation.

RF discharges may be classified in three categories on the basis of the excitation method or more precisely, the form of the electromagnetic field/plasma interaction. The first type is the so-called *inductive RF discharge.* It can be produced when the RF field in the plasma is induced by a change in the internal magnetic flux and the electric field lines close within the plasma. The second type of discharge is the *capacitative discharge* maintained between planar electrodes, which may be inside or outside the plasma region. In this case, the electric field lines close outside the plasma through the sheaths and metal electrodes. For both types of RF discharges, the RF field/plasma interaction manifests a quasi-steady state nature, with the wavelength of the electromagnetic field being significantly greater than the plasma dimensions. The third RF discharge type is the *wave discharge,* which occurs under conditions where the electromagnetic field wavelength in the plasma is significantly less than the plasma dimensions; this is the microwave discharge operating at frequencies greater than about 500 MHz. In the work reported here, we will concentrate on the steady state capacitative RF discharge with particular attention being devoted to its use in CO_2 gas lasers.

As with DC discharges, the properties of RF discharges are determined to a significant degree by the gas pressure and the gas composition. A change in pressure from a fraction of a torr to tens of torr radically changes the kinetic properties of the plasma. For RF discharges, an important parameter is the ratio of the field angular frequency ω to the electron/atom or molecule collision

frequency, ν, which is proportional to the pressure p. For the case where $\omega/\nu << 1$ the RF discharge plasma is similar to a DC discharge plasma, although the current-voltage characteristic of the discharge may vary significantly. In the opposite case where $\omega/\nu >> 1$ and the dispersion phenomena of the plasma are clearly expressed, the RF discharge manifests rather exotic behaviour. This behaviour includes the formation of plasmoids [6,7], resonant state phenomena [7], and non-collision absorption of RF field energy [8]. The pioneer plasma physicists, Wood and Hatch [6], both observed plasmoid formation, while Taillet [7] studied the resonant state phenomena. The work of Allis and Brown [9] related the spatial distribution of the ionization function in a microwave discharge to the visible emission profile and resonant behaviour. The regions of high visible emission near each electrode were taken to be the regions of greatest electric field. The proposed explanation was that in these regions the plasma was in resonance and was shielding the central part of the discharge. The RF frequencies considered here are too low for plasma resonance effects to occur as $\omega/\nu << 1$.

The pioneering research in investigating the mechanism of capacitative RF discharges for $\omega/\nu << 1$ was conducted by Levitskii [10]. Levitskii was the first to give a qualitative explanation of the origin of the significant DC potential differences between the RF plasma and the electrodes. He proposed that the DC voltages were the result of the formation of uncompensated space charge sheaths near the RF electrodes, with widths equal to the amplitude of electron oscillations, resulting from electron escape to the RF electrodes. He deduced that diffusion processes can dominate in the centre of the discharge, with mobility being significant near the electrodes. Levitskii postulated that electrons are swept out of the sheath, of thickness a_0 where a_0 is the electron oscillation amplitude near the electrode boundaries, once every cycle of the applied RF field. For the electrode separation L, the majority of electrons are therefore confined to a region of width $L-a_0$, the virtual discharge gap. The electrons are removed from this region by diffusion. For electron densities, n, greater than $\sim 10^6/cm^3$ ambipolar diffusion is

dominant over free diffusion. At high frequency and gas pressure, charge production is often treated as a purely volume process with ion losses occuring by ambipolar diffusion or recombination and attachment, according to the particular pressure conditions. This description is appropriate when the amplitude of the electron oscillations are much smaller than the electrodes separation, so that the electron loss to the electrode is small. A simple expression has been derived [41] for the electron ambit, a_0, in terms of the collision frequency, ν, of the electron with gas atoms, the electric field amplitude, E, and the angular frequency, ω, of the RF field. For $\nu >> \omega$, it can be shown that $a_0 = eE/\nu\omega m$, where e and m are the charge and mass of the electron respectively.

Capacitative RF discharges may be classified into two general categories which differ in the physical appearance of the discharge and in the detailed mechanism of electron and ion production and their losses. Levitskii was the first to observe that the capacitative RF discharge at intermediate pressure can occur in two distinct stable regimes, which he named the alpha and gamma type RF discharges, according to whether the predominant electron production mechanism is a volume or boundary ionization process. The alpha and gamma designations are used in analogy with Townsend's ionization coefficients. Levitskii offered the hypothesis that the secondary ion impact emission processes occuring at the electrode are necessary in maintaining the capacitative RF discharge in the gamma regime as they are in DC glow discharges. If the applied interelectrode voltage in a capacitative RF discharge is not very high, an alpha type RF discharge occurs, but a high voltage results in a transition into the gamma regime.

Yatsenko [11] demonstrated that the change in luminosity with increasing RF voltage and the alpha to gamma transition was accompanied by a sharp increase in the discharge current density from .012 to .24 A/cm^2 at a pressure of 30 torr, with an electrode spacing of 10 mm. It was noted by Yatsenko that the RF voltage corresponding to the gamma regime change is a function of pressure,

electrode separation and of the electrode material, and was nearly equal to the normal cathode fall in a DC glow discharge.

The lower power density alpha RF discharge has relatively poorly conducting and positively charged sheaths near each electrode boundary and relatively low current density. As indicated earlier, the alpha discharge is sustained largely by volume ionization. By contrast the gamma discharge has been linked to the DC glow discharge [11]; it tolerates high current densities, is sustained by wall ionization processes, and has relatively thin electrode boundary sheaths. These space charge sheaths along the boundaries of the plasma determine to a significant degree the properties of RF discharges. The gamma discharge is highly localised and arc like. It is the lower power density alpha discharge that is used to excite CO_2 lasers.

For the alpha discharge a number of theoretical models have been proposed. These include Raizer's [12], where an estimate of sheath voltage is made and Smirnov's [13] which assumes that all the interelectrode voltage is dropped off across the space charge sheaths. Griffith [14] in his theoretical model applied to waveguide CO_2 lasers ignored the presence of the sheaths near each electrode and assumed that the voltage distribution in the plasma was uniform. By using a low pressure alpha type RF discharge model [15], Parazzoli and Chien [16] have described some of the behaviour of RF excited CO_2 gas lasers, allowing for the neutral gas temperature, but having to assume uniform energy deposition.

The most comprehensive work to date on the alpha to gamma transition is that of Godyak and Khanneh [17]. These authors obtained good agreement with experiments by assuming that the alpha to gamma transition occured when fast electrons, produced in the alpha discharge positive sheath and diffusing into the plasma zone, generate a critical concentration of additional charge. The theory predicts a transition of a threshold nature that is accompanied by a sharp increase

in plasma charge density, n and decrease in plasma mean electron energy, ϵ, which consequently results in a discharge that is dominated by wall ionization processes. Yatsenko [11] proposed that the alpha to gamma transition occurs simply as a breakdown of the alpha regime positive ion sheaths and was determined by the same criteria which are used to determine the DC glow discharge breakdown, except that in the calculation of S, the discharge positive sheath thickness, is substituted for L, the interelectrode separation. Yatsenko did not offer numerical predictions for comparison with experimental results.

RF capacitative discharges were frequently used for the excitation of gas lasers in the early days of laser research [18–22]. For example, the first He–Ne and CO_2 gas lasers were excited by RF capacitative discharges [18, 2, 23]. However, despite several apparently very promising experiments in the late 1960s and early 1970s, when combinations of RF and DC fields were used to excite CO_2 gas lasers [24, 25], the technique of RF discharge excitation of lasers was ignored in favour of DC discharge pumping. The interest in RF excitation of CO_2 gas lasers re–emerged in the mid 1970s [26, 27], with the arrival of better RF power sources and the first published report of the successful operation of an RF excited CO_2 waveguide laser [28]. The importance of this technique was quickly realised and research activities on the combination of transverse RF discharges and optical propagation in hollow dielectric waveguides began. Since then many research papers on RF excited gas lasers have been published, notably in the last few years where there have been a number of significant developments in terms of laser device performance [29, 30]. Progress in understanding the physics of waveguide resonators and RF discharge lasers has also been observed [31–32, 33–37].

RF discharges have also been used for the pulsed excitation of gas lasers. Lachambre *et al.* [28] reported both CW and pulsed operation of their original RF excited CO_2 waveguide laser. Sutter [38] demonstrated an improvement in amplitude and frequency stability, with a sealed off Aluminium electrodes and

Beryllium Oxide side walls waveguide laser, using an RF excitation frequency of 144 MHz. Christensen *et al* [39] studied both rectangular hollow dielectric guides with alumina/silica walls (axial gas flow) and alumina strip guides without side walls (transverse flow). They obtained laser outputs from CO_2, Xe, F, and HF discharges and recently XeCl [40].

In spite of the rapid development of RF excited gas lasers, very little has been published on the parametric dependence of laser properties, and it is clear that the physics of RF discharge processes involved in laser excitation is not well understood. For CO_2 lasers there are two urgent requirements concerning the RF discharge. Firstly, the region of stability of the alpha type discharge needs to be mapped out so that data can be generated on the maximum power which can be coupled into the system without a transition to the arc like gamma discharge occuring. Secondly, a fuller understanding of the benefits and drawbacks caused by the electrode boundary sheaths or "striations" is essential given the small electrode separations used in transverse RF laser structures and the consequently large degree of intrusion of these sheaths into the central gain zone. The work of this thesis is aimed at linking experimental and theoretical work on the RF discharges to the performance of the CO_2 laser with a view to optimising the latter.

1.2 OUTLINE OF THESIS CONTENTS

This thesis is presented in 10 chapters comprising theoretical analysis, description of experiments, results obtained, discussions and conclusions, and finally proposals for future work. The sequential presentation of the thesis is as follows. In Chapter 2, a theory has been developed that, using readily measured discharge parameters, allows the calculation of the discharge internal electric fields, electron energies, electron number densities, plasma resistance, power factors and sheath capacitance and thickness. Chapter 3 describes the principle diagnostic techniques that were used in most of the experimental studies. Chapter 4 contains results on

alpha discharges in nitrogen at low powers, which are representative in many ways of the RF discharges used to excite CO_2 lasers. Pure N_2 simplifies the theoretical modeling of the discharge. The input power used lies in the range of 10 to 100 W/cm^3. The transition from alpha to the higher current, more localised and arc like gamma discharge (power densities > 100 W/cm^3) has also been monitored. Experiments were done using Aluminium, Gold-plated Aluminium, and PTFE covered, 4 cm diameter disc electrodes for the following range of parameters; pressure 10 to 100 torr, RF frequency 10 to 30 MHz and electrode separation 5 to 12 mm. The discharge characteristics monitored were; current, voltage, power, time dependent and time averaged spectra of the visible emission, discharge neutral gas temperatures and the alpha to gamma transition point voltages and powers.

Chapter 5 deals with the formation times of electrode sheaths or striations. It is well known that the positive column of an alpha RF discharge is a very useful environment for the population inversion in CO_2 gas lasers. This positive column is surrounded by the positively charged sheaths near each electrode which encroach on the usable gain volume. In the case of pulsed RF discharge CO_2 laser excitation, one would like to know how these sheaths are formed and how they depend on the other discharge parameters with a view to, perhaps, producing a pulsed discharge without striations and thereby increasing the gain volume. Experiments are described on the times of formation of striations in N_2. The manner in which the striation formation time changes with RF discharge parameters such as RF frequency, electrode separation, input power and pressure is discussed and a simple model proposed.

In Chapter 6 the results of a brief investigation into multiple striations in He are given as there is no mention of the phenomenon in the literature to describe the behaviour that we observed. The phenomena of the formation of striations in the central gain zone was first noted in the CO_2 gas laser mixture richer in helium than $3He:1CO_2:1N_2$ and was deemed to be sufficiently interesting for some

time to be given over to taking a closer look in pure He where the effect was strongest. Results are presented and discussed for Al electrode separations 4 to 20 mm, pressure 20 to 300 torr and RF frequency between 9 and 60 MHz.

Experimental results on the stability region (alpha to gamma transition) and spectroscopy of alpha and gamma RF discharges in CO_2 laser mixture ($3He:1CO_2:1N_2$) are discussed in Chapter 7, including the effect of Xe addition on the electron and neutral gas temperatures.

Chapter 8 presents and discusses experiments on the stability region of alpha and gamma pulsed RF discharge in a typical CO_2 gas laser mixture ($3He:1CO_2:1N_2$). The time dependence of the alpha to gamma transition was investigated for different He concentrations in the CO_2 gas laser mixture, RF frequencies and gas pressures.

Chapter 9 is divided into two parts. The first presents a modification of the theoretical model of the N_2 alpha type RF discharge of Chapter 2, adapted for the case of a CO_2 gas laser mixture. The second part is a report of the experimental and theoretical results from a simultaneous investigation of the laser discharge electrical properties and laser power output characteristics. The discharge electrode separation was varied between 4 and 10 mm, while the RF frequency and pressure ranged from 32 to 85 MHz and 5 to 70 torr respectively. The experimental results include the measurements of laser power, RF voltage, current and neutral gas temperature for a square cross-section of length 200 mm. Theoretical calculations are made of the internal discharge parameters. In particular the electron energy and density plasma gain zone reduced fields (E/N) and excited CO_2 densities. A comparison of the excited CO_2 densities and the laser power output concludes this chapter.

Finally, a summary of the work presented in this thesis and proposals for

future work are suggested in Chapter 10.

The reader is not bound by this order of presentation as each chapter is self contained and suitable cross-references are given.

REFERENCES

[1] C.B. Zarowin, J.Appl.Phys., Vol.57, 929 (1985).

[2] A.C. Eckbreth and J.W. Davies, Appl.Phys.Lett., Vol.21, 25 (1972).

[3] N. Tesla, Elect.Engg.Lond., Vol.7, 549 (1981).

[4] J.J. Thomson, Phil.Mag., Vol.32, 321 (1891).

[5] E. Wiedmann and Ebert H. Wiedmann, Phil.Mag., Vol.1, 549 (1893).

[6] R.W. Wood, Phys.Rev., Vol.35, 673 (1930).

[7] J. Taillet, American J. of Phys., Vol.37, 423 (1969).

[8] V.A. Godyak, Sov.Phys.Tech.Phys., Vol.16, 1073 (1972).

[9] W.P. Allis and S.C. Brown, Phys.Rev., Vol.84, No.3, 519 (1951).

[10] S.M. Levitskii, Sov.Phys.Tech.Phys., Vol.2, 856 (1957).

[11] N.A. Yatsenko, Sov.Phys.Tech.Phys., Vol.26, 679 (1981).

[12] Yu.P. Raizer, Sov.J.Plasma Phys., Vol.5, 232 (1979).

[13] A.S. Smirnov, Sov.Phys.Tech.Phys., Vol.29, 34 (1984).

[14] G.A. Griffith, SPIE, Vol.227, 6 (1980).

[15] V.A. Godyak, Sov.J.Plasma Phys., Vol.2, R78 (1976).

[16] C.G. Parazzoli and K.R. Chien, IEEE J.Quant.Elect., Vol.QE-22(3), 479 (1986).

[17] V.A. Godyak and A.S. Khanneh, IEEE Plasma Sci. PS 14 (1986).

[18] A. Javan, W.R. Bennett Jr. and D.R. Herriot, Phys.Rev.Lett., Vol.6, 106 (1961).

[19] W.R. Bennett Jr., W.L. Faust, R.A. MacFarlane and C.K.N. Patel, Phys.Rev.Lett., Vol.8, 470 (1962).

[20] C.K.N. Patel, W.L. Faust and R.A. MacFarlane, Appl.Phys.Lett., Vol.1, 84 (1962).

[21] R.A. Paananen and D.L. Bobroff, Appl.Phys.Lett., Vol.2, 99 (1963).

[22] C.K.N. Patel, Phys.Rev., Vol.136, A1187 (1964).

[23] C.K.N. Patel, Phys.Rev.Lett., Vol.13. 617 (1964).

[24] A. Crocker and M.S. Wills, Elect.Lett., Vol.5, 33 (1969).

[25] C.O. Brown and J.W. Davies, Appl.Phys.Lett., Vol.21, 480 (1972).

[26] K.D. Laakmann, Proc. of Laser, 78 Conf. Orlando, Florida, (1978).

[27] K.D. Laakmann, Proc. of Laser, 79 Conf. Orlando, Florida, (1979).

[28] J.L. Lachamber, J. MacFarlane, G. Otis and P. Lavigne, Appl.Phys.Lett., Vol.32, 652 (1978).

[29] D. He and D.R. Hall, Opt.Commun. Vol.56, No.3 185 (1983).

[30] P. Vidaud and D.R. Hall, Opt.Commun. Vol.56, No.3 185 (1985).

[31] C.A. Hill and D.R. Hall, App.Optics, Vol.24, No.9, 1283 (1985).

[32] P.E. Jackson, C.A. Hill and D.R. Hall, Submitted to Appl. Optics March (1988).

[33] G. Allcock and D.R. Hall, Opt.Comm., Vol.37, No.1, 49 (1981).

[34] D. He and D.R. Hall, IEEE J.Quant.Elect., Vol.QE-20, No.5, 509 (1984).

[35] S.M.A. Durrani, P. Vidaud and D.R. Hall, Paper ThT4, CLEO, Anaheim, California (1988).

[36] G.N. Pearson and D.R. Hall, Paper ThT6, CLEO, Anaheim, California (1988).

[37] J.G. Xin and D.R. Hall, Opt.Comm., Vol.58, No.6, 420 (1986).

[38] L.V. Sutter, Proc.SPIE, Meeting, Washington D.C. 227 (1980).

[39] C.P. Christensen, F.X. Powell and N. Deju, IEEE J.Quant.Elect., Vol.QE-16, 949 (1980).

[40] C.P. Christensen, B.J. Feldman and A. Huston, Paper TuU3, Conference on Lasers and Electrooptics (CLEO), Anaheim, California (1988).

[41] G.E.C. Francis, "Ionisation Phenomena in Gases", Academic, Press, New York (1960).

CHAPTER 2

THEORETICAL MODEL FOR ALPHA TYPE RF CAPACITATIVE DISCHARGE AT INTERMEDIATE PRESSURE IN N_2

2.1 INTRODUCTION

The variety of the types and features of the RF discharge has attracted an increasing interest among physicists in connection with the eventual application of RF discharge for gaseous lasers [1-3]. For this purpose the mechanism of the RF breakdown has been studied quite thoroughly [4] but the processes which occur in a steady state capacitative RF discharge are not completely understood, especially the relationship between the internal discharge characteristics (i.e. electron temperature, plasma density and current voltage characteristics) on the one hand and on the other hand the external discharge parameters (i.e. input power, pressure, electrode separation, RF frequency and the gas employed).

A specific feature of capacitative RF discharges is the existence of two distinct regimes (alpha and gamma). These two types are distinguished by their characteristic breakdown and by the luminosity of the plasma. If the voltage is not very high an alpha-type regime takes place. A higher voltage results in a transition into the gamma-regime. Pointing out a similarity of discharge luminosity in the case of gamma-regime and of d.c. glow discharge [5] put forward a hypothesis that in the gamma-regime of the capacitative RF discharge, electron emission from electrodes (gamma-processes) plays an essential role in the breakdown and maintenance of the discharge as in the d.c. glow discharge case. In contrast with this, in the alpha-regime the surface phenomena are less important and electron generation is determined by bulk ionization

(alpha-processes). Any transition from an alpha-type capacitative RF discharge used in CO_2 lasers to the high current gamma-type capacitative RF discharge can be considered as an undesirable instability. The alpha-type capacitative RF discharge consists basically of two different regions, i.e. positively charged sheaths near each electrode and a central positive column. To explain the capacitative RF discharge excited CO_2 laser behaviour it is necessary to know the value of the reduced field and hence the excitation rate in the central positive column. This in turn requires a knowledge of discharge internal electric fields upon which electron energies and densities depend.

In the last twenty years a number of theoretical models have been proposed for the RF alpha-type discharge that is used to derive CO_2 lasers, these include that of Godyak [6] which applies only at low gas pressures, when the collision length of the particles exceeds the thickness of the layers. Levitskii [5] proposed a model in which the electrode layers are free of electrons and the ion density is equal to the charge density in the positive column. The electron density in the layer is thus equal to zero and the electric circuit is closed by the displacement currents. This model can explain the low currents observed in capacitative RF discharges, but it does not describe the fundamental properties of such a discharge - the sheath thickness and the voltage drop across the sheaths. It was suggested by Raizer [9] that if the electrodes are coated by an insulating film, the electrons do not reach the electrodes, but instead form a thin space charge layer near the electrodes. Although this reduces the voltage drop in the layer, as compared with [5], the qualitative behaviour of the current remains the same. Griffith [9] in his theoretical model ignored the presence of the sheaths near each electrode and assumed that the voltage distribution in the plasma was uniform. For the medium pressure capacitative RF discharges Smirnov [8] proposed a model in which he assumes that all the interelectrode voltage is dropped off across the sheaths. By using the low pressure RF discharge model of Godyak [6], Panazzoli and Chien [10] have described some of the behaviour of RF excited CO_2 lasers, allowing for

the neutral gas temperature, but having to assume uniform charge deposition.

In the present chapter we use a time dependent model for alpha-type discharges, developed by Dr P. Vidaud, the candidate and Professor D.R. Hall [18]. This model gives electron energy, and density, internal potentials, discharge current, and power dissipation given the measured parameters of interelectrode voltage and separation, gas pressure and RF frequency. The model predicts considerable energy dissipation in the near electrode sheaths and elucidates the increasing stability of the alpha discharge for higher input power as the RF frequency is raised.

2.2 DESCRIPTION AND ASSUMPTIONS

The model, see Figure 2.1, assumes that the electrical equivalent circuit of alpha-type RF capacitative discharges consists of a condenser of time dependent capacitance, C, representing the sheath zone in contact with the instantaneous cathode and a series constant resistance, R, representing the rest of the discharge or plasma zone. The effect of secondary electrons ejected from the instantaneous cathode and accelerated across the sheath, important in the alpha to gamma discharge transition and the ionisation processes of gamma discharge [11, 12], is ignored. The analysis is executed over half of a cycle of the applied RF, the model is applicable for N_2 discharges for the range of parameters shown in figure 2.1 and its predictions are compared, where possible, to the experimental results obtained in N_2, (Table 4.2). The main assumptions are listed below.

(i) Discharge covers an area A m^2 of a set of infinite plane parallel electrodes.

(ii) $L >> (a + \lambda_D)$ where L is the interelectrode separation, a the electron oscillation amplitude and λ_D the Debye length. From [4],

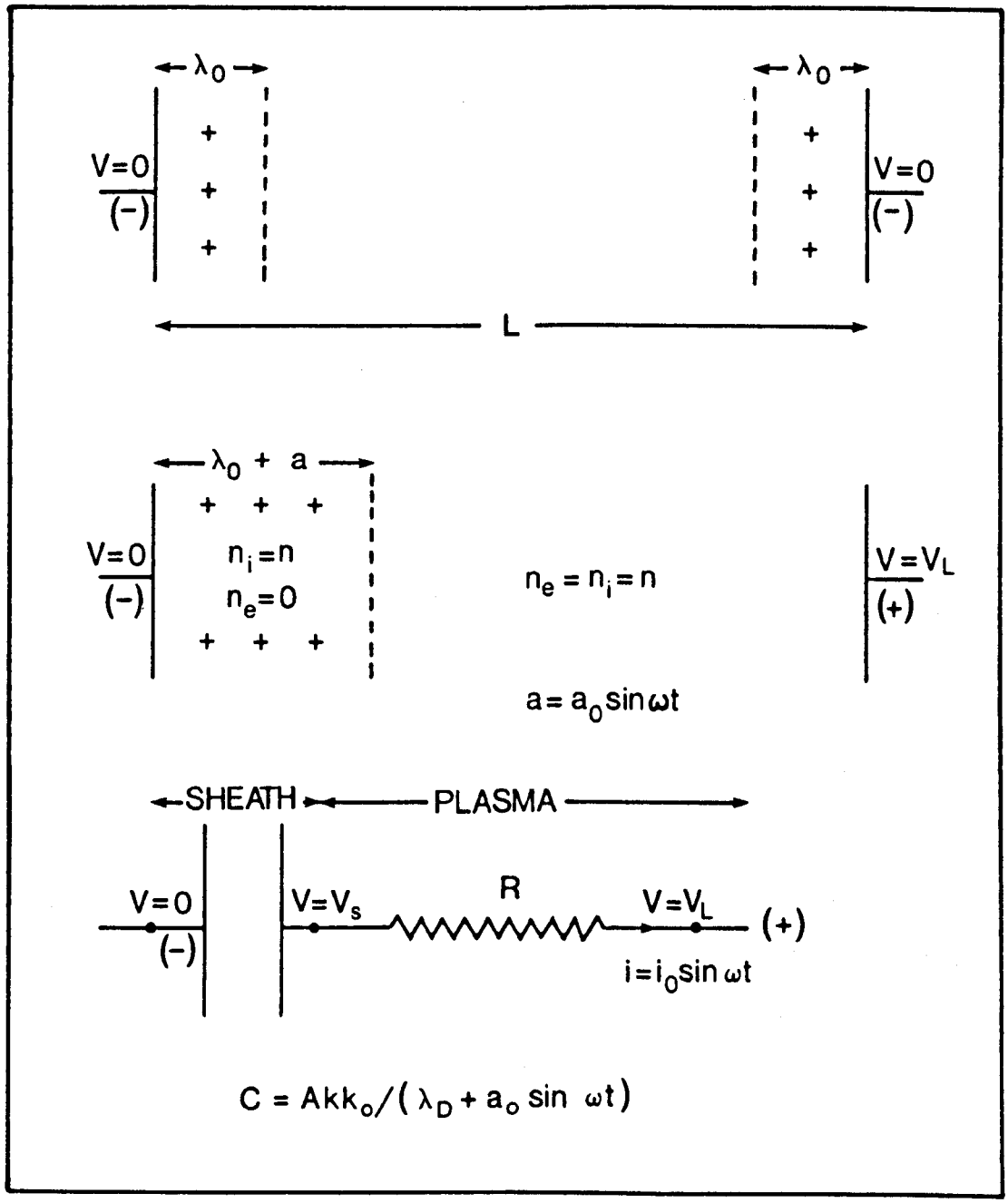

FIGURE 2.1 Charge Distribution and Equivalent Circuit for "α" Type Discharge in N_2. C, R, λ_D, n_i and n_e are Respectively the Sheath Capacitance, the Plasma Zone Resistance, Debye Length, the Ionic and Electronic Charge Densities. A is the Area of the Electrodes Covered by the Discharge and $i_0 \sin\omega t$ the Discharge Current.

$$a = eE/mp\nu_1\omega \qquad (2.1)$$

where e/m is the electronic charge to mass ratio, E/p the plasma zone reduced field, ν_1 the electron momentum transfer collision frequency at 1.0 torr and 300°K, ω the applied RF radian frequency and p the pressure in torr. With ω = 9.68 x 10^7 radians s^{-1} (15.4 MhZ), a plasma zone mean electron energy ϵ = 1.0eV, ν_1 = 2.4 x 10^9 s^{-1} (see Equation (2.20)) and E/p = 500 volts/torr-m (see Table 4.2, Chapter 4), a = 4 x 10^{-4}m. λ_D = 6.07 x 10^3 $(\epsilon/n)^{1/2}$m, where ϵ is the mean electron energy in eV, with an electron density of n = 5 x $10^{16}m^{-3}$, λ_D = 3 x 10^{-5}m. The smallest L used experimentally was 10^{-3}m (1.0 mm).

(iii) $\nu_1 p >> \omega$. For 10 torr and 60 MHz $\nu_1 p/\omega$ = 64. This allows the RMS RF fields to be equated to the DC fields of electron transport data [4].

(iv) Charge is produced in the plasma zone by electron collisions at a rate $z_1 pn$ m^{-3} s^{-1}, where z_1 is the ionisation rate at 1.0 torr, and charge is lost by volume dissociative recombination at a rate σn^2 m^{-3} s^{-1} where σ is the recombination coefficient. From the continuity equation,

$$z_1 pn = \sigma n^2 \qquad (2.2)$$

This condition means that n is constant and independent of position in the plasma zone. To establish that volume recombination of charge rather than ambipolar diffusion to the electrodes controls the charge loss from the system, consider half the discharge volume. To a first approximation, the diffusion loss is

$$\frac{D_1^a}{p}\frac{dn}{dx} = \frac{D_1^a}{p}\frac{n}{L/2}$$

where D_1^a = 0.2ϵ m^2 s^{-1} is the ambipolar diffusion coefficient for N_2^+ at 1.0

torr [13]. Volume recombination loss from the same volume is $\sigma n^2 L/2$. Ratio is $\Phi = \sigma n L^2 p / 4 D_1^a$. With p = 25 torr, ϵ = 1.0 eV, $\sigma = 5 \times 10^{-14}\ \epsilon^{-0.4}\ m^3\ s^{-1}$ [17], $n = 5 \times 10^{16}\ m^{-3}$ and $L = 6 \times 10^{-3} m$, Φ = 2.8.

(v) Charge separation occurs in the sheath. When the electric field E_s in the sheath due to the applied field drives the electrons away from the instantaneous cathode, they will back diffuse over a distance b. If $b = a + \lambda_D$ (the sheath thickness) charge separation will not occur. Back diffusion is checked by the applied field when $n\ \mu_e\ E_s = D_e\ dn/dx = D_e\ n/b$, where μ_e and D_e are respectively the electron mobility and free diffusion coefficient, i.e. $b = D_e/(\mu_e E_s)$ or $b = \epsilon/eE_s$. Taking $E_s = V_s/a$ where V_s is the RMS potential drop across the sheath, $a/b = eV_s/\epsilon$. With, Table 2, Chapter 4, V_s = 100 volts, a >> b.

(vi) The electron energy is assumed to be constant over half the RF cycle. If n and Δ are respectively the number of collisions required to deactivate an electron of energy ϵ and its fractional energy loss per collision $n\Delta\epsilon = \epsilon$ and $n = 1/\Delta$. Time in which electron loses its energy is then $t_\epsilon = (\nu_1 p\Delta)^{-1}$. For 60 torr and ϵ = 1.0eV where $\Delta = 2 \times 10^{-3}$ [14], $t_\epsilon = 3.5 \times 10^{-9} s$. This is a minimum as Δ decreases with decreasing ϵ. For 15.4 MHz, the time between peak energising RF voltages is $t_{RF} = 5 \times 10^{-9} s$. Thus for the highest pressure and lowest RF frequency, the electron energy will be modulated. Although this variation of electron energy is confirmed by the observed modulation of the visible light emission (Section 4.3.4, Chapter 4), the model will assume ϵ to be effectively constant.

(vii) The electron density is assumed to be constant over half the RF cycle. As $dn/dt = -\sigma n^2$, the time taken for the charge density to drop by one half is $t_{1/2} = (\sigma n)^{-1} = 2 \times 10^{-8} s$ with $n = 10^{21}\ m^{-3}$ and ϵ = 1.0eV (see iv). From (vi), the longest time between peak ionising voltages is $t_{RF} = 5 \times 10^{-9} s$. Thus n is constant provided $n < 10^{21}\ m^{-3}$.

(viii) The discharge current is of the form $i_0 \sin\omega t$. This approximation allows an analytical solution for the discharge sheath voltage V_s to be obtained from which other internal discharge characteristics can be derived. This approximation is reasonable provided the derived expression for V_L, the interelectrode voltage, repeats itself over the applied RF half cycle. Expression (2.13) for V_L below fulfils this requirement.

2.3 SHEATH VOLTAGE V_s

Consider a discharge covering an area A m^2 of the electrodes. Let the discharge current, the plasma zone resistance and the plasma zone reduced field be respectively

$$i = i_0 \sin\omega t \qquad \text{amps} \qquad (2.3)$$

$$R = \rho L/A = m\nu_1 pL/Ane^2 \qquad \Omega \qquad (2.4)$$

$$\text{and} \quad E/p = \frac{R\, i_0 \sin\omega t}{pL} = \frac{m\nu_1 i_0 \sin\omega t}{A\, ne^2} \qquad \text{volts/m-torr} \qquad (2.5)$$

where ρ is the resistivity.

From (2.1) and (2.5), the electron oscillation amplitude is then

$$a = \frac{i_0 \sin\omega t}{Ane\omega} \qquad \text{m} \qquad (2.6)$$

and the time dependent capacitance of the sheath condenser

$$C = Ak_0/(\lambda_D + a) = G/(1 + F \sin\omega t) \qquad \text{farads} \qquad (2.7)$$

where k_0 is the permittivity of free space, $G = Ak_0/\lambda_D$ and $F = i_0/Ane\omega\, \lambda_D$.

Equating the sheath displacement and discharge currents

$$\frac{d[V_s C]}{dt} = i_o \sin\omega t \qquad \text{amps} \qquad (2.8)$$

and $$\frac{dV_s}{dt} = \frac{V_s F \cos\omega t}{(1 + F \sin\omega t)}$$

$$= \frac{i_o \sin\omega t \ (1 + F \sin\omega t)}{C} \qquad \text{volts s}^{-1} \qquad (2.9)$$

solving (2.9) with the boundary condition that at t = 0, C = G

$$V_s = \frac{i_o}{\omega G} \ (1 + F \sin\omega t)(1 - \cos\omega t) \qquad \text{volts} \qquad (2.10)$$

with $F = i_o/Ane\omega\lambda_D \sim 12$($i_o$ = 250ma, A = 8 x $10^{-5}m^2$,

n = 2 x $10^{17}m^{-3}$, ω = 4 x 10^8 radians s^{-1} = 60 MHz and

λ_D = 2 x 10^{-5}m, Table 2, Chapter 4)

F >> 1.0 and

$$V_s = \frac{i_o F}{\omega G} \sin\omega t \ (1 - \cos\omega t) \qquad \text{volts} \qquad (2.11)$$

For F >> 1 both (2.10) and (2.11) yield the same expressions for the RMS interelectrode voltage $(V_L)_{RMS}$, (2.15), and the discharge power dissipation <W>, (2.17). The approximation for V_s, (2.11), is used expressly to meet the physical requirement, assumption (viii), that the interelectrode voltage repeat itself over the RF half cycle.

2.4 INTERELECTRODE VOLTAGE V_L

As the potential across the plasma zone is

$$V_p = R i_o \sin\omega t \qquad \text{volts} \qquad (2.12)$$

from (2.11) and (2.12) the instantaneous interelectrode voltage is

$$V_L = V_S + V_P$$

$$= \frac{i_0 F}{\omega G} \sin\omega t \ (1 - \cos\omega t) + R i_0 \sin\omega t \qquad \text{volts} \qquad (2.13)$$

The time averaged value of V_L is

$$\langle V_L \rangle = \int_0^{\pi/\omega} V_L \, dt/(\pi/\omega) = \frac{2F i_0}{\pi\omega G} + \frac{2R i_0}{\pi} \qquad \text{volts} \qquad (2.14)$$

the RMS interelectrode voltage is then

$$(V_L)_{RMS} = \frac{\pi}{2\sqrt{2}} \langle V_L \rangle = \left[\frac{i_0}{A\omega}\right]^2 / (k_0 ne\sqrt{2}) + \frac{R i_0}{\sqrt{2}} \qquad \text{volts} \qquad (2.15)$$

2.5 DISCHARGE POWER DISSIPATION

The instantaneous power dissipation of the discharge is

$$W = (V_S + V_P)\, i_0 \sin\omega t \qquad \text{Watts} \qquad (2.16)$$

From (2.13) and (2.16) the time averaged power dissipation is

$$\langle W \rangle = \int_0^{\pi/\omega} V_L \, dt/(\pi/\omega) = \frac{F i_0^2}{2\omega G} + \frac{R i_0^2}{2} \qquad \text{Watts} \qquad (2.17)$$

The first and second terms in (2.17) are respectively power dissipated in the sheath and the plasma. Substituting the expression for F/G into (2.17)

$$\langle W \rangle = \langle W_S \rangle + \langle W_P \rangle$$

$$= 3.53 \times 10^{29} \, i_0^3/(A^2\omega^2 n) + R i_0^2/2 \qquad \text{Watts} \qquad (2.18)$$

2.6 EMPIRICAL AVERAGE ELECTRON ENERGY FUNCTIONS

These functions relate, for the given approximate validity ranges, the plasma

zone reduced field and various electron collision processes to the average electron energy, ϵ, in the N_2 plasma at a gas temperature of 300°K.

Reduced plasma zone electric field,

$$Ri_0/(pL/2) = 400\ \epsilon^4 \qquad \text{volts/torr-m} \qquad (2.19)$$

$$0.7 < \epsilon < 1.5 \text{ [15]}$$

Electron momentum transfer collision frequency at one torr

$$\nu_1 = 2.4 \times 10^9\ \epsilon\ s^{-1} \qquad (2.20)$$

$$0.2 < \epsilon < 1.8\text{eV [14]}$$

Dissociative recombination rate, $N_2^+ + e$

$$\sigma = 5 \times 10^{-14}\ \epsilon^{-0.4}\ m^3 s^{-1} \qquad (2.21)$$

$$0.03 < \epsilon < 1.0\text{eV [17]}$$

Volume rate of ionization per electron at one torr

$$z_1 = 3.63 \times 10^8\ p\epsilon^{0.9}\ e^{-15.5/\epsilon}\ \epsilon \qquad (2.22)$$

$$\epsilon < 8\text{eV [13]}$$

2.7 n, R, i_0 AND $(V_L)_{RMS}$ IN TERMS OF ϵ AND THE CALCULATION OF ϵ

From the continuity equation (2.2) and expressions (2.21) and (2.22), the plasma zone charge density is

$$n = z_1 p/\sigma = 7.26 \times 10^{21}\ p\epsilon^{0.9}\ e^{-15.5/\epsilon} \qquad m^{-3} \qquad (2.23)$$

From (2.4), (2.20) and (2.23), the plasma zone resistance is

$$R = m\nu_1 pL/Ane^2 = 1.7 \times 10^{-5}\ \frac{L\epsilon^{-0.9}e^{15.5/\epsilon}}{A} \qquad \Omega \qquad (2.24)$$

From (2.19) and (2.24), the discharge current is

$$i_0 = (\sqrt{2})400\ \varepsilon^4\ pL/R \qquad \text{amps}$$

$$= 4.82 \times 10^7\ pA\ \varepsilon^{0.9}\ e^{-15.5/\varepsilon} \qquad \text{amps} \qquad (2.25)$$

Substituting (2.19), (2.23) and (2.25) into (2.15) the RMS

interelectrode voltage is

$$(V_L)_{RMS} = 1.6 \times 10^{23}\ p\ \frac{\varepsilon^{6.9}\ e^{-15.5/\varepsilon}}{\omega^2}$$

$$+ 400\ \varepsilon^4 pL \qquad \text{volts} \qquad (2.26)$$

The average electron energy in the plasma zone is finally obtained by substituting into (2.26) the readily measured parameters $(V_L)_{RMS}$, p, ω and L and solving for ε. With ε the values of n, R and i_0 can be calculated from (2.23), (2.24) and (2.25).

2.8 DISCUSSION

The theory developed here is used in analysing the work on N_2 in Chapter 4 and to some degree the work on $3He{:}1CO_2{:}1N_2$ in Chapter 9. The principle limitation of the theory is that it does not allow for the effect of the energetic electrons that are produced at the instantaneous cathode and projected into the gain zone. A model that included this effect would explain the high small signal gain found near electrode boundaries [16].

REFERENCES

[1] A.C. Eckbreth and J.W. Davice, Appl.Phys.Lett., Vol.21, 25 (1972).

[2] C.O. Brown and J.W. Davies, Appl.Phys.Lett., Vol.21, 480 (1972).

[3] E.L. Latush, V.S. Makhalevskii, M.F. Sem, G. Tolmachov and V.Ua. Khasilev, JEPT Lett., Vol.24, 69 (1976).

[4] G.E.C. Francis, "Ionisation Phenomena in Gases", Academic, Press, New York (1960).

[5] S.M. Levitiskii, Sov.Phys.Tech.Phys., Vol.2, 887 (1957).

[6] V.A. Godyak and A.A. Kuzovnikov, Sov.J.Plasma Phys., Vol.1, 276 (1975).

[7] Yu.P. Raizer, Sov.J.Plasma Phys., Vol.5, 232 (1979).

[8] A.S. Smirnov, Sov.Phys.Tech.Phys., Vol.29, No.1, 34 (1984).

[9] G.A. Griffith, SPIE CO_2 Laser Devices and Application, Vol.227, 6 (1980).

[10] C.G. Parazzoli and K.R. Chien, IEEE J.Quant.Elect., Vol.QE-22(3), 479 (1986).

[11] N.A. Yatsenko, Sov.Phys.Tech.Phys., Vol.26, 678 (1981).

[12] V.A. Godyak and A.S. Khanneh, IEEE Plasma Sci., PS14, 112 (1986).

[13] A. Von Engel, "Ionised Gases", Oxford: OUP (1965).

[14] E.W. MacDanial, "Collision Phenomena in Ionised Gases", New York, Wiley (1964).

[15] J. Dutton, J.Phys.Chem., Ref. Data 4, 64 (1975).

[16] R.C. Sharp, J.Appl.Phys., Vol.61, No.11, 5184 (1987).

[17] F.J. Mehr and M.A. Bionoi, Phys.Rev., Vol.181, 264 (1969).

[18] P. Vidaud, S.M.A. Durrani and D.R. Hall, J.Phys.D., Vol.21, 57 (1988).

CHAPTER 3

DIAGNOSTIC TECHNIQUES

3.1 INTRODUCTION

In this chapter we describe diagnostic techniques that were used in several of the experimental studies. These are the measurement of RF voltages, current, input power, electron and neutral gas temperatures, time dependent and time averaged visible light emission, pressure and RF frequency. The complete experimental set up (i.e. electrode systems, power supplies, vacuum vessel etc.) used for the different experiments are described at the beginning of each particular chapter. Section 3.2, discusses the techniques that were used for the measurement of RF voltage, current, electron and neutral gas temperatures, time dependent and time averaged visible emissions. Section 3.3 gives the techniques used for the measurement of input power, pressure (including vacuum system) and RF frequency. Finally Section 3.4 gives a discussion and estimated errors.

3.2 MEASUREMENTS OF RF VOLTAGE, CURRENT, ELECTRON AND NEUTRAL GAS TEMPERATURES, TIME DEPENDENT AND TIME AVERAGED VISIBLE EMISSIONS

3.2.1 RF Voltage Measurements

The RF voltage measurements were performed by using a capacitative divider [1]. The capacitative divider consists basically of two series capacitors in parallel with the discharge gap as shown in Figure 3.1. If V_i is the RF voltage (voltage across the discharge gap), V_o is the voltage on the oscilloscope or electronic

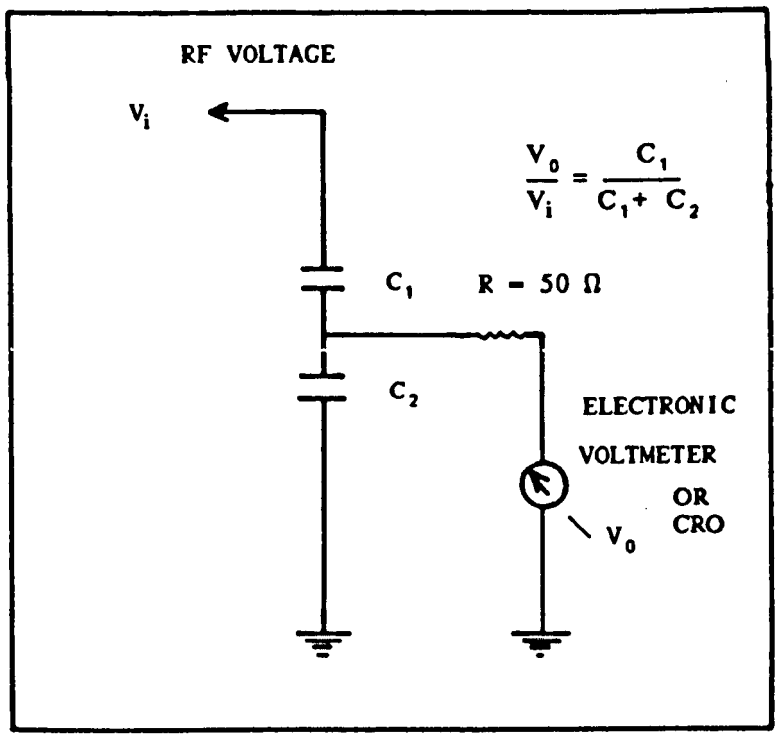

FIGURE 3.1a The Capacitative Voltage Divider

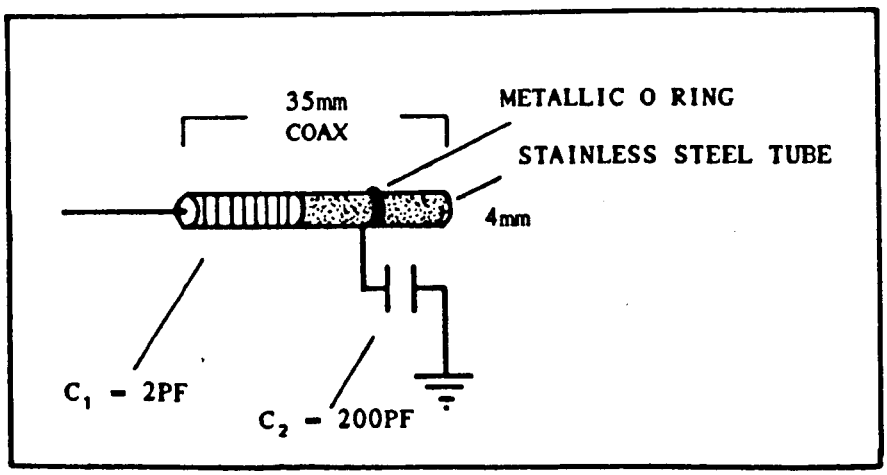

FIGURE 3.1b The Construction of Capacitative Divider

voltmeter, C_1 and C_2 are capacitors of known value, then the ideal capacitative divider equation can be written as

$$V_o/V_i = C_1/(C_1 + C_2) \qquad (3.1)$$

Corrections in the calibration due to different cable lengths can be made.

For an accurate calibration of the capacitative divider to allow measurements of RF voltage, the value of the capacitors C_1 and C_2 has to be known with suitable precision. A further requirement is that the value of capacitor C_1 must be kept as small as possible (say a few picofarads). For the present experimental studies, a capacitative divider was designed with C_1 and C_2 equal to 2pf and 200pf respectively. Its construction is shown in Figure 3.1(a). The capacitor C_1 is basically a 35mm long length of coaxial cable, with an overall outside diameter of 4mm and a core of single strand Cu wire 1mm in diameter. One end of coaxial cable was left open as an input, while the other end was sheathed in a stainless steel tube of I.D. 4mm and length 15mm. The capacitor C_2 is connected in series with C_1 by soldering one side of C_2 to a metallic "O" ring, and this "O" ring was sleeved on the stainless steel tube as shown in Figure 3.1(b). The other side of C_2 was earthed. Finally, the capacitative divider is shielded in an aluminium box. Figures 3.2 shows the calibration curve of the capacitative divider used. The output of a Marconi TF2002B signal generator, for different RF frequencies, was fed into the input of capacitative divider. Output from the capacitative divider was measured on the oscilloscope and the ratio V_i/V_o was plotted against RF frequency.

3.2.2 Current Measurements

For the measurement of current a simple technique was employed involving the use of a non-inductive carbon film resistor placed between earth and the

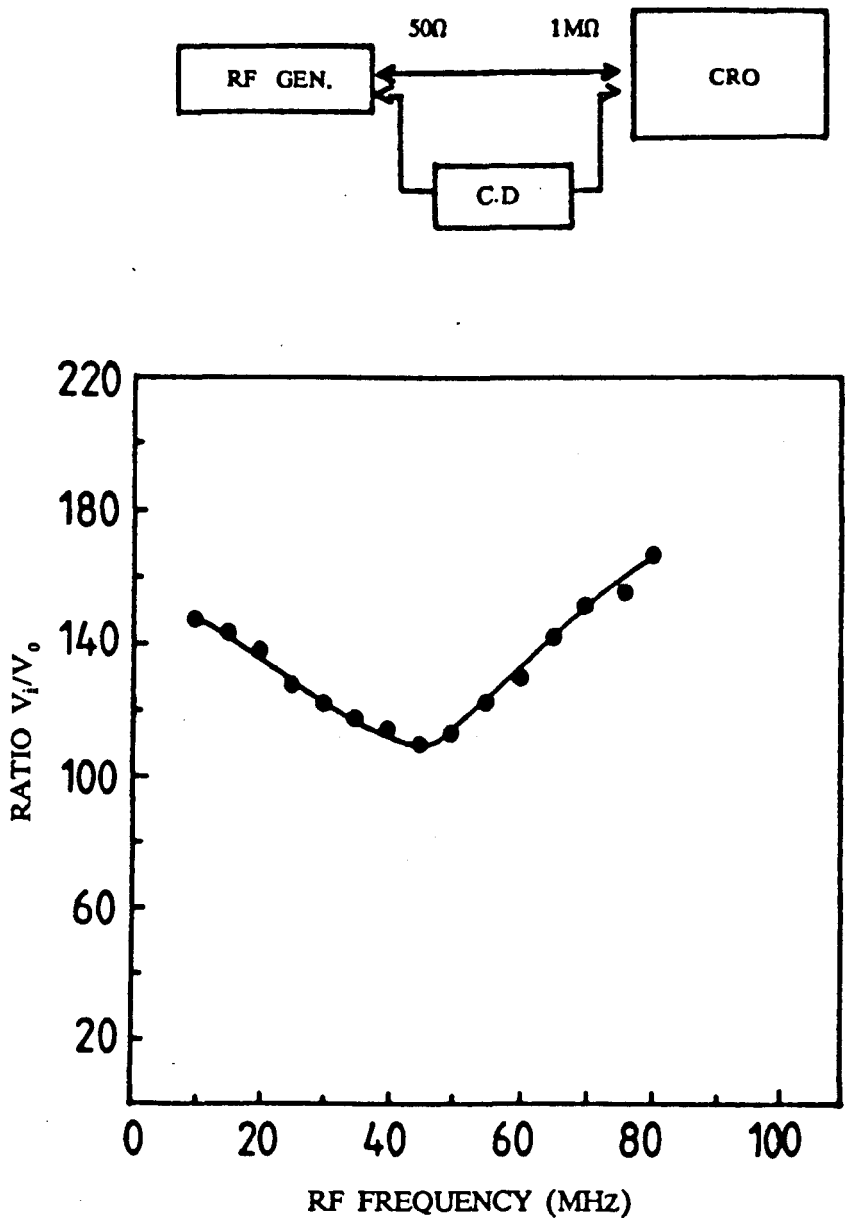

FIGURE 3.2 The Capacitative Divider Calibration Curve.

bottom electrode. In order to avoid error in measuring RF voltage (due to the discharge resistance being in series with the carbon film resistor) the value of the carbon film resistor must be kept below 1 Ohm. For this three 3.5 Ohm resistors in parallel were used, giving a net value of 0.9 Ohm as shown in Figure 3.3. Power rating for each resistor was equal to 2 W, this gives a net value of 6 W.

3.2.3 Electron Temperature Measurements

In order to measure the electron temperatures a floating double electrostatic probe technique [3] was utilised suitably adapted for RF discharges at intermediate pressure [4]. A double electrostatic probe consists of two identical electrodes, usually wires, a few mm apart and immersed in the plasma, as shown in Figure 3.3. The probe current is measured as a function of the applied (±) voltage between the probes 1 and 2 (for theory see References 4 and 5). Figure 3.4 shows the typical S shaped current and voltage characteristic of a double probe. From [4] and [5] if Δ is the width (in volts) of the curve Figure 3.4, then the electron temperature in ^{0}K can be written as, [5]

$$T_e = 0.25 \times \Delta \times 11700 \qquad (3.2)$$

The measured electron temperature in Degrees Kelvin can easily be converted into electron volts. From [6]

$$0.025\text{eV} = 290^0\text{K}$$

therefore

$$T_e \text{ (in eV)} = (0.025/290) \times (\text{electron temp. in } ^0\text{K})$$

The electron temperature was measured using platinum wire electrostatic

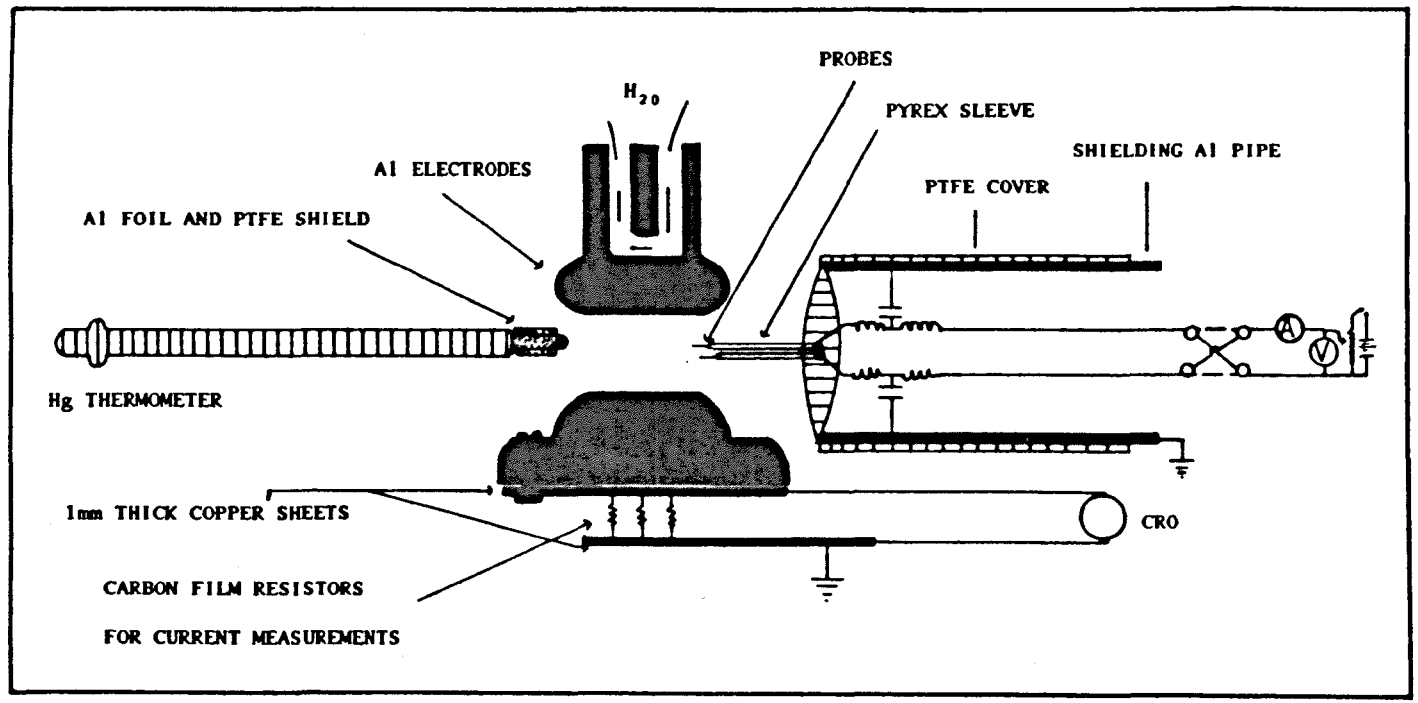

FIGURE 3.3 Experimental Setup for Measurements of Current and Electron and Neutral Gas Temperatures

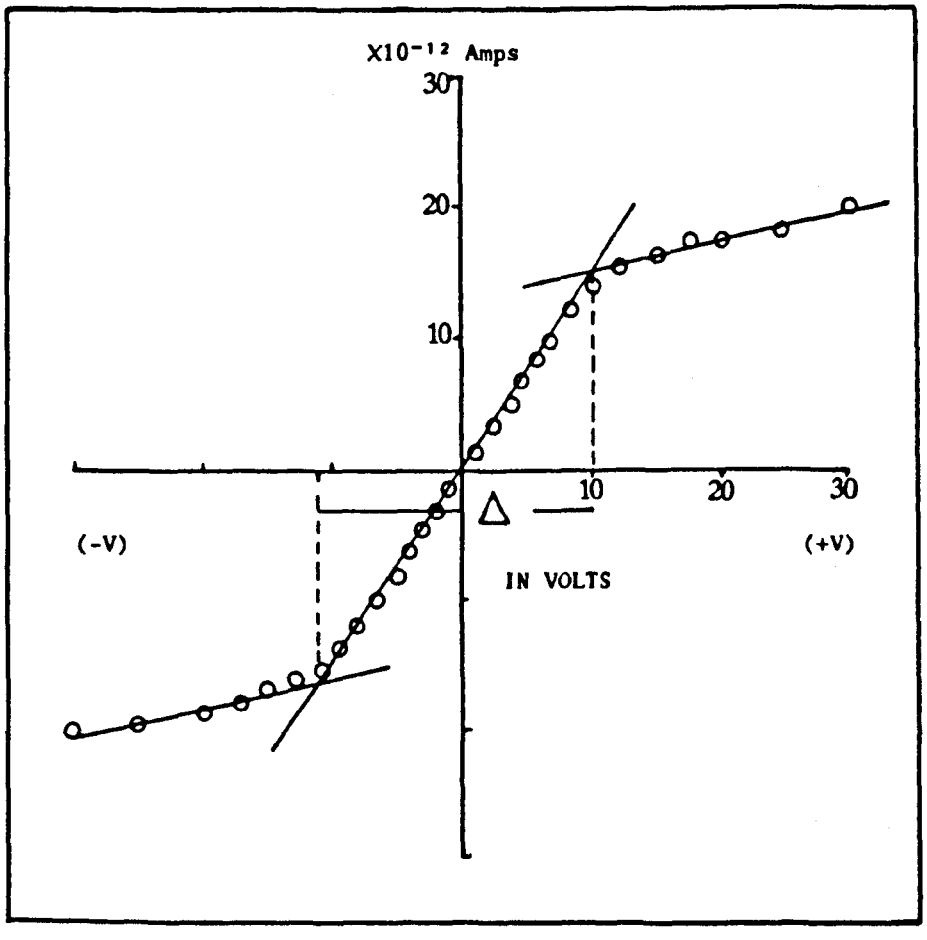

FIGURE 3.4 Double Probe Current - Voltage Characteristic Curve

probes each 0.5 mm in diameter and sheathed in pyrex as shown in Figure 3.3. The probes were inserted into the discharge in a direction parallel to the electrode surfaces. Conventional filtering of the electrostatic probe circuit was used to eliminate the distorting effect of RF pickup [9] (see Figure 3.3). A typical current and voltage characteristic is shown in Figure 3.4. The S-shaped curve is analyzed yielding a value for the electron temperature.

3.2.4 Neutral Gas Temperature Measurements

The average discharge neutral gas temperatures were directly measured with a small, RF shielded, mercury in glass thermometer, inserted via a vacuum feed through into the open end of the discharge as shown in Figure 3.3. The reliability of this technique was verified in different ways (for details see Chapter 4, 5 and 7). The neutral gas temperatures were measured in close proximity to, but not in the discharges. This means that our values of neutral gas temperatures are a minimum. Spectroscopic measurements of neutral gas temperatures in similar discharges of carbon monoxide [2] give values that are not very different from those obtained in Chapter 9.

3.2.5 Time Dependent and Averaged Visible Emission Measurements

In both the experiments on the time dependent visible emission of the discharge and the time averaged spectroscopic analysis of the discharge visible emission, four optical fibres, five meters in length, with peak transmission at 650 nm were used to duct the discharge visible emission away from the discharge and so reduce the effect of RF noise on the detection instruments. In the time dependent measurements, the optical fibres were taken into an RF shielding cage containing an EMI 9813KB photomultipler, a DC voltage supply and Tektronix 2445 150Mhz oscilloscope (See Figure 4.2). Photographs of the scope traces were taken with a Shackman 7000 polaroid camera. For the spectroscopic (time

averaged) analysis results, the fibres were fed directly into the entrance slit of a Jobin Yvon H.10 double monochromator fitted with an EMI 9785QB photomultiplier on its exit slit. The photomultiplier output as a function of wavelength, in the range 300 to 780 nm, was recorded on a chart recorder. The detection system comprising photomultiplier, monochromator voltage supply and oscilloscope was contained in an RF-shielded cage.

3.3 MEASUREMENT OF PRESSURE, INPUT POWER AND RF FREQUENCY

3.3.1 Pressure Measurements

The gases used for all the experiments were pure N_2, He, Xe and laser mixtures such as $3He:1CO_2:1N_2$ and $3He:1CO_2:1N_2$ + 5% Xe. The mixing of gases was performed in a gas mixing chamber with multiple gas inlet ports. The gases used were all research grade. The gas pressure in the discharge chamber and laser vessel was monitored with an absolute pressure gauge, having a resolution of 0.5 torr. The vacuum system consisted of rotary and diffusion pumps.

3.3.2 Input Power Measurements

Measurements of forward and reflected powers were made with a bi-directional Bird Thru-line power meter model 4431. Power was transferred to the discharge via 50 Ω coaxial cable and an LC impedance matching network (see Figure 4.2 and Figure 9.2). For the pulsed RF discharge measurements (Chapter 5 and Chapter 8), the above described CW power meter could not be used. This problem was solved by calibrating an oscilloscope by using CW power. A simultaneous measurement of power and voltage for each RF frequency was made. The power was recorded from a Bird Thruline meter and the voltage on the oscilloscope. The calibration technique is illustrated in Figure 3.5. CW power was

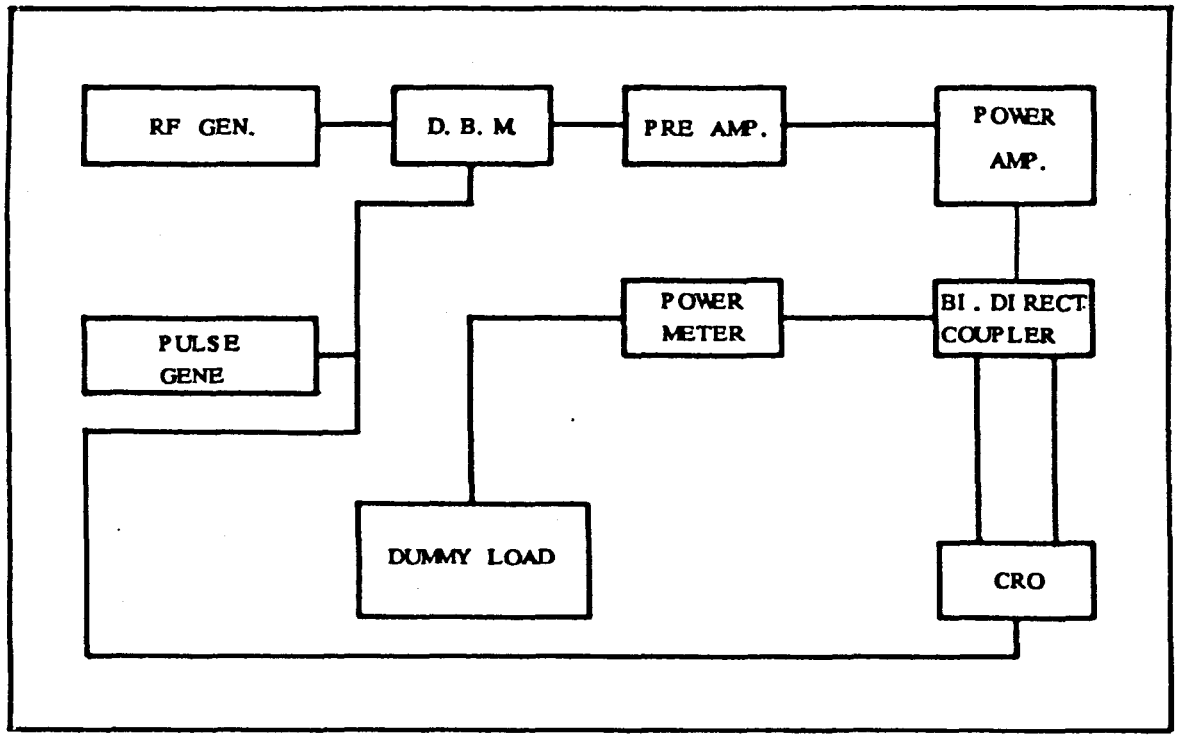

FIGURE 3.5 Experimental Setup for Power and Generator Voltage Calibration

fed into the dummy load and measured with a power meter (model is shown above) and the voltage signal for the oscilloscope was picked off by using an inline bi-directional coupler (model 4522-002-1) as shown in Figure 3.5. From the typical calibration curve (Figures. 3.6 and 3.7) i.e. voltage (from scope) versus power (from meter), the power was obtained for pulsed RF discharge, by measuring the pulsed voltage from the scope. By adjusting the external matching circuit, for each single measurement, the reflected power was kept below 10% of the forward power.

3.3.3 RF Frequency Measurements

The RF frequency measurements were performed with a frequency counter, Black Star Meter 600.

3.4 DISCUSSION AND ESTIMATED ERRORS

The cross electrode RF discharge voltage could also have been determined by the discharge resistance substitution technique [6]. However there are two main problems associated with this approach, firstly it is extremely difficult and time consuming to perform a resistor substitution for every single measurement of RF voltage, especially in the case where hundreds of RF voltage measurements were required, and secondly for the higher power densities, it does not provide an accurate measurement of RF voltage, due to the dependence of discharge resistance on neutral gas temperature (the authors of Ref. 7, in their calculations have ignored the influence of neutral gas temperature on the discharge resistance). An alternative for the current measurements is a technique using the Rogowiki loop, [8], but the calibrations required for this technique are complicated. The estimated errors of the parameters are as follows:-

(i) RF voltage. A comparison at the limiting frequencies of 25 and 80MHz

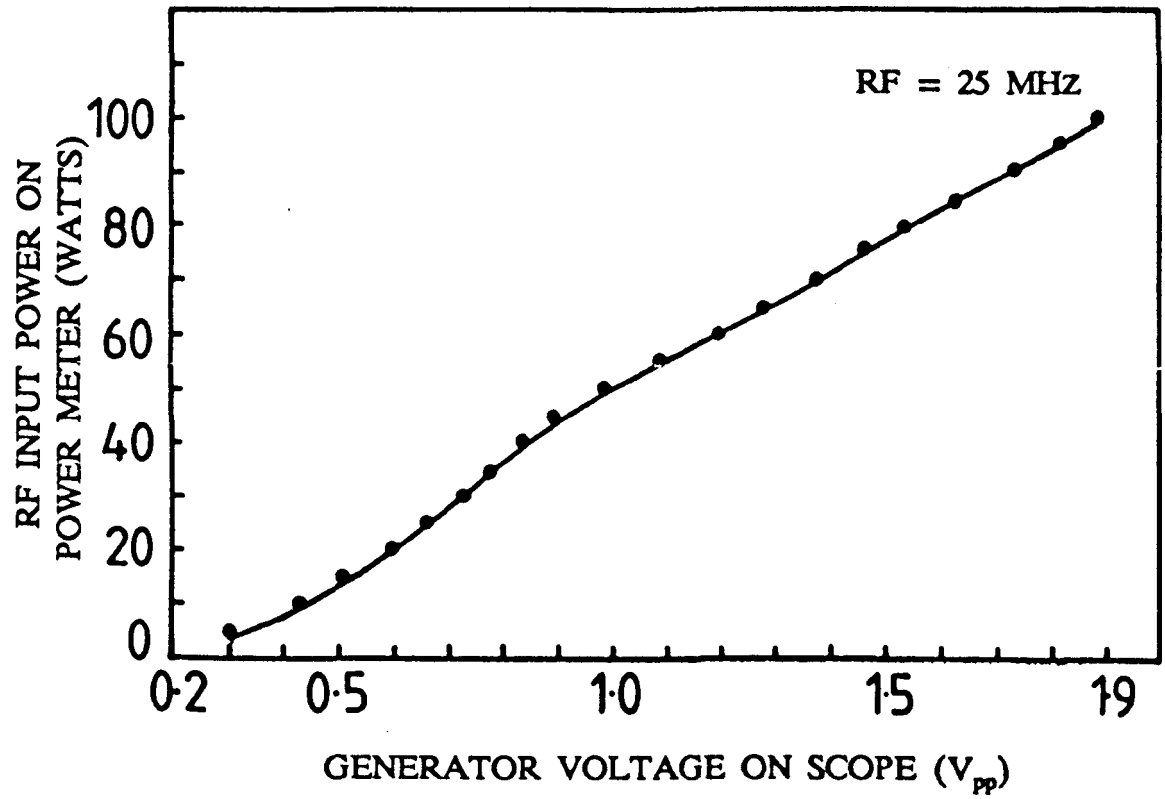

FIGURE 3.6 Power and Generator Voltage Calibration Curve, RF = 40 MHz

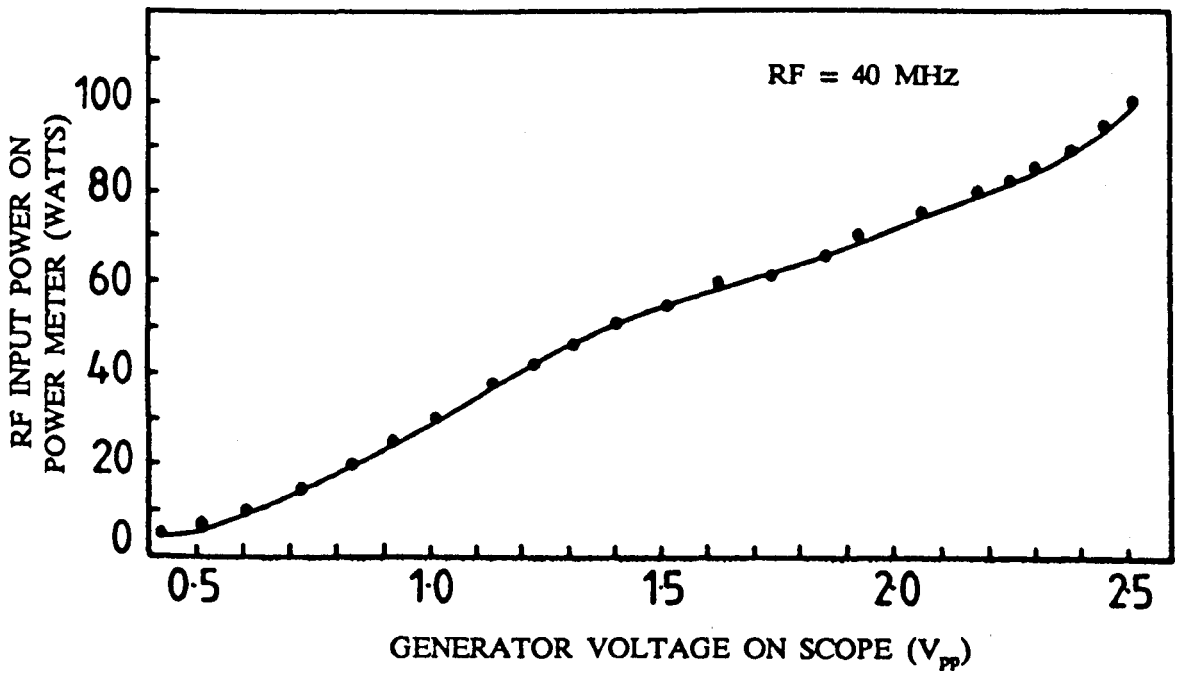

FIGURE 3.7 Power and Generator Voltage Calibration Curve, RF = 25 MHz

of the measured voltages across various dummy loads that are equivalent to the discharge (R = 100 to 1,000 Ω, C = 3 and 25 pF) using the capacitative dividers and the substitution technique [7] and the error in reading voltage of the electrode and oscilloscope give the error as ~ 10%.

(ii) RF current. From the error in the standard resistance and the reading of voltage off the oscilloscope we estimate the error is ~ 10%.

(iii) Gas pressure. On the analogue pressure meter the minimum pressure readable was 0.5 torr in 20 torr this gives an error of ~ 2.5%.

(iv) Electron temperature. For the laser to operate the maximum and minimum of electron energy are ~ 1 and 5 eV [10], the measured range was 2.5 to 4.0 eV. This gives the greatest error of between 50 and 100%.

(v) Neutral gas temperature. The measured values of gas temperature will all be on the low side because the thermometer was kept outside the actual discharge. Measured values of the gas temperature in CO_2 laser mixture discharges [12] range up to 600 ^{0}K on the centre line. Maximum values recorded here were 400 ^{0}K. This suggests an error of ~ 50% on the low side.

(vi) RF frequency. On the calibrated digital frequency counter, the estimated error in measuring the RF frequencies was negligible.

(vii) RF input power. On the analogue power meter the minimum power readable was 0.5 Watt in 50 Watts, this gives an error of 1%.

REFERENCES

[1] M.M. Brady and K.G. Dedrick, Rev. of Sci.Ins. Vol.33, No.12, 1421 (1962).

[2] G.N. Pearson, Ph.D. Thesis, Heriot-Watt University (1988).

[3] E.O. Johnson and L. Malter, Phys.Rev., Vol.80, No.1, 58 (1950).

[4] J.R. Cozens and A. Von Engel, Int.J.Electron, Vol.19, 61 (1965).

[5] A. Von Engel, "Ionized Gases", Oxford University Press (1965).

[6] B. Chapman, "Glow Discharge Processes", John Wiley and Sons (1980).

[7] J.G. Xin, G. Allock and D.R. Hall, J.Phys.E.Sci.Ins., Vol.19, 210 (1986).

[8] N.A. Yatsenko, Sov.Phys.Tech.Phys., Vol.26, No.6, 678 (1981).

[9] A. Cantin and R.R.J. Gagne, Appl.Phys.Lett., Vol.30, No.7, 16 (1977).

[10] J.J. Lowke, A.V. Phelps and B.W. Irwin, J.Appl.Phys., Vol.44, 4669 (1973).

[11] Y. Sakai, S. Kaneko, H. Tagashira and S. Sakamoto, J.Phys.D., Vol.12, 23 (1979).

[12] A.J. Laderman and S.R. Byron, J.Appl.Phys., Vol.42, No.8, 3138 (1971).

CHAPTER 4

INVESTIGATION OF THE STABILITY REGIONS IN N_2

4.1 INTRODUCTION

Transverse capacitative RF discharges in the pressure range of 10 to 200 torr and frequency between 10 to 200 MHz, which are being increasingly used to excite CO_2 lasers, exhibit a number of advantages over their DC counterparts [1-3]. These advantages include low interelectrode voltages, improved discharge stability and higher efficiencies [4]. RF discharges at intermediate pressures, however, cannot yet be fully exploited because at present they are not very well understood [5]. Of particular interest in laser work, where a large uniform gain medium is required and narrow transversely excited discharges are employed, is the nature and methods of control of the non-homogeneities or "striations" that occur in these discharges close to the boundaries [6]. Again it is necessary to establish what determines the stability region for the alpha type discharge used in CO_2 lasers. The work presented in this Chapter concerns experimental observation on the characteristics of the alpha and gamma regimes in N_2. N_2 was chosen to simplify the theoretical work as there is a lot of information on N_2 discharge properties in the literature and the behaviour of the N_2 discharge is similar to that of the usual CO_2 gas mixture discharges. Arrangement of the present chapter is such that, Section 4.2 shows the discharge chamber with the experimental set up and Section 4.3 gives the experimental results. Among these experimental results Section 4.3.1 is based on the current, voltage and power characteristics. Section 4.3.2 gives the stability regime results. Section 4.3.3 shows the electron temperature measurements in the alpha and gamma regimes. Sections 4.3.4 and 4.3.5 are based on the time dependent visible emission the spectroscopy of the time averaged visible emission,

and the time averaged visible emission and spatial profile respectively. Finally, using the theoretical model of Chapter 2, Section 4.4 gives calculated values of the discharge parameters, a discussion and conclusions.

4.2 THE DISCHARGE CHAMBER AND EXPERIMENTAL APPARATUS

The discharge chamber is shown in Figure 4.1. It consists of a cubic aluminium box with centrally located disc electrodes and four ports, each at right angles to the discharge. One port contained a glass tube terminated in an optically flat window. The glass tube was sufficiently wide, diameter 4 cm, for an array of fine optical fibres, to be tracked vertically on a micrometer slide mount close to the discharge. The capacitative divider was fixed on the second port. The third port was used for the current measurements, and finally the fourth port, on the front side of the chamber, was used for viewing of the discharge. The experimental arrangements are shown in Figure 4.2. The aluminium electrodes were "Bruce" profiled discs of diameter 4 cm that were independently water cooled and could be moved to a separation of up to 4 cm. For the measurements with gold surfaces, gold was evaporated directly onto the aluminium electrodes. Discharge power was supplied by an oscillator driving a wide band EN1 5100L power amplifier fed through a Bird Thruline 4431 watt meter and an external matching circuit consisting of a variable inductor L_M and capacitor C_M. The gases were research grade and the metal vacuum chamber enclosing the electrodes could be evacuated to 10^{-2} torr. The discharge current was obtained by measuring the voltage across a $\sim$ 1 Ω thick carbon film resistor R placed between the bottom electrode and earth. The interelectrode voltage was measured using a capacitative divider. The impedance of the capacitative divider at 30 MHz was ~5000 Ω. Visible emission from the discharge was detected with the array of five optical fibres that could be tracked in three dimensions. For the time dependent light measurements, the fibres were fed into a photomultiplier and fast oscilloscope. The time averaged spectroscopic measurements were taken using a Spex

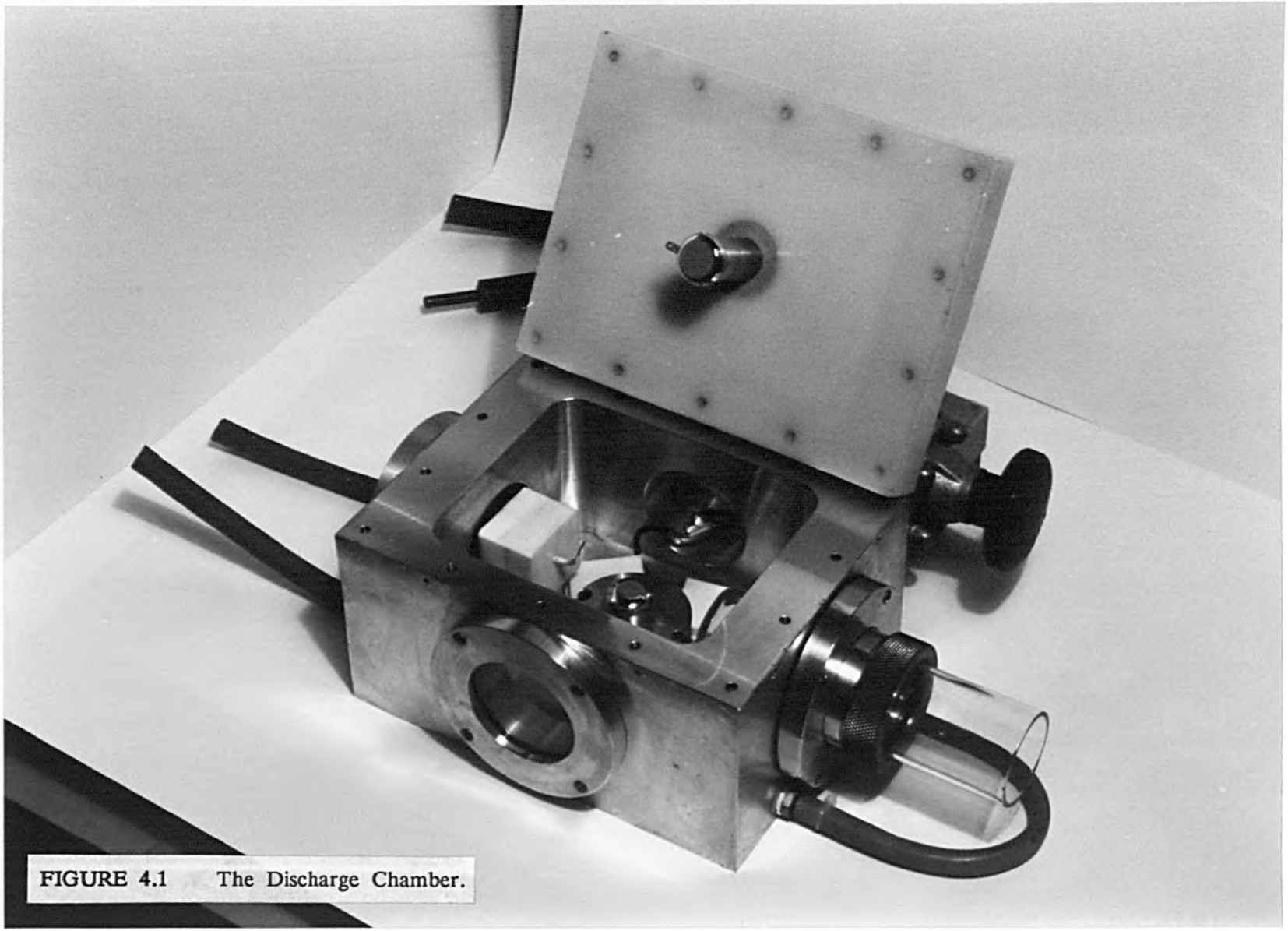

FIGURE 4.1 The Discharge Chamber.

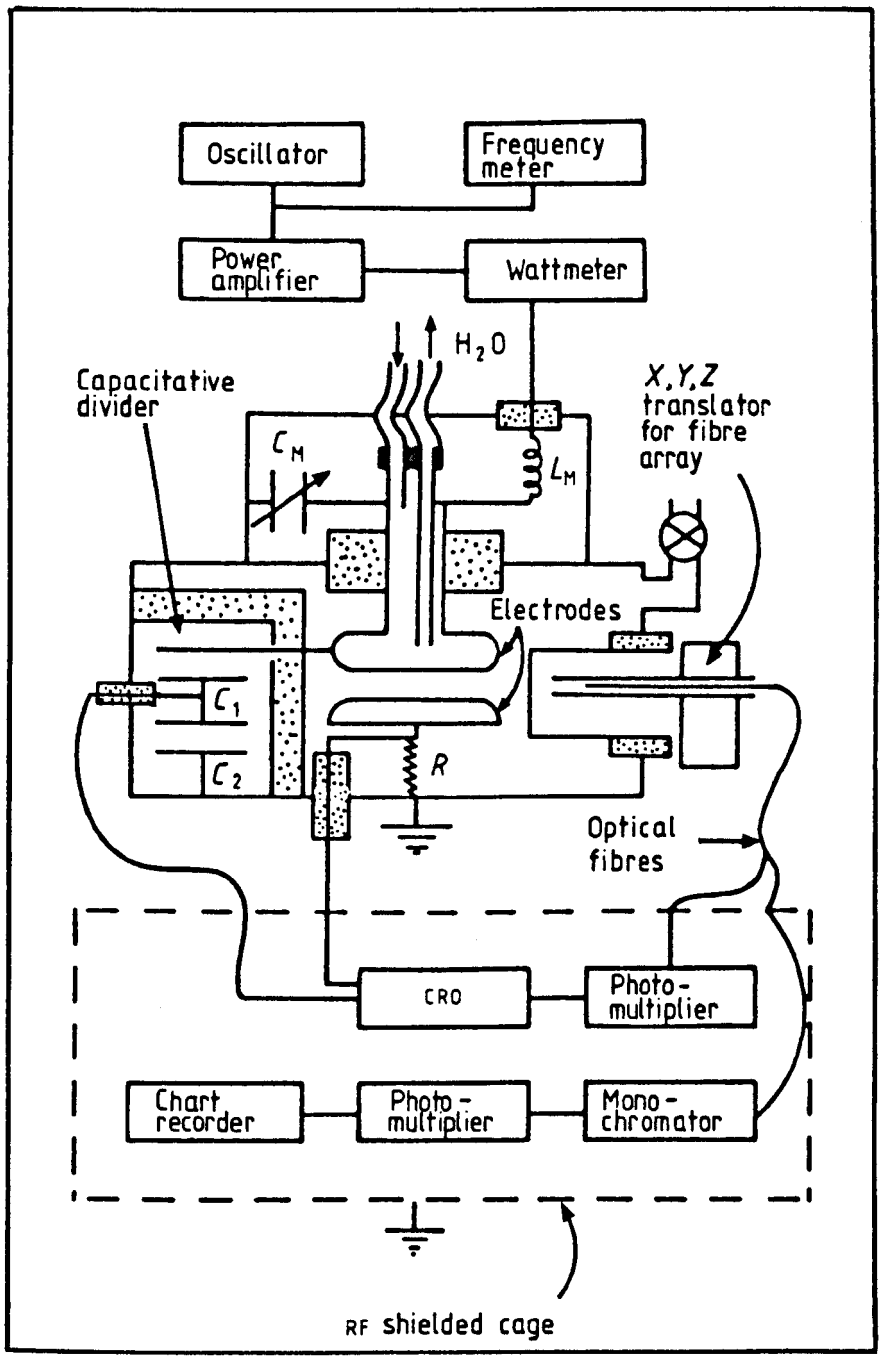

FIGURE 4.2 Schematic of Apparatus.

monochromator with line calibration provided by a mercury-cadmium lamp. The equipment for the voltage, current and light measurements was contained in an RF shielded cage.

4.3 EXPERIMENTAL RESULTS AND DISCUSSIONS

4.3.1 Current, Voltage and Power Characteristics

Figures 4.3(a) and (b) are photographs, on the same scale, of alpha and gamma discharges respectively in N_2; (c) and (d) are the corresponding visible light oscilloscope traces. Figures 4.4 and 4.5 show typical characteristics obtained with aluminium electrodes of constant separation. In Figure 4.4(a), as the voltage is raised from the alpha discharge minimum maintenance value ${}_{\alpha}V_L^{MIN}$, the current rises almost linearly to the alpha-to-gamma transition point $({}_{\alpha}V_L^{TR}, {}_{\alpha}i_{TR})$ where an abrupt drop in voltage to a value ${}_{\gamma}V_L$ and rise in current to a value ${}_{\gamma}i_{TR}$ occur. Points $({}_{\alpha}V_L^{TR}, {}_{\alpha}i_{TR})$ and $({}_{\gamma}V_L, {}_{\gamma}i_{TR})$ are connected by a dashed line with arrows indicating the one way only direction of the transition. Variation of the power input to the gamma discharge produced no detectable variation in the voltage ${}_{\gamma}V_L$: when the power to the gamma discharge was lowered to the point $({}_{\gamma}V_L, {}_{\gamma}i_{MIN})$ it was usually extinguished. Under certain conditions it was found that the gamma and alpha regime characteristics touched for low V_L and i. When this happened, lowering the power to the gamma discharge resulted in a transition back to the alpha regime $({}_{\gamma}V_L, {}_{\gamma}i_{MIN})$. If this occurred, return to the gamma regime could only be effected by following the alpha characteristics up to the $({}_{\alpha}V_L^{TR}, {}_{\alpha}i_{TR})$ transition point. Due to the close proximity of the electrodes it was not possible to measure accurately the area of the electrode covered by the discharges. What could be seen was that as ${}_{\alpha}V_L$ was raised from ${}_{\alpha}V_L^{MIN}$, the alpha discharge very quickly filled the electrode gap and then grew with ${}_{\alpha}V_L$ in visible light intensity up to the transition point. In the gamma regime the area of the electrode covered, or spot size, was small, Figure 4.3(b), and grew very slowly

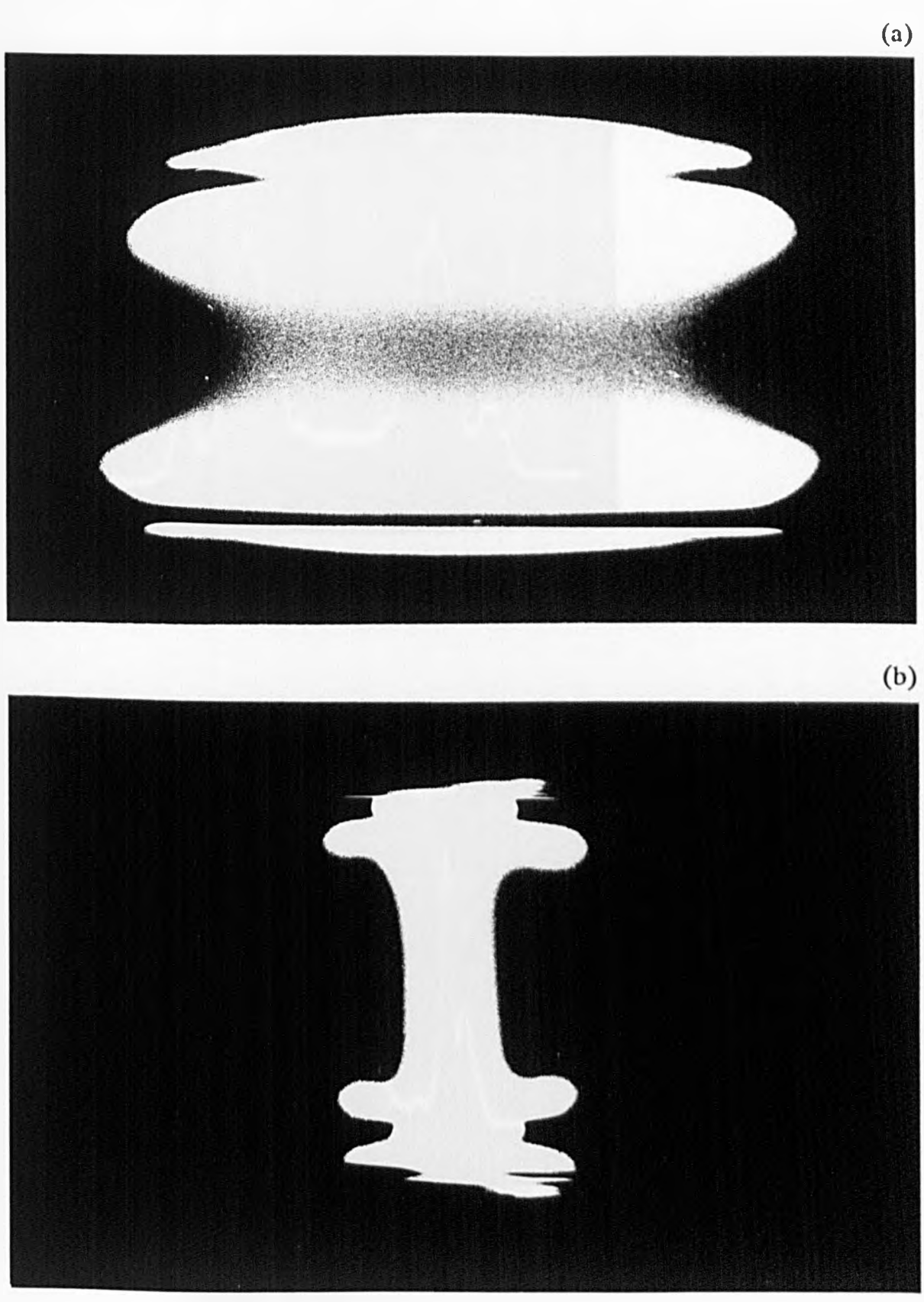

FIGURE 4.3 RF discharge in N_2, L = 2.0 cm, 20 MHz, (a) α discharge, 20 torr, 40 W, (b) γ discharge 40 torr, 50 W.

(c)

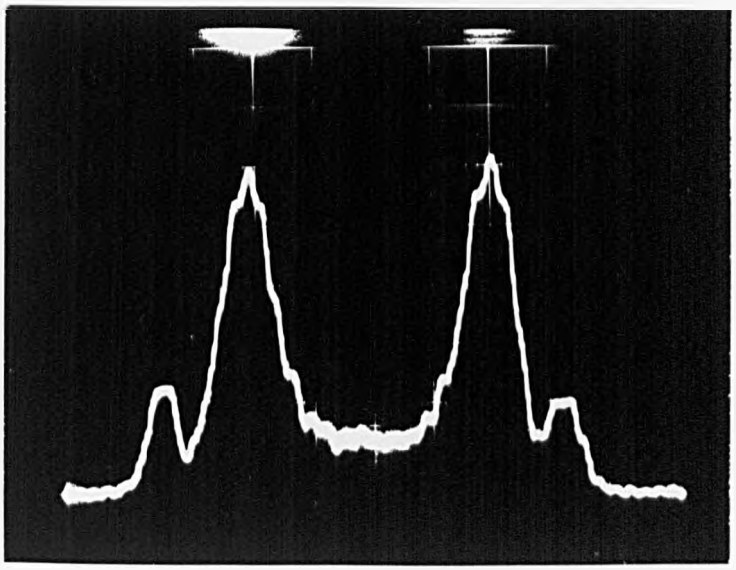

(d)

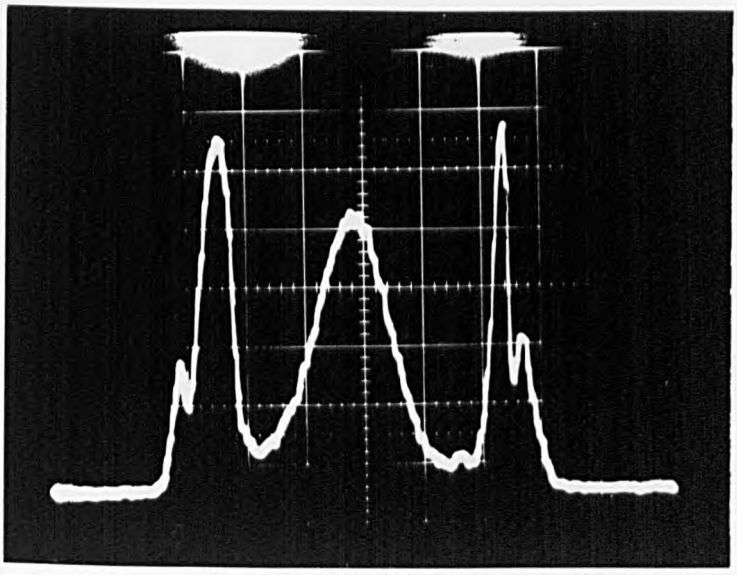

FIGURE 4.3 Oscilloscope photographs of RF discharge visible light emission profile in N_2, L = 2.0 cm, 20 MHz, (c) α discharge 20 torr, 40 W (d) γ discharge 40 torr, 50 W.

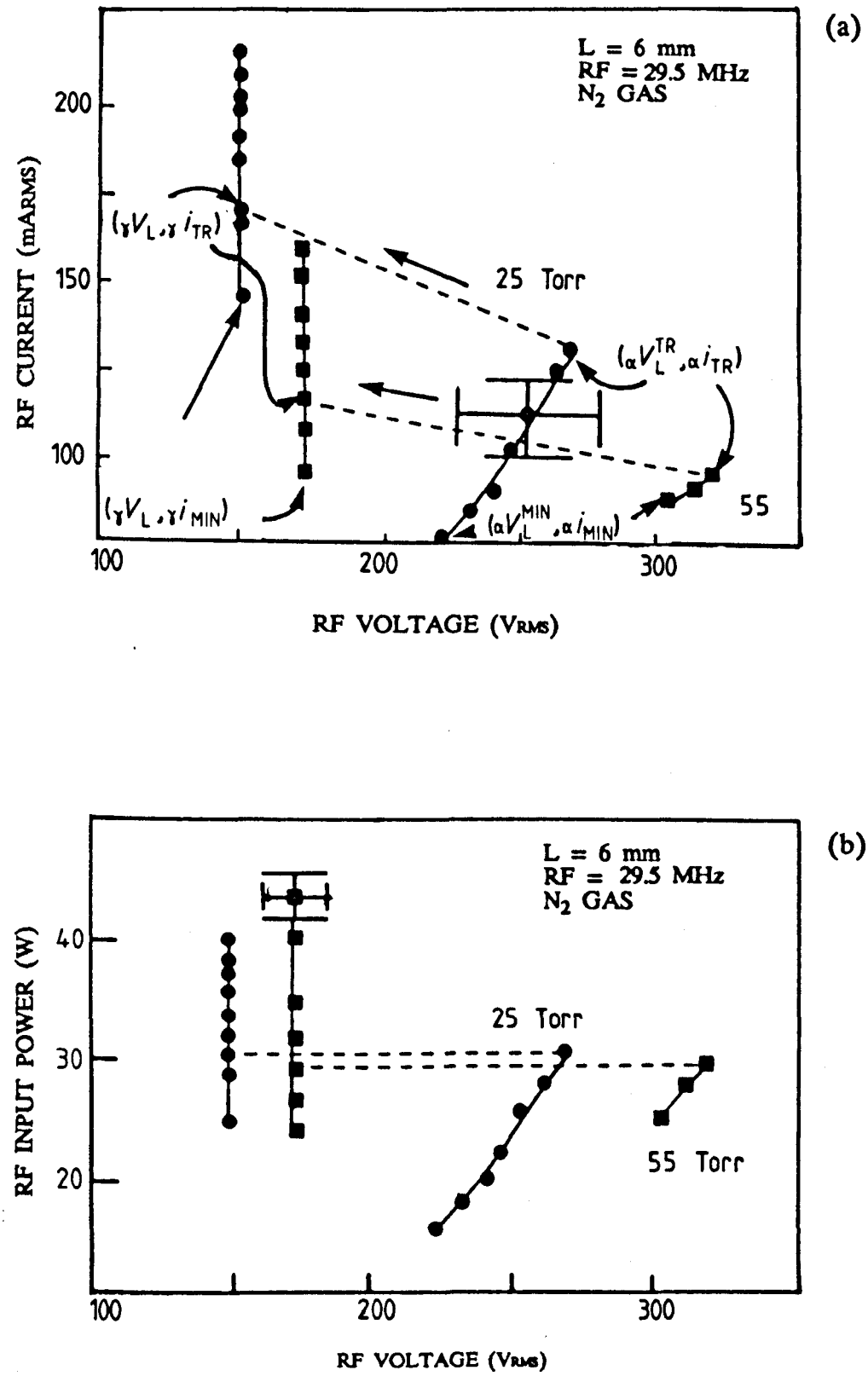

FIGURE 4.4 α and γ Current/Voltage and Total Discharge Power/Voltage Characteristics, Aluminium Electrodes.

with applied power. With rising pressure at constant power its contraction was again slow. At the transition point ($_{\gamma}V_L$, $_{\gamma}i_{TR}$) for Al electrodes at 29.25 MHz and 55 torr, Figure 4.4(a), we estimate the spot size as ~ 1.76 cm^2. The area, A, of the electrode covered by the alpha discharge was, for most conditions constant and equal to ~ 12.6 cm^2. This gives a gamma regime current density of ~ 67.18 mA rms/cm^2 as compared to ~ 7.5 mA rms/cm^2 at the alpha regime transition point ($_{\alpha}V_L^{TR}$, $_{\alpha}i_{TR}$). At the lowest frequency of 15 MHz it was found that for constant pressure and approximately equal power loading there was little difference between the interelectrode voltages for the two fixed electrode separations of 5.9 x 10^{-3} and 1.2 x 10^{-2}m. The fact that $_{\alpha}V_L$ does not increase appreciably for these small values of L is in agreement with the theory presented in Chapter 2 which predicts (see Table 4.2) that the proportion of $_{\alpha}V_L$ that falls off across the sheaths is quite large, rises with falling frequency and is about 70% for L = 5.9 x 10^{-3}m and 15 MHz. This prediction is further supported by absolute time resolved measurements of field in the sheaths of alpha RF discharges at a tenth of a torr where it was established that by far the greatest potential drop in the whole discharge occurs in the sheath adjacent to the instantaneous negative electrode [9]. In Figure 4.5 it is seen that $_{\alpha}i_{TR}$ and $_{\gamma}i_{TR}$ increase while $_{\alpha}V_L^{TR}$ decreases with rising frequency. The same effect has been observed in air at lower pressure and frequencies (~ 1.0 torr and 3 and 9 MHz) by Godyak and Khanneh [7, 8]. The increased currents with increased RF frequency, ω, will follow from the effect on the total discharge current of the sheath displacement current in both alpha and gamma discharges [10]. The sheath displacement current is directly proportional to ω and the sheath capacitance. In the alpha discharge the electron energy rises with ω, this results in larger conduction currents, (see Chapter 2, Equations 2.1 and 2.7) a thinner sheath and larger sheath capacitance. The fact that at the same frequency the gamma discharge current is greater than that of the alpha type is due to the gamma's very much thinner sheaths. At 25 torr characteristics similar to those of Figures 4.5(a) and 4.5(b) were obtained using aluminium electrodes coated with gold. The main difference between aluminium and gold

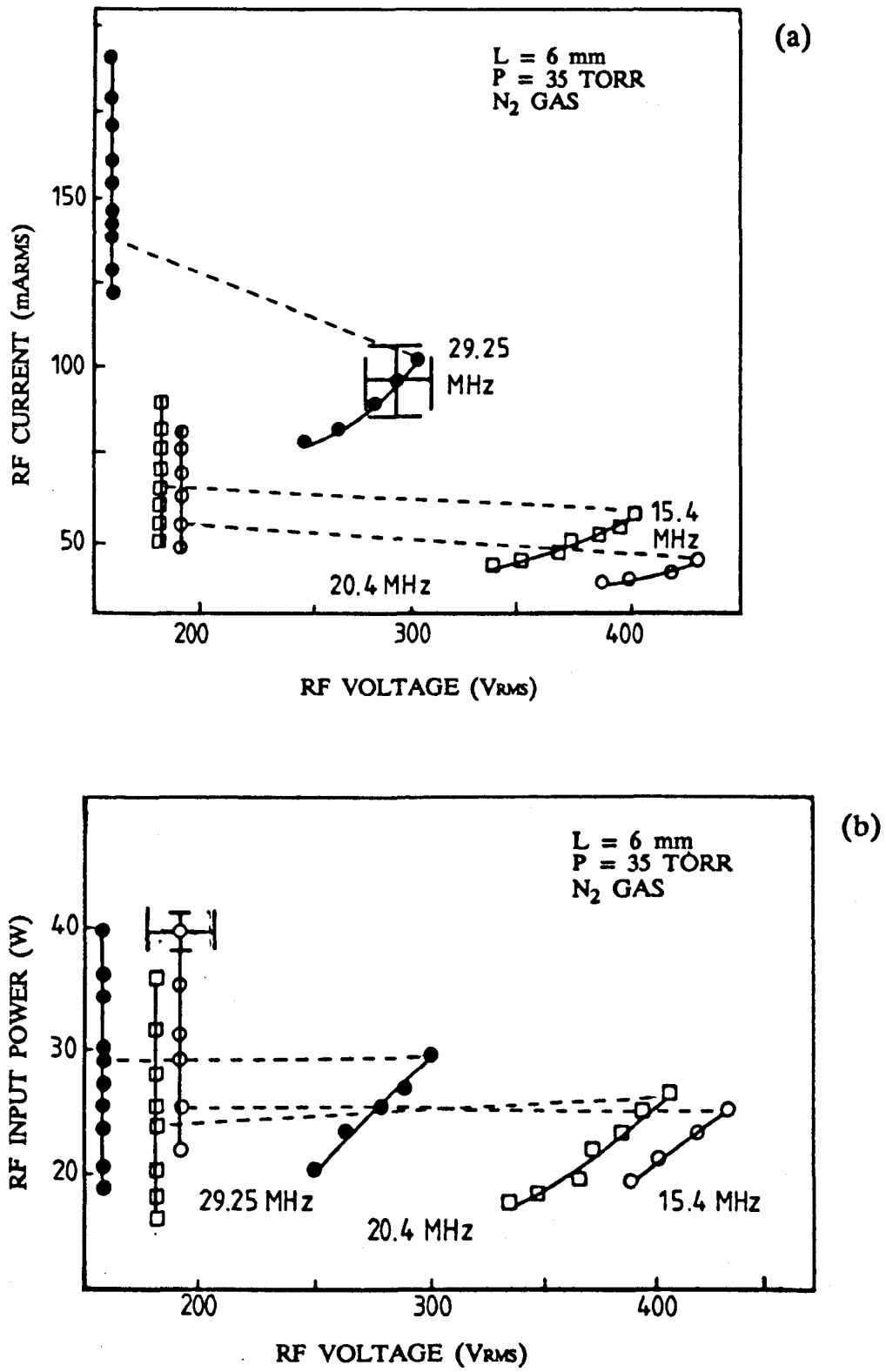

FIGURE 4.5 α and γ Current/Voltage and Total Discharge Power/Voltage Characteristics Aluminium Electrodes.

coated electrodes was that at constant pressure and frequency the voltages and currents were higher with gold. It was not possible to obtain measurements for p > 30 torr with the gold coated electrodes because of the greater powers needed.

Working up to 30 torr at a fixed frequency of 13 MHz, Yatsenko [11] has observed i-V characteristics similar to those reported here for N_2. By applying small ancillary voltages, Yatsenko found that the relatively thick alpha regime sheath had a much greater resistivity than the thinner gamma one for which the values were close to that for a DC glow. This again suggests that the gamma discharge sheath is traversed by appreciable currents originating at or close to the electrode. In helium Yatsenko notes that it is only at high pressures, > 100 torr, that a discontinuity is found in the i-V characteristic. For argon and xenon, here it is found that the alpha regime was stable up to pressures around 200 torr when transition to a filamentary discharge occurred. For constant pressure the alpha discharge is more stable with rising input power density the higher the RF frequency, Figure 4.5(b). A rough comparison was made of the neutral gas temperatures of the alpha and gamma discharge regimes using a mercury thermometer placed outside the discharge field zone and .2 cm from the luminous edge of the discharge. Figure 4.6(a) shows the variations in neutral gas temperature with the discharge input power for the alpha and gamma discharge regimes at a fixed pressure, RF frequency and electrode separation. In the first instance it shows that the neutral gas temperature increases with power, which is similar to the results of Ecker and Zoller [12] working with DC discharges. They also found that the neutral gas temperature increased with current. Figure 4.6(a) also shows that the observed neutral gas temperature, Tg, in the gamma regime is higher than that in the alpha regime for otherwise the same conditions of pressure, input power, RF frequency and electrode separation. Figure 4.6(b) shows the power densities in the alpha and gamma regimes versus input power. Due to these higher power densities, the neutral gas temperature is higher in the gamma regime. The higher power densities in the gamma regime as compared with those

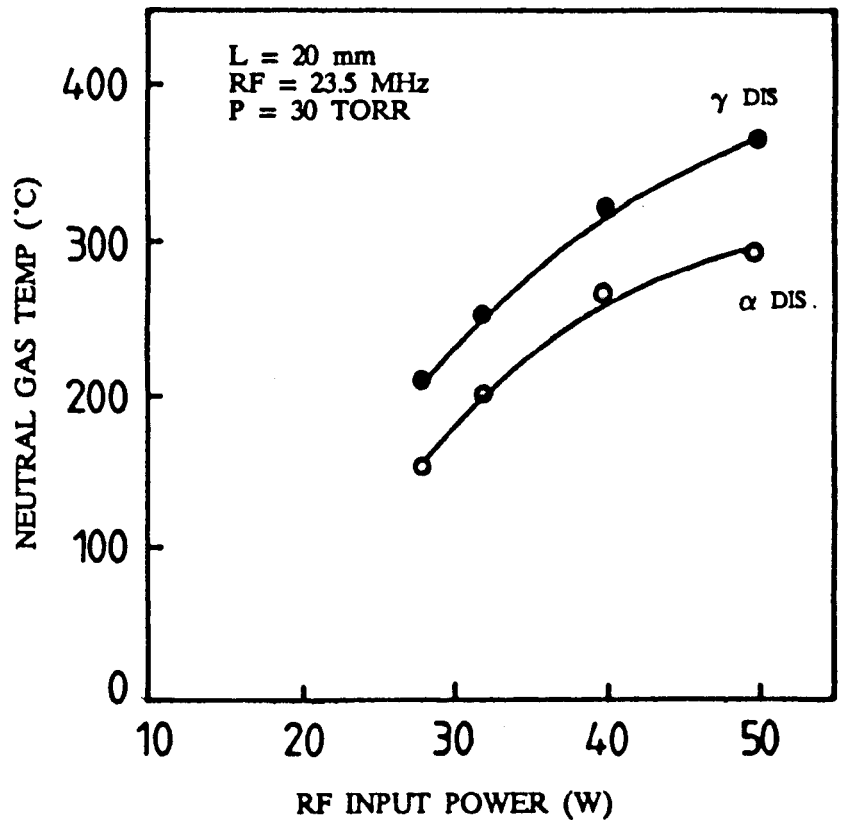

FIGURE 4.6a Variation of Neutral Gas Temperature with Input Power in α and γ Regimes

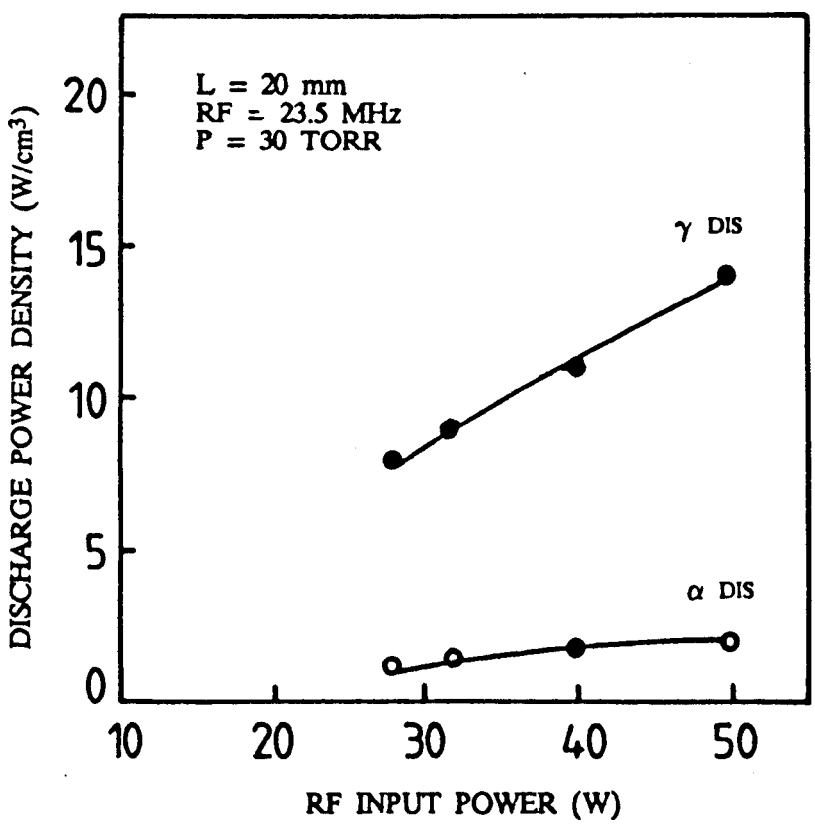

FIGURE 4.6b Discharge Power Density as a Function of Input Power in α and γ Regimes

in the alpha regime, are due to their different discharge volumes, for similar discharge conditions. (For details of alpha and gamma discharge sizes, see Section 4.3.1 and Figure 4.3.)

4.3.2 Stability Region for Alpha and Gamma RF Discharges as a Function of Gas Pressure, Input Power, RF Frequency, RF Voltage and Electrodes Material and Separation

The transition from the alpha to the gamma type RF discharge which occurs when power to the alpha discharge is raised to a critical value is important in devices such as gas lasers (CO_2, CO) as it places an upper limit on the power density that the alpha discharges used can accommodate.

The transition from the alpha to gamma discharge occurs when the interelectrode voltage in the alpha discharge reaches a critical value ${}_{\alpha}V_L^{TR}$, see Figures 4.4 and 4.5. Under certain, not fully investigated, conditions when, for low voltages and currents, the alpha and gamma current and voltage curves meet a transition from the gamma back to the alpha can occur (for backward transition see Chapter 7) if the voltage to the gamma discharge is lowered to the meeting point. A return to the gamma discharge has then to proceed up along the alpha curve and through the transition point $({}_{\alpha}V_L^{TR}, {}_{\alpha}i_{TR})$. ${}_{\alpha}V_L^{TR}$, see Figures 4.7(a) and 4.7(b) rose with rising pressure P at constant frequency ω and decreased with rising frequency at constant pressure. For constant pressure, the power loading to the discharge at the transition was higher the higher the frequency. The gamma discharge transition voltage, ${}_{\gamma}V_L$, increased with electrode separation L; within experimental errors ${}_{\alpha}V_L^{TR}$ appeared to be independent of L for RF frequencies beneath 30 MHz. Due to lack of available RF power it was not possible to effect the alpha and gamma transition for 57 MHz where the alpha discharge was stable to pressures over 100 torr, see Table 4.2. The experiments showed that ${}_{\alpha}V_L^{TR}$ is affected by the material of the electrode being greater at constant P, L and ω for

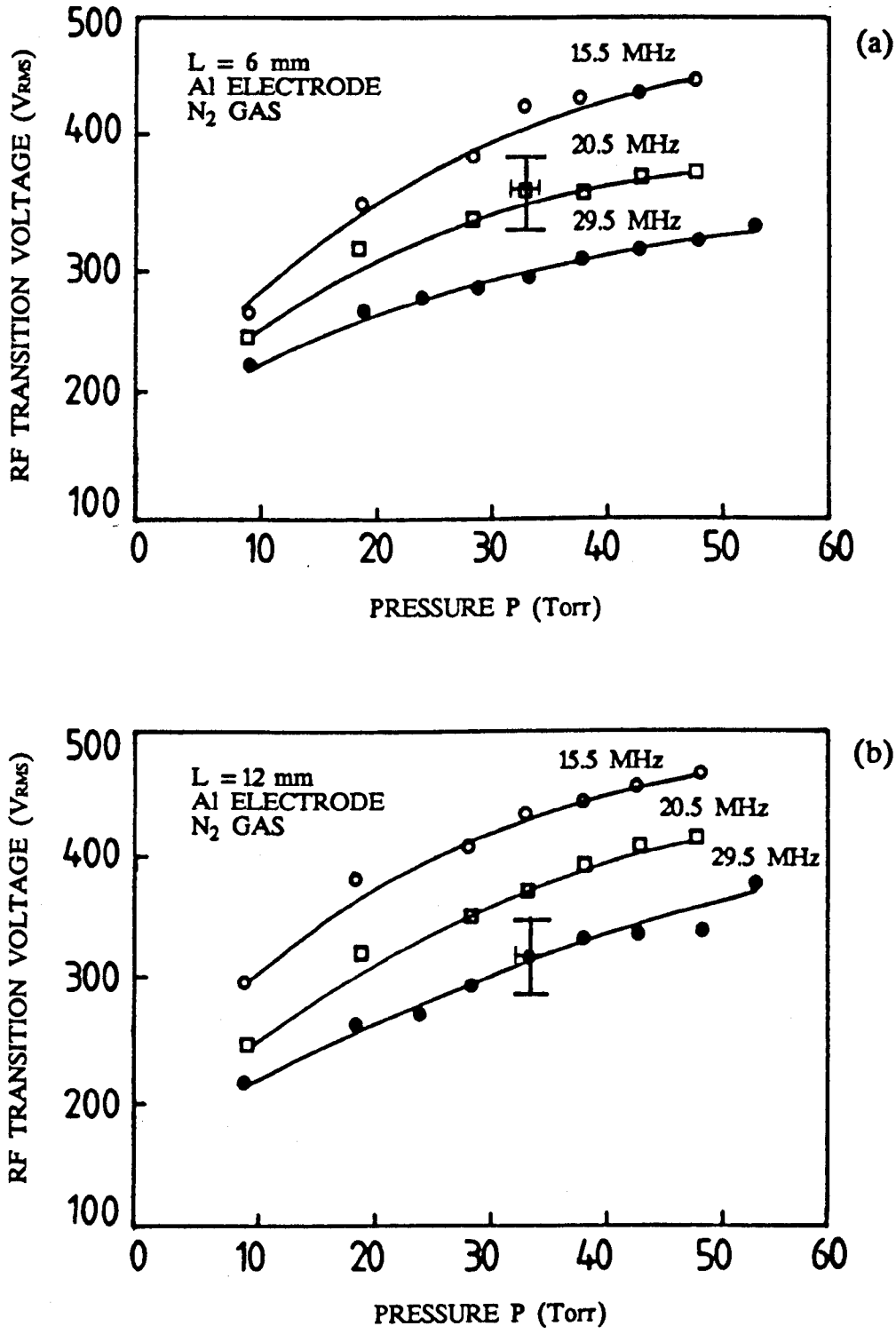

FIGURE 4.7 α Discharge Transition Voltage as a Function of Pressure for Different Electrode Separations, Aluminium Electrodes.

gold than for aluminium, Figure 4.8(a) shows RF transition voltage as a function of pressure at different RF frequencies, for gold coated aluminium electrodes of separation 0.59 cm. The RF transition voltage, as mentioned before, is increased significantly with gold coated aluminium electrodes for otherwise the same discharge conditions as aluminium electrodes, Figure 4.7(a). The picture is further clarified by looking at Figures 4.8(b) and 4.8(c) which show RF transition power as a function of pressure, for various RF frequencies at constant electrode separation, for respectively, aluminium and gold coated electrodes. A comparison of RF transition power and voltage for gold and aluminium is shown again in Figures 4.8(d) and 4.8(e) respectively, for a frequency of 20.5 MHz. These clearly show that the gold has increased significantly both the RF transition power and voltage. Finally Table 4.1 shows similar results for an electrode separation of 1.2 cm. Measurements with the gold coated aluminium electrodes could not be extended above 30 torr because of the large powers required. It was also found that when the electrodes were covered with PTFE it was not possible to generate a gamma discharge. Yatsenko [11] found that when his electrodes were covered with glass or PTFE the transitions voltage was raised by ~ 10 and 50% respectively. Our failure to obtain a gamma discharge with PTFE covered electrodes was probably due to the limited power and hence cross electrode voltage we had available. If the transition is controlled by secondary electron emission from the instantaneous cathode, the observed dependence of transition voltage on electrode surface material can be explained in terms of the work functions of the materials. In general, the lower the work function the more secondary emission. For the three materials used, aluminium, gold coated and PTFE, aluminium has the lowest and PTFE the highest work function.

The theory presented in Chapter 2 shows (see Table 4.2) that the voltage dropped across the sheath, V_s, where the secondary electrons that affect the alpha to gamma transition gain energy, is greater the smaller the RF frequency. This gives a possible explanation as to why the alpha discharge is more stable with

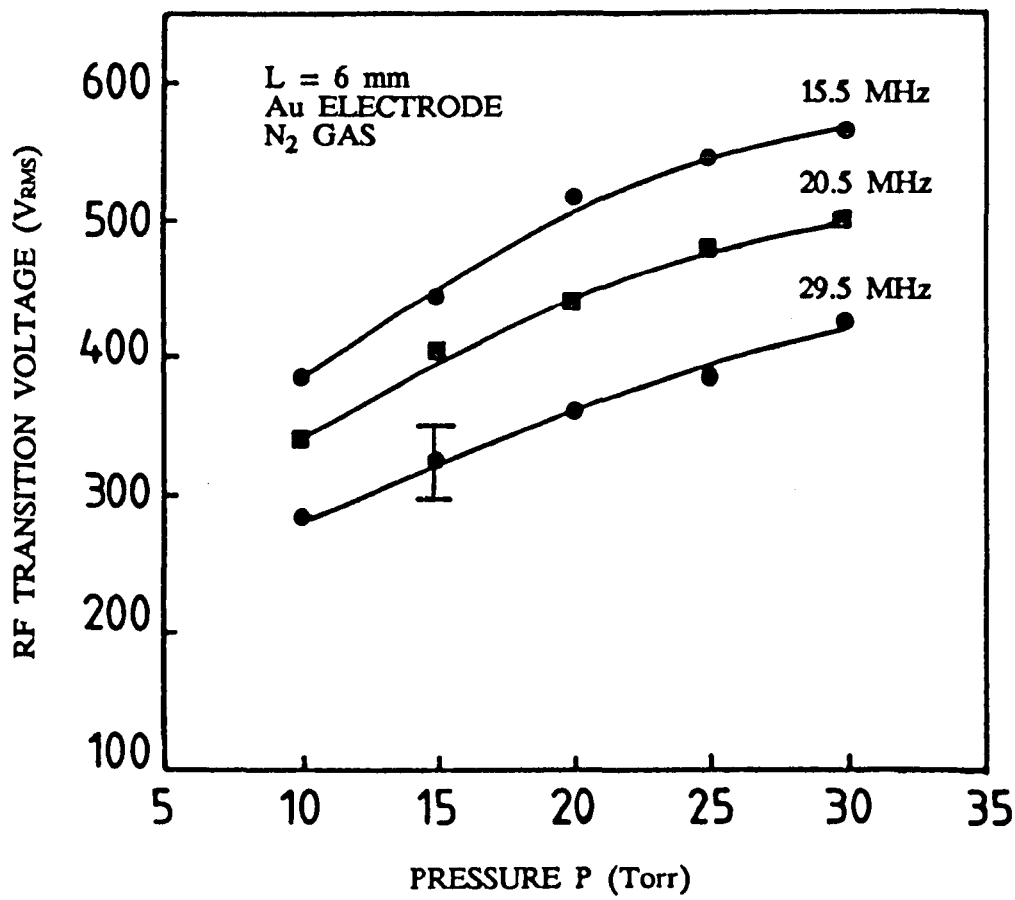

FIGURE 4.8a Alpha to Gamma Transition Voltage as a Function of Pressure, Au Coated Electrodes

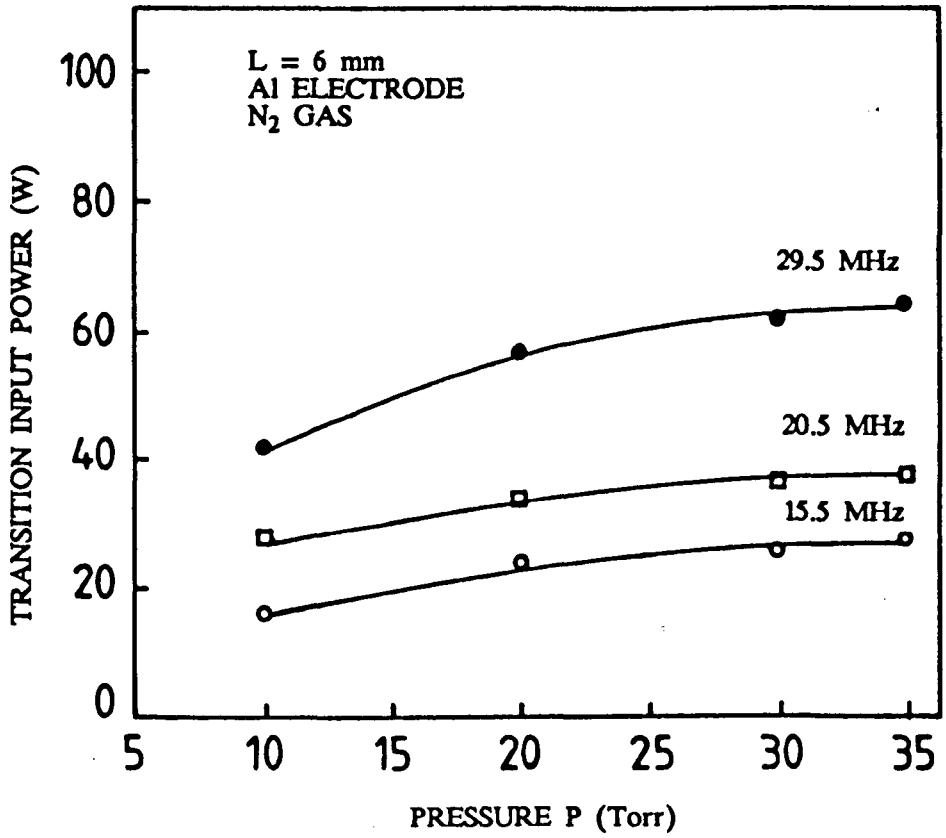

FIGURE 4.8b Alpha to Gamma Transition Power as a Function Pressure Al Electrodes

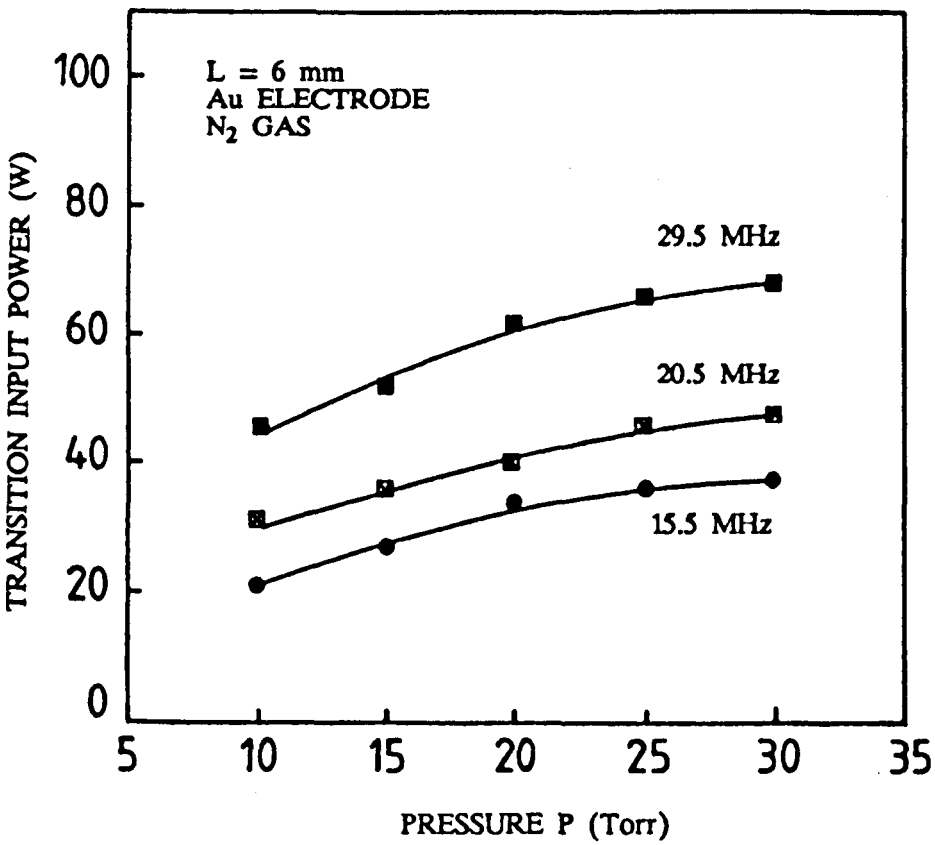

FIGURE 4.8c Alpha to Gamma Transition Power as a Function of Pressure, Au Coated Electrodes

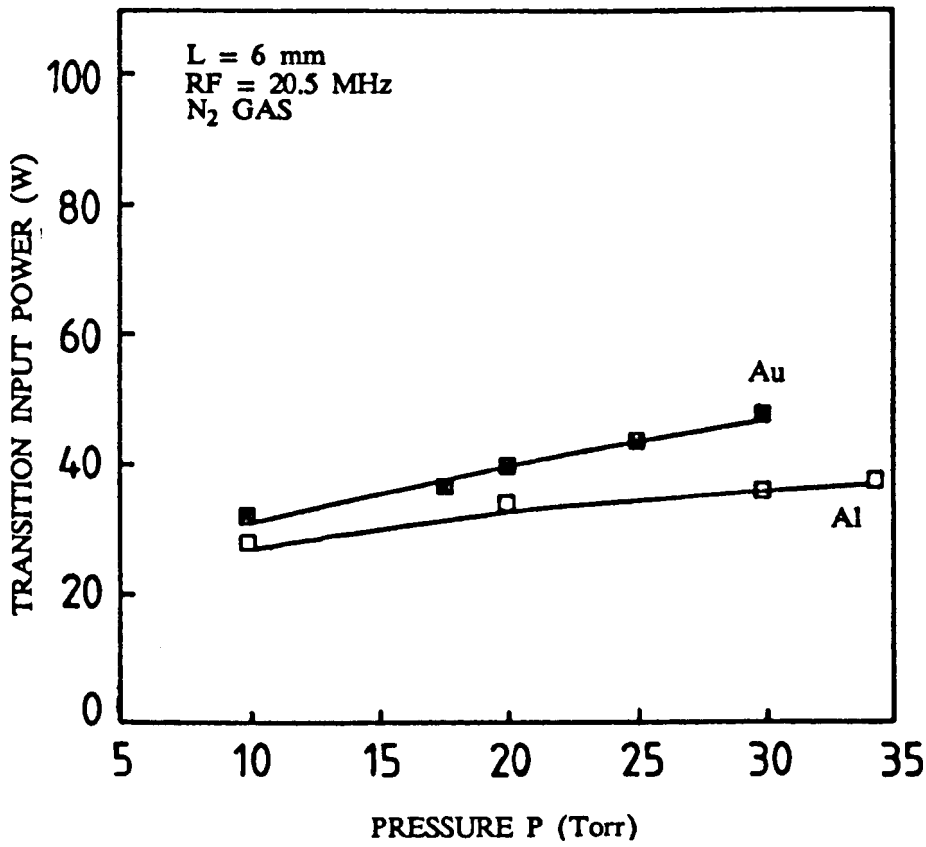

FIGURE 4.8d Alpha to Gamma Transition Power as a Function of Pressure for Au Coated and Al Electrodes

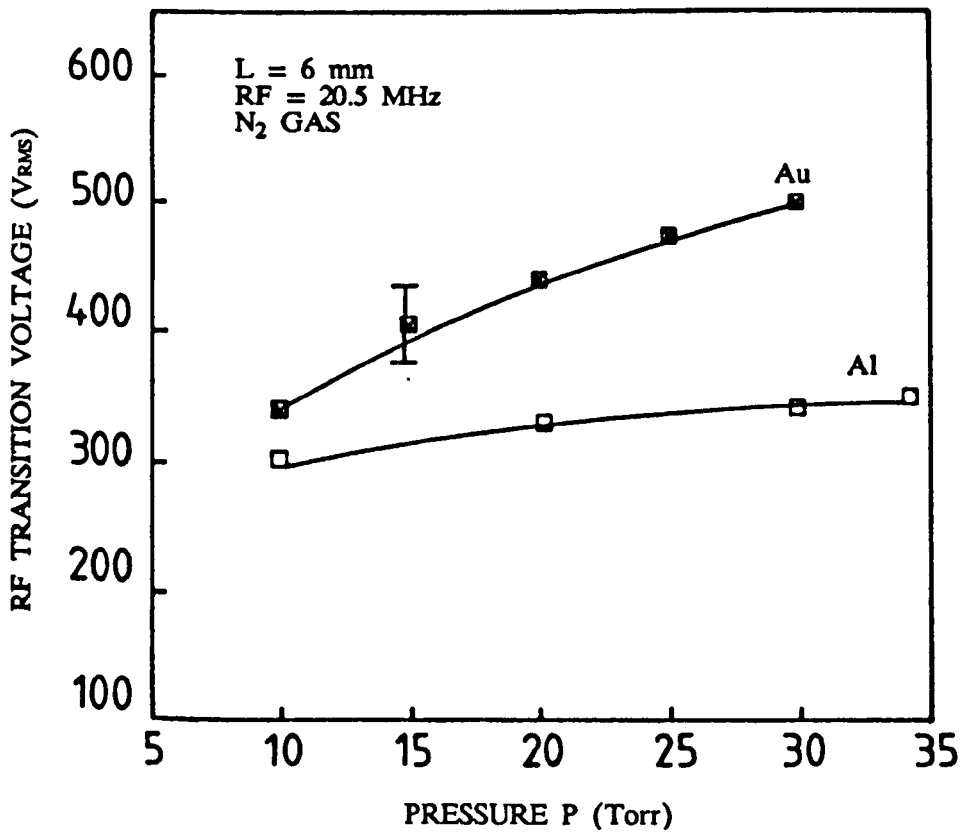

FIGURE 4.8e Alpha to Gamma Transition Voltage as a Function of Pressure for Au Coated and Al Electrodes

P	f	αV_L^{TR}
Torr	MHz	Volts rms
10	15.4	385
15	15.4	445
20	15.4	500
30	15.4	580
10	29.25	300
15	29.25	325
20	29.25	350
30	29.25	400

TABLE 4.1 The α to γ transition voltage αV_L^{TR} for different pressure and RF frequency. N_2 between Au electrodes separation 1.2 x 10^{-2}m.

increasing power loading the higher the RF frequency.

4.3.3 The Electron Temperature Measurements in Alpha and Gamma Regimes

Figure 4.9 shows the electron temperature Te as a function of pressure for the alpha and gamma discharge regimes at constant input power, RF frequency and electrode separation. It can be seen from this figure that firstly, the electron temperature decreases with pressure in both the alpha and gamma discharge regimes and secondly, the electron temperature in the alpha discharge regime is higher than that in the gamma discharge regime. The decrease in the electron temperature in both the alpha and gamma discharge regimes with pressure is due to the plasma zone reduced field (E/N), which decreases with increasing pressure at constant input power [13]. The electron temperature, which depends on the plasma zone reduced field will therefore also decrease. The lower electron temperature in the gamma regime is due to the lower plasma zone reduced field and higher charge density in the gamma regime [10] for otherwise the same discharge conditions as the alpha regime. Godyak and Khanneh [10], in their calculations of the gamma regime plasma zone reduced fields, did not however take account of the neutral gas temperature though the higher neutral gas temperature in the gamma regime (Section 4.3.2) will effect their calculations of E/N due to its effect of lowering the neutral gas density, N.

4.3.4 The Time Dependent Visible Emission as a Function of Pressure and RF Frequency

Figure 4.10 compares the visible light from the centre of the discharge to that from close to one electrode for an alpha and gamma discharge. It is seen that (i) the percentage of modulation is greatest for the gamma, (ii) modulation of the light from the centre of the discharge is at twice the RF frequency, ω, for both discharge types and (iii) light from near the electrode is modulated at ω for the

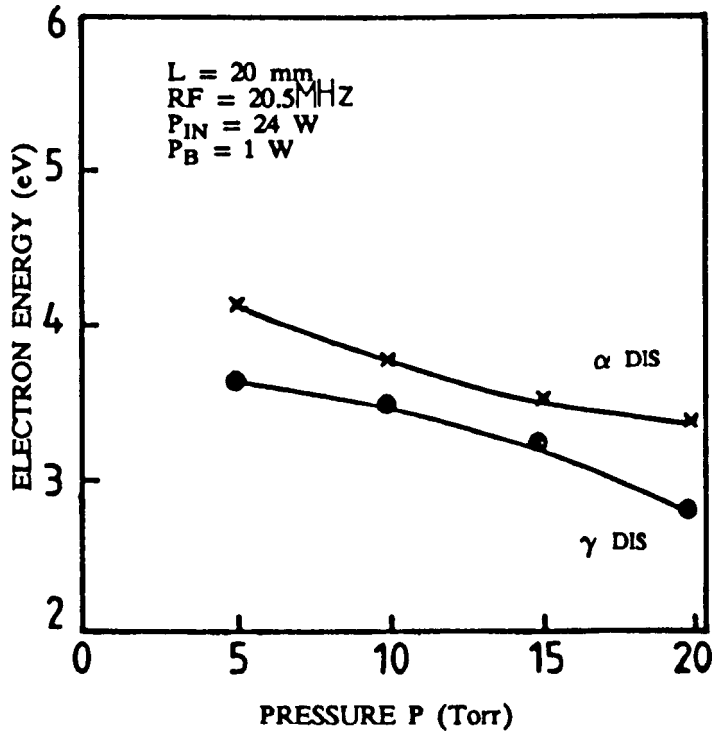

FIGURE 4.9 Electron Energy as a Function of Pressure in α and γ Regimes

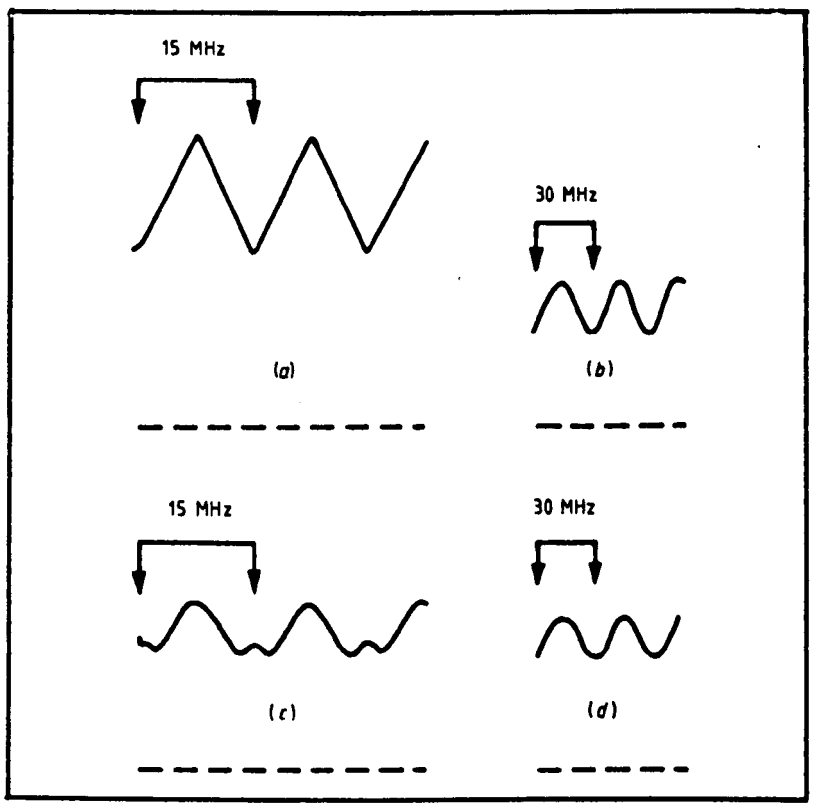

FIGURE 4.10 Visible Emission from the Electrode Region (a) and (c), and from the Discharge Centre (b) and (d). (a) and (b) γ Discharge, (c) and (d) α Discharge. Dotted Line Denotes Trace Baseline N_2, 35 torr, 15 MHz, 35 W.

gamma but with the alpha the waveform has become asymmetric. The most likely explanations for these observations are as follows. In the gamma discharge a strong pulse of light is generated at one electrode once per cycle of the applied RF. The light signal of both discharge types is modulated at 2ω because the light from the discharge central plasma is excited twice per RF cycle each time the plasma electron energy peaks and/or the spatial resolution of the detector was not good enough to prevent it seeing equal signals generated in turn at one electrode and the other. The fact that there are two signals of different amplitude per RF cycle for the light from near the electrode in the alpha discharge is probably because there is a relatively smaller light pulse generated there at a frequency ω and because the plasma modulated at 2ω extends closer towards the electrode.

The emission of light modulated at the applied RF field frequency from close to the electrodes was observed by Kuzovnikov and Savinov [14] working with alpha discharges in He at 8 MHz and 0.5 torr. These authors ascribed the relatively intense and modulated emission from the electrode region to excitation by the once per RF cycle ejection of a pulse of energetic electrons from the electrode boundary when it is driven at a negative voltage. The fast electrons are ejected from the instantaneous cathode by positive ion, photon and excited species bombardment and gain their energies by being accelerated across the positive sheath zone. In the alpha type discharge, the pulsed electrons supplement the volume ionisation to a degree that increases with increased energy input to the discharge until at the alpha to gamma transition point they provide the dominant source of ionisation. Recently spatially and temporarily resolved work by Hebner and Verdeyen [15], again in He in the 1 torr and 1 MHz pressure and frequency range, confirmed experimentally that firstly, the light pulses occur at the instantaneous negative electrode and secondly, by placing a quartz slide in front of and parallel to one electrode so as to obstruct the stream of energetic ejected electrons, the electrons causing these light pulses do indeed follow ballistic trajectories in a direction away from and perpendicular to the negative electrode. Figure 4.11 shows the

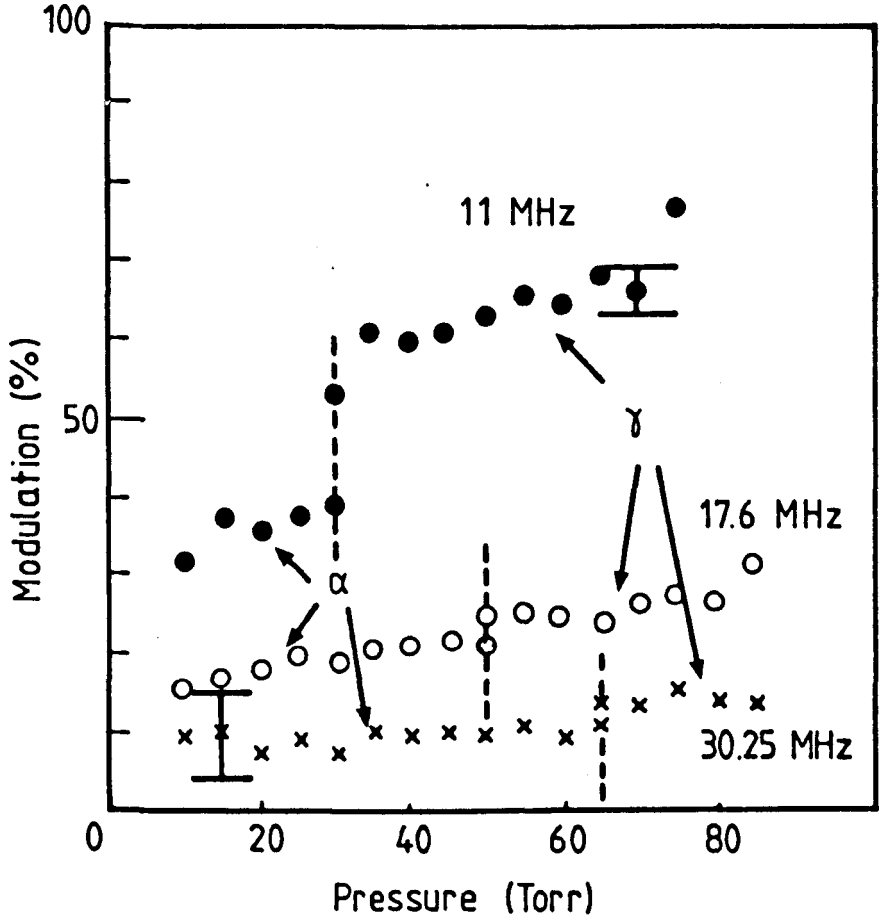

FIGURE 4.11 Percentage Modulation of Visible Emission from Discharge Centre as a Function of Pressure and Frequency N_2. Dotted Vertical Lines Denote Position of α to γ Transition.

modulated emission signal from the centre of the discharge as a percentage of the total light detected. The signal is from the discharge centre as the electrodes had to be brought fairly close together for a reasonable variation in pressure and RF frequency to be obtained. The dashed vertical lines denote the pressures at which the transition from alpha to gamma occurred. It is seen that the modulation increases with increasing pressure and decreasing frequency of the applied RF. These two trends were found in all the gases investigated. Comparing nitrogen, air and the laser mixture $3He:1N_2:1CO_2$ to pure helium, argon and xenon, it was always found that the modulation was greatest in the molecular rather than noble gases. Again it was noted that it was not possible for the electrode separations used (~ 0.3 to 2.0cm) to obtain a transition for alpha to gamma for argon and xenon at pressures beneath about 200 torr. The explanation for the pressure and frequency dependence of the modulation appears to be that the maximum electron energies and hence atomic/molecular excitation rates follow the peak RF fields. If $\Delta\tau$ is the time in the RF cycle when excitation is at a minimum and $\nu_1 p$ is the collisional deactivation rate of excited species at pressure p then, to a first approximation, the depth of modulation will be proportional to the product $\nu_1 p\Delta\tau$, that is greatest at low frequency and high pressure. The modulation would be more pronounced in molecular rather than atomic gases because the rates of collisional quenching in molecular gases are higher due to the greater number of states in close resonance to the excited states.

4.3.5 Spectroscopy of the Time Averaged Visible Emission

Scrutiny of the emission of alpha and gamma discharges between 3000 and 7000Å emitted from the middle of the discharges showed differences in the range 3800 to 5300Å. The alpha spectrum, Figure 4.12(a), consisted almost exclusively of the second positive N_2 ($C^3\Pi_u \rightarrow B^3\Pi_g$) system. Superimposed on this N_2 emission, the gamma spectrum, Figure 4.12(b), shows strong N_2^+ emission due to the N_2^+ ($B^2\Sigma_u^+ \rightarrow X^2\Sigma_g^+$) 1st negative system (3914, 4237 and 4278Å).

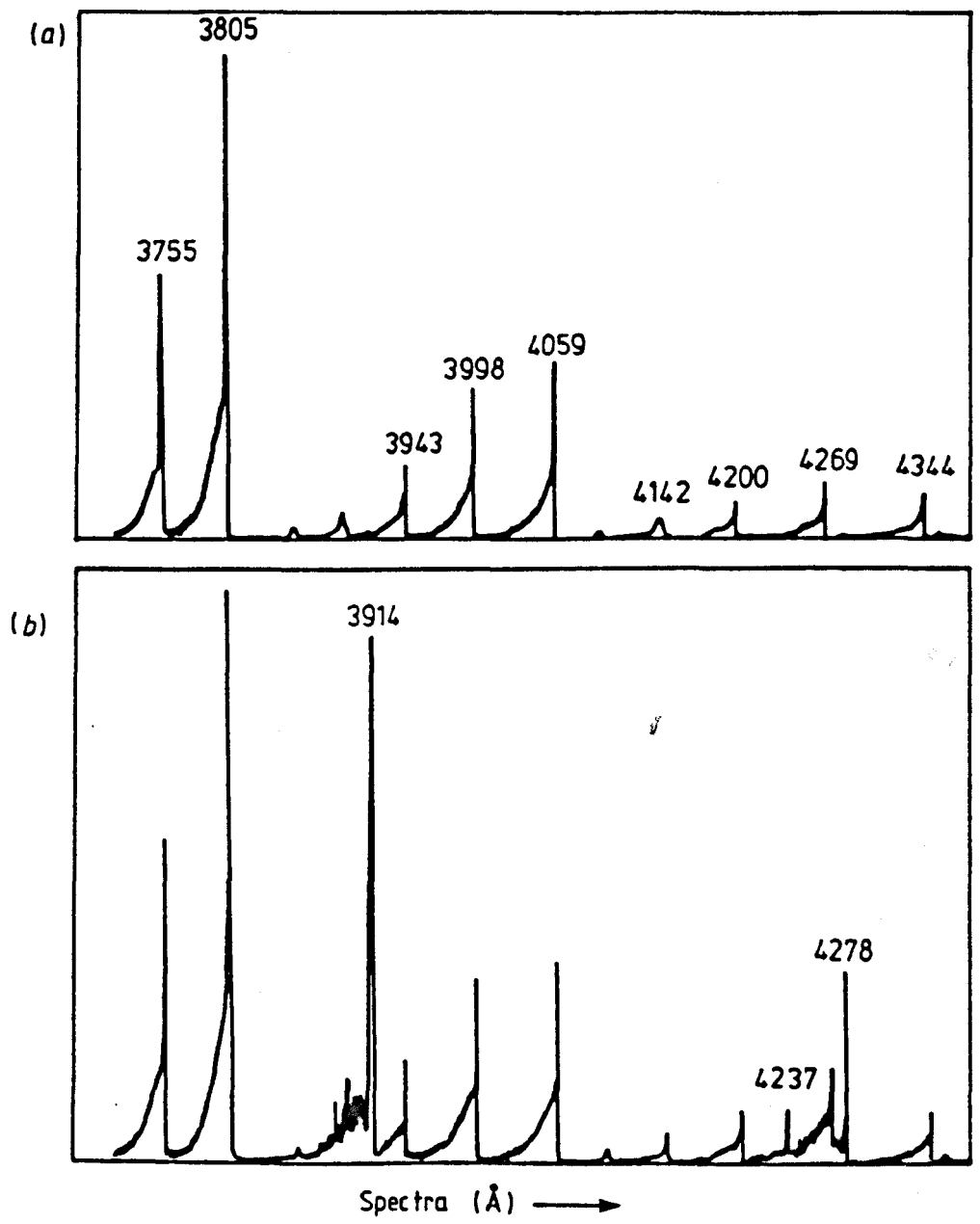

FIGURE 4.12 N_2 Emission Spectra 3700 to 4300Å for (a) α Discharge and (b) γ Discharge. L = 0.59 cm, 40 W, 30 torr, 20 MHz. Intensity in Arbitrary Units.

Magnification of the alpha spectrum revealed that the N_2^+ lines found in the gamma are present but at about one hundredth of the gamma spectrum intensities. Due probably to poor spatial resolution, no detectable differences were found between the spectra for the middle and near electrode regions of the discharges. The enhanced molecular nitrogen ion emission in the gamma is consistent with an increase in N_2^+ or charge density in the gamma discharge as compared to the alpha. No detectable difference was found in the spectra when gold as opposed to aluminium electrodes were used.

4.3.6 Time Averaged Visible Emission Spatial Profile of Gamma Discharge

Returning to the photo densitometer trace, Figure 4.3(d), of the gamma emission profile between the electrodes, some similarity was observed between the DC glow discharge cathode fall region and the electrode boundary region of the gamma discharge when the latter's boundary layers were measured. At 40 torr in N_2 with aluminium electrodes, starting in towards the discharge centre, the thin intensely bright layer, thickness 0.3 mm, was followed by a dark region of thickness 0.1 mm and then a diffuse layer that was finally separated by another dark region from the central plasma zone. If these layers are RF analogues of respectively the cathode layer, the cathode dark space, the negative glow and the Faraday dark space, the thickness of the cathode dark space analogue, 0.1 mm above, is close to the predicted value of 0.07 mm for N_2 with aluminium electrodes in DC glows [16].

4.4 DISCUSSION AND CONCLUSIONS

Table 4.2 lists some measured and calculated alpha discharge characteristics for nitrogen between aluminium electrodes, using the theory of Chapter 2. When compared to the experimental results, the calculated currents and discharge powers give the observed trends and the agreement is fair. Noteworthy is the prediction

OBSERVED						CALCULATED								
ω radians s^{-1}	P torr	L m	V_L volts rms	I mamps rms	$\langle W \rangle$ Watts	I mamps rms	$\langle W \rangle$ Watts	$\langle W_s \rangle$ Watts	$\langle W_p \rangle$ Watts	ϵ eV	n m^{-3}	R Ω	V_s volts rms	E/p volts $torr^{-1}m^{-1}$
3.58×10^8	35	5.9×10^{-3}	188	183	22	202	35	12.9	22.1	1.1	2.1×10^{17}	542	64	600
(57 MHz)			220	353	46.5	279	58.6	25.5	32.1	1.12	2.8	411	91	625
	105		275	229	36.5	102	27.5	2.5	25.0	1.00	1.4	2416	24	405
			353	398	62	216	73	12.8	60.2	1.04	2.6	1285	59	474
1.84×10^8	25	5.9×10^{-3}	220	78	16	122	10.7	6.1	4.6	1.09	1.3×10^{17}	630	142	564
(29.25 MHz)			270	134	31	144	14.3	8.7	5.6	1.10	1.5	540	173	584
	35		250	76	20	127	13.0	6.4	6.6	1.072	1.4	820	140	528
			300	108	28	145	15.9	8.4	7.5	1.08	1.6	715	148	544
	55		310	86	26	142	18.1	7.4	10.7	1.053	1.7	1060	150	492
			320	95	30	156	21.5	9.3	12.2	1.058	1.8	1000	166	501
9.68×10^7	35	5.9×10^{-3}	390	35	18	79	12	8.3	7.4	1.045	0.95×10^{17}	1200	264	477
(15.4 MHz)			440	50	25	91	15.1	11.0	4.1	1.053	1.1	1040	346	491
	25	1.2×10^{-2}	418	44	14	68	11.0	6.2	4.8	1.056	0.8	2080	262	497
			520	61	20	91	18.9	12.0	6.9	1.073	1.0	1660	370	530

TABLE 4.2 Comparison of measured and predicted α discharge characteristics. N_2 between Al electrodes.

that energy is dissipated in the oscillating sheath zone as well as in the plasma zone. The high intensity visible emission "wings" close to the electrodes, Figure 4.3, can thus be explained as due in part to the energetic oscillation of electrons at the plasma/sheath boundary rather than being caused solely by high energy secondary electrons that have been ejected from the instantaneous cathode and accelerated across the sheath [14]. Considering the stability of alpha discharges, how they flip over to the gamma discharge when the power density is increased to a critical value, the theory predicts that the sheath voltage V_s is largest for lower frequency where, see Figure 4.5(b), the alpha to gamma transition occurs for lower power density. In other words, for the same P and L and about the same $<W>$, the theory from Chapter 2 and Table 4.2, predicts that V_s increases with decreasing RF frequency. If the transition is due to breakdown of the sheath [10], the lower frequency discharge with its greater cross sheath voltage might well be expected to be less stable. Again Table 4.2 and the theory (Chapter 2), predicts that the proportion of power dissipated in the sheath decreases as the frequency is raised. Advantages from a laser point of view of high over low frequency illustrated by the model are higher charge density, n, thinner sheaths and greater discharge stability as the power is raised. If however the plasma zone reduced field, E/N, is optimum for the desired laser pumping at a lower frequency, the advantages of higher frequency may be off-set. Concerning the calculated discharge parameters of Table 4.2, it should be noted that the discharge gas temperature was taken to be constant and at room temperature. This will tend to overestimate N the gas density and underestimate the reduced field E/N. This in turn will underestimate the electron energy ϵ and charge density n, see Chapter 2. Systematic neutral gas temperature measurements were not made in these experiments because confidence in the technique used was not yet established.

REFERENCES

[1] P.P. Chenausky, R.A. Hart, L.A. Newman and N.N. Hoffman, Proceedings of CLEO Phoenix, Arizona, USA, Opt.Soc.Am., 88 (1982).

[2] H. Hugel and W. Schock Proceedings of CLEO Phoenix, Arizona, USA, Opt.Soc.Am., 90 (1982).

[3] D. He and D.R. Hall, App.Phys.Lett., Vol.43, 726 (1983).

[4] P. Vidaud, D. He and D.R. Hall Optics Communications Vol.56, 185 (1985).

[5] C.G. Parazolli and K.R. Chien IEEE J.Quant.Electron., QE-22, 479, (1986).

[6] D. He, C.J. Baker and D.R. Hall, J.Appl.Phys., Vol.55, 4120 (1984).

[7] V.A. Godyak, Special Issue, IEEE J.Quant.Electron. (1986).

[8] V.A. Godyak and A.S. Khanneh, IEEE Plasma Science, PS 14, 112, (1986).

[9] C.A. Moore, G.P. Davis and R.A. Gottscho Phys.Rev.Letters, Vol.52, 538, (1983).

[10] N.A. Yatsenko, Sov.Phys.Tech.Phys., Vol.25, 1454 (1980).

[11] N.A. Yatsenko, Sov.Phys.Tech.Phys., Vol.26, 678, (1981).

[12] G. Ecker and O. Zoller, Phys.Fluids, Vol.7, 1996 (1964).

[13] A. Lompe and R. Seeliger, Ann.Phys., Vol.15, 300, (1932).

[14] A.A. Kuzovnikov and V.P. Savinov Bull University of Moscow, Physics, Vol.18, 215, (1973).

[15] G.A. Hebner and J.T. Verdeyen, IEEE Plasma Science PS 14, 132, (1986).

[16] A.H. Von Engel "Ionised Gases", OUP, Oxford, (1965).

CHAPTER 5

STRIATION FORMATION TIME MEASUREMENTS IN N_2

5.1 INTRODUCTION

A universal property of gas discharge plasmas, independent of the method of generating such a plasma, is the existence of a space charge sheath along the plasma boundaries. These positively charged sheaths are always present along the electrodes bounding the plasma [1-5]. In the simplest case, where the total electron and ion current normal to the plasma boundary is equal to zero, the width of the sheath amounts to several Debye lengths while the negative jump in the potential from the plasma to the electrode amounts to several electron volts. This negative potential retards the penetration of plasma electrons into the sheath and accelerates the plasma ions so as to equalize their rates of arrival at the electrode boundary. As a result, the number of electrons is negligible in the sheath and its conductivity is significantly lower than the plasma conductivity. These sheaths are easily observed in experiments as dark layers separating the plasma from the electrodes.

The alpha type capacitative RF discharge, which has been used extensively for the excitation of CO_2 gas lasers, has positively charged sheaths near each electrode boundary. These space charge sheaths along the boundaries of the plasma determine to a considerable degree the properties of RF discharges since a significant portion of the interelectrode voltage is dropped across them and they can provide extra ionization for the volume of the discharge. Sheaths also play an important role in the transition, from alpha to gamma RF discharges [6-8, see also Chapter 4]. Considering pulsed CO_2 gas lasers, if a pulsed discharge is short

enough the gas remains cool and the discharge is free of the sheath in-homogeneities of the fully developed discharge. In-homogeneities and hot gas both vitiate the CO_2 gas laser performance.

To explain the structure of striations in RF discharges, several theoretical models have been proposed [9-12]. However, none of these give information on the striation formation time and its dependence on RF discharge parameters such as RF frequency, pressure, electrode separation and input power. Because there is again no experimental data available, a set of experiments were performed on RF striation formation times in N_2. Based on the results obtained, a simple theoretical model for the observed striation formation times is proposed. The experimental set up is described in Section 5.2, while Section 5.3 contains the experimental results. The theoretical model is described in Section 5.4. and compared with experimental results in Section 5.5.

5.2 EXPERIMENTAL SET UP

The experimental set up for the striation formation time measurements is shown in Figure 5.1. A double balanced mixer was used to control the RF drive amplitude level in a square wave fashion. The pulsed RF frequency signal from the double balanced mixer was then pre-amplified and fed into the wide band power amplifier. Power was supplied to the discharge through an inline bi-directional Bird Thru-line coupler and power meter. Forward and reflected powers were measured on the oscilloscope (for details see diagnostic techniques Chapter 3). For the striation formation time measurements, we simply observed the distribution of visible light in a transverse direction, from the discharge. A schematic representation of the visible light profile from the discharge is shown in Figure 5.2(a). Decreasing the RF pulse width decreases the brighter wings of Figure 5.2(a), until a distribution as shown in Figure 5.2(b) is reached. Actual experimental results similar to Figure 5.2, are shown in Figure 5.3. The RF pulse

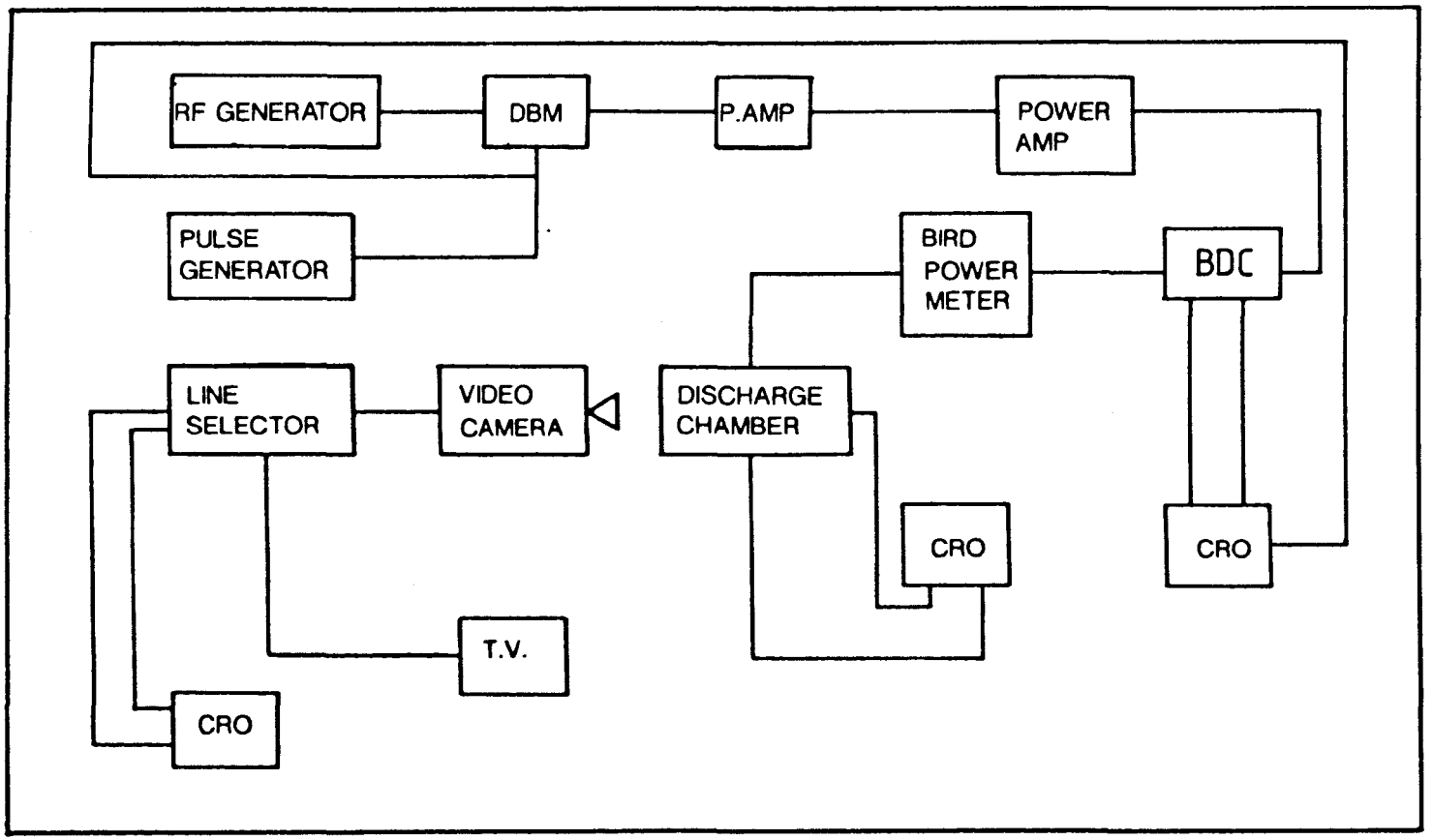

FIGURE 5.1 **Experimental Set Up for Striation Formation Time Measurements.**

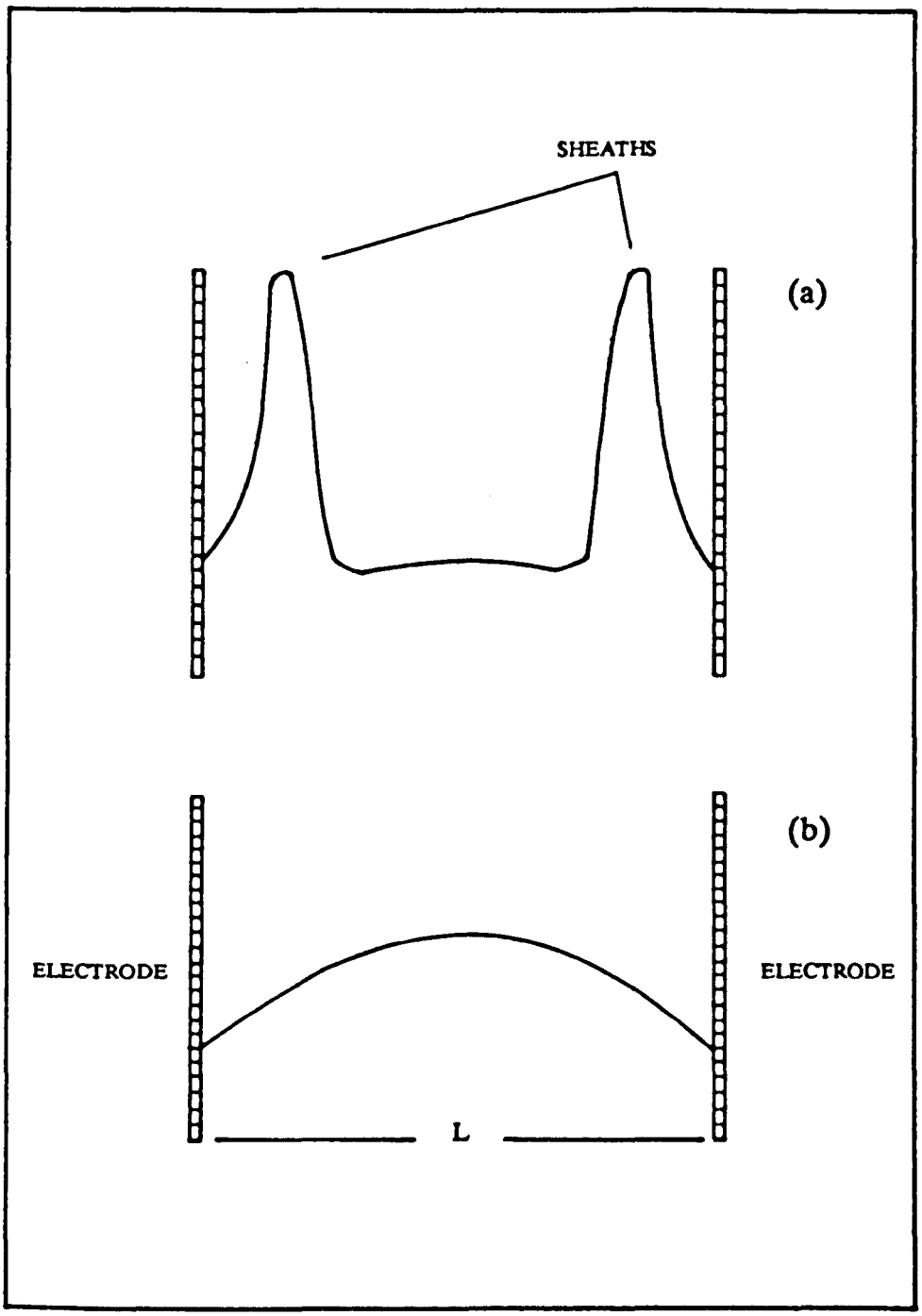

FIGURE 5.2 Characteristics Visible Light Emission Profiles from the Discharge Across the Electrodes (a) with Striations, (b) without Striations.

(a)

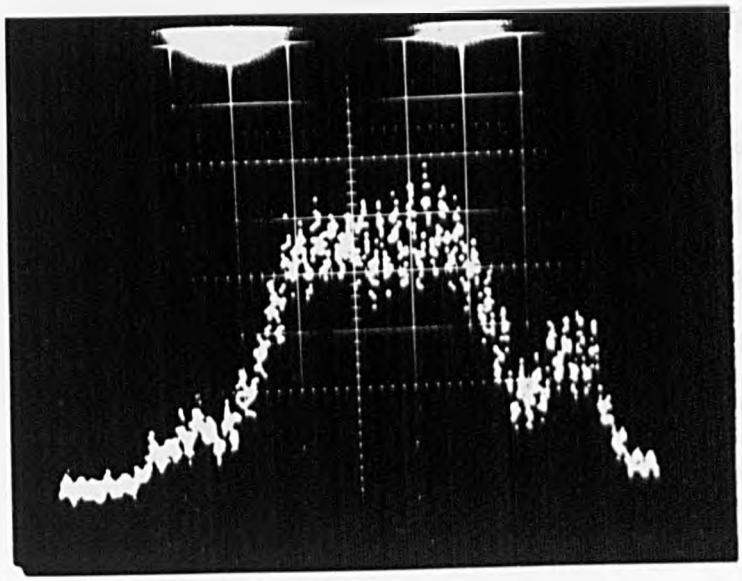

(b)

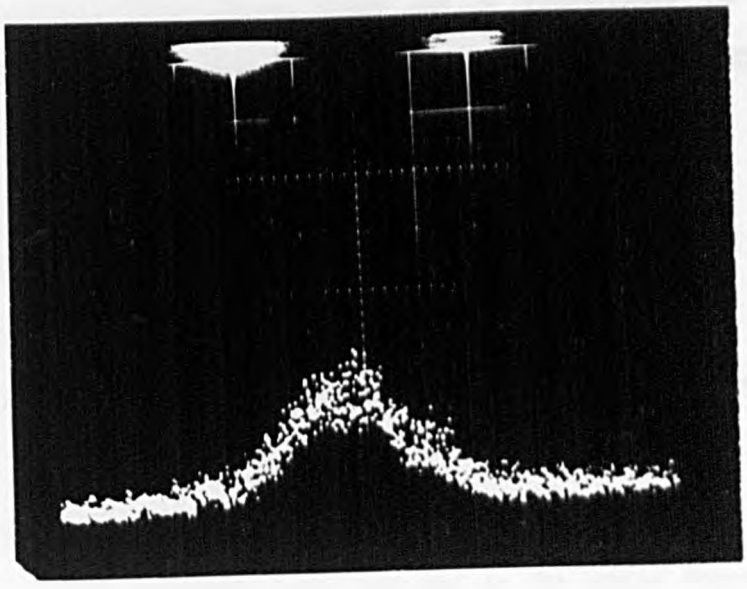

FIGURE 5.3 Oscilloscope photographs of visible light emission profile from the discharge across the electrodes (a) discharge with striations (b) discharge without striations.

width at which the striation wings appear near the electrodes is taken to be the striation formation time for the particular RF discharge conditions.

To observe the distribution of visible light from the discharge, a video camera was used along with a T.V. screen line selector, oscilloscope and television. The video camera displayed the discharge on a typical 650 line television screen. Using the television screen line selector, connected to a HAMEG Digital storage oscilloscope (model HM 208), we observed the distribution of visible light in a transverse direction of the discharge from the television screen across a single line. The discharge current, voltage, input and reflected powers were measured by using the techniques described in Chapter 3. For all the experimental investigations reported in this chapter we used the same discharge chamber shown in Chapter 4, except that the diameter of the Al electrodes for the present work was 2.8 cm. Finally for all the experiments, the pulsed RF duty cycle was kept constant at 0.25%.

5.3 STRIATION FORMATION TIME AS A FUNCTION OF POWER, GAS PRESSURE, ELECTRODE SEPARATION AND RF FREQUENCY

Figure 5.4 shows striation formation time as a function of pressure for different input powers at a constant electrode separation of 5 mm and RF frequency of 40 MHz. The striation formation time increases with pressure at constant input power, and it is decreased with increasing power at constant pressure. From Figure 5.4 it can also be seen that at 10 torr, the difference in striation formation time with increasing power is less than it is at a higher pressure of 28 torr. This difference is in part due to the strong dependence of striation formation time on the discharge impedance matching conditions. For perfect discharge impedance matching conditions, where the reflected powers were below 5% of the input power, the striation formation time was much less than for those where the reflected power exceeded 5%, with otherwise similar discharge conditions.

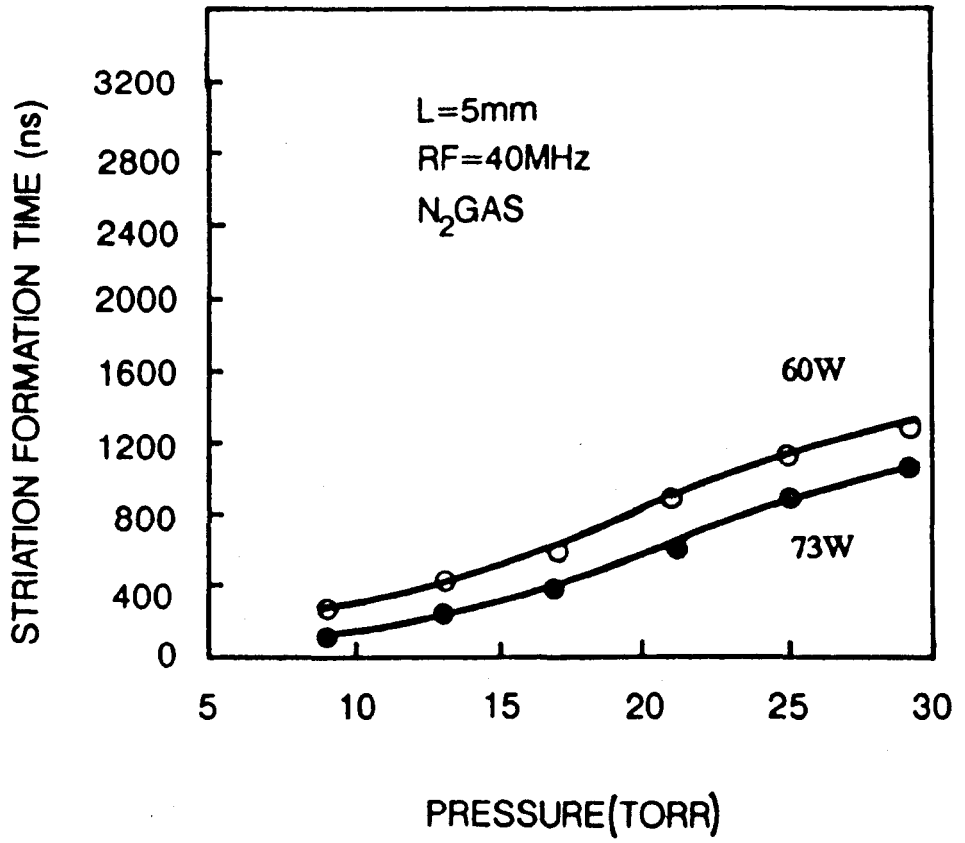

FIGURE 5.4 Striation Formation Time as a Function of Pressure for Different Input Powers.

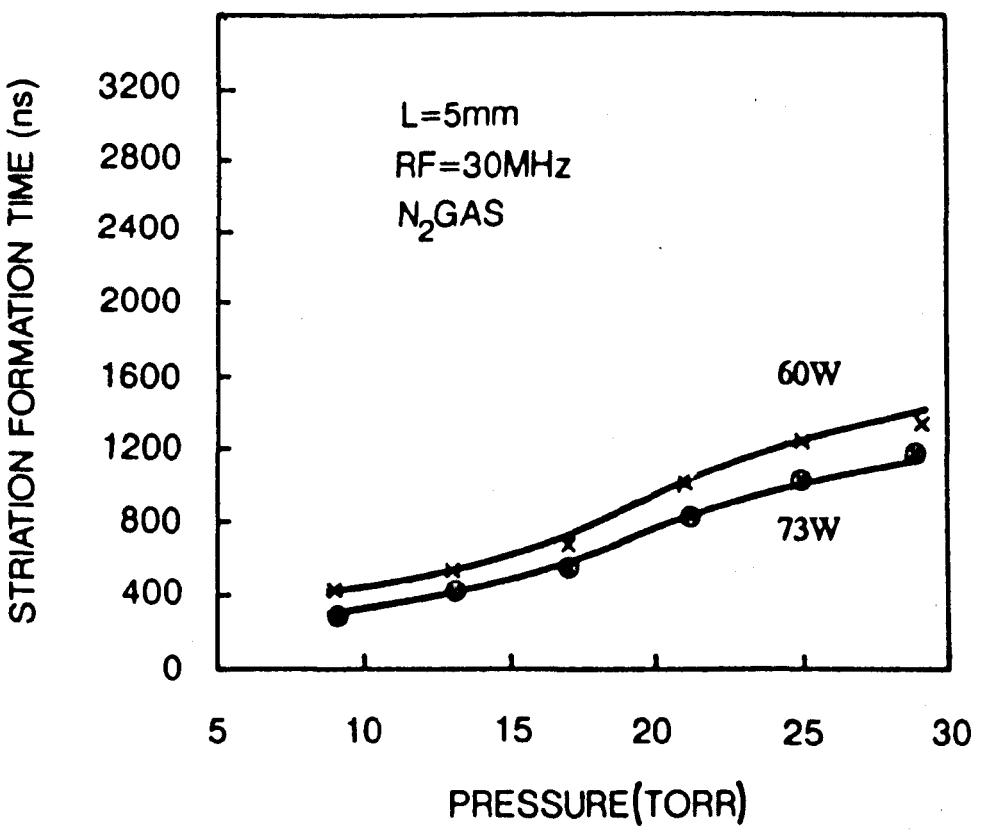

FIGURE 5.5 Striation Formation Time as a Function of Pressure for Different Input Powers.

This was one of the reasons for trying to keep the reflected RF power low as much as possible. Except in few cases for most of the experimental work presented in this chapter, we succeeded in keeping the reflected RF power below 5%. Results similar to those in Figure 5.4 are repeated in Figure 5.5 for the RF frequency of 30 MHz. The striation formation time as a function of pressure and RF frequency for constant power and electrode separation of 60 W and 5 mm respectively, is shown in Figure 5.6. Increasing RF frequency decreases the striation formation time. Striation formation time as a function of pressure and electrode separation at constant RF frequency and power is shown in Figure 5.7. By increasing the electrode separation from 5 mm to 10 mm, the striation formation time is increased. Finally the results of Figures 5.4, 5.5 and 5.6 are repeated in Figures 5.8, 5.9 and 5.10 respectively for the electrode separation of 10 mm. In Figures 5.8, 5.9 and 5.10, the matching conditions were not as good as far the other figures above about 20 torr. The dashed portions of the curves mark the boundary between good matching and reliable results at low pressure and the not so good or reliable results at higher pressure.

5.4 THEORETICAL MODEL FOR STRIATION FORMATION TIME

The model assumes that striations in an RF discharge are formed when the plasma charge density reaches some critical value n_s at which the space charge distorts the interelectrode field. Space charge distortion occurs when the field due to the space charge becomes comparable to the applied field. This causes the onset of ambipolar diffusion as the electrons are no longer able to move in the applied field independently of the positive ions. With the ions speed increased and the electrons speed decreased to the common ambipolar diffusion speed, the rate of loss of electrons is effectively reduced. This, coupled with the enhancement of the effective electric field by the space charge, results in a rapid increase in the rate of ionization. The net effect of a large and equal density of positive and negative ions at each point in the volume of the discharge is that a considerable voltage

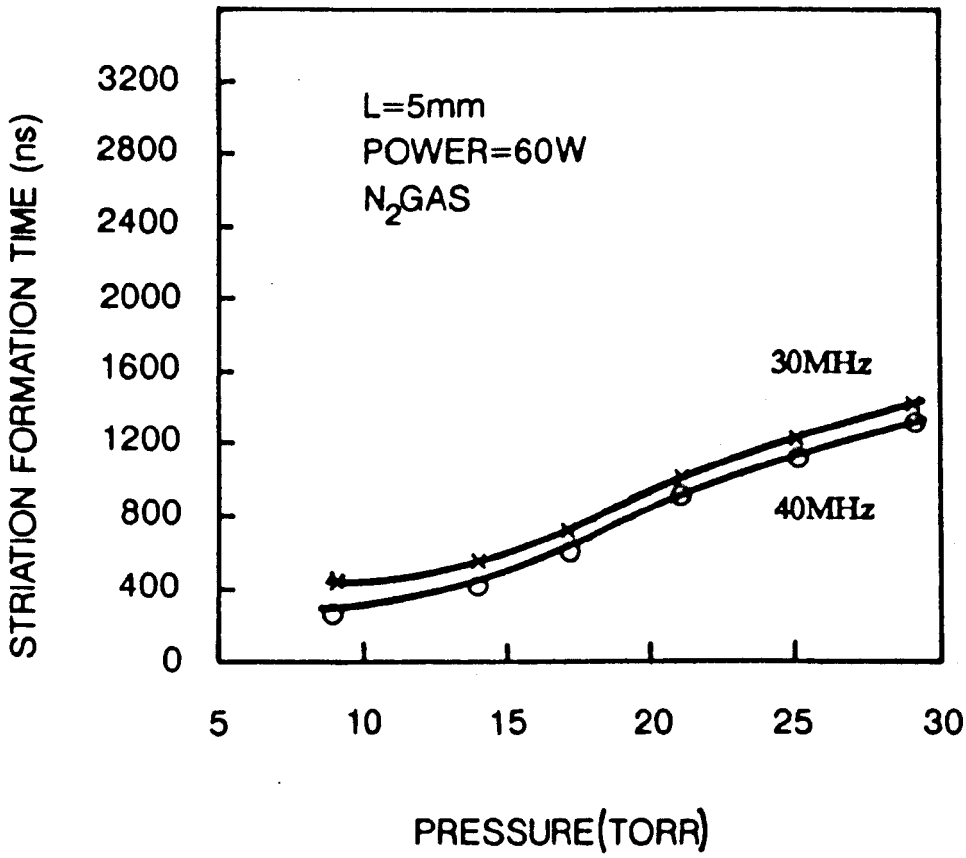

FIGURE 5.6 Striation Formation Time as a Function of Pressure for Different RF Frequencies.

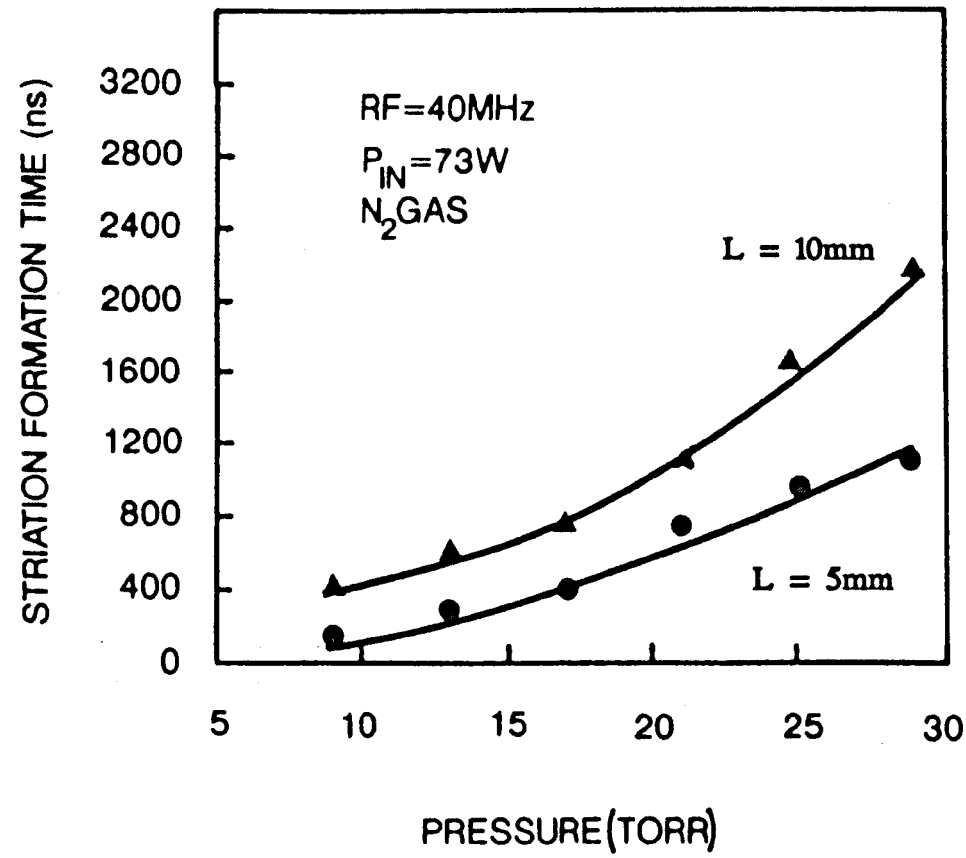

FIGURE 5.7 Striation Formation Time as a Function of Pressure for Different Electrode Separations.

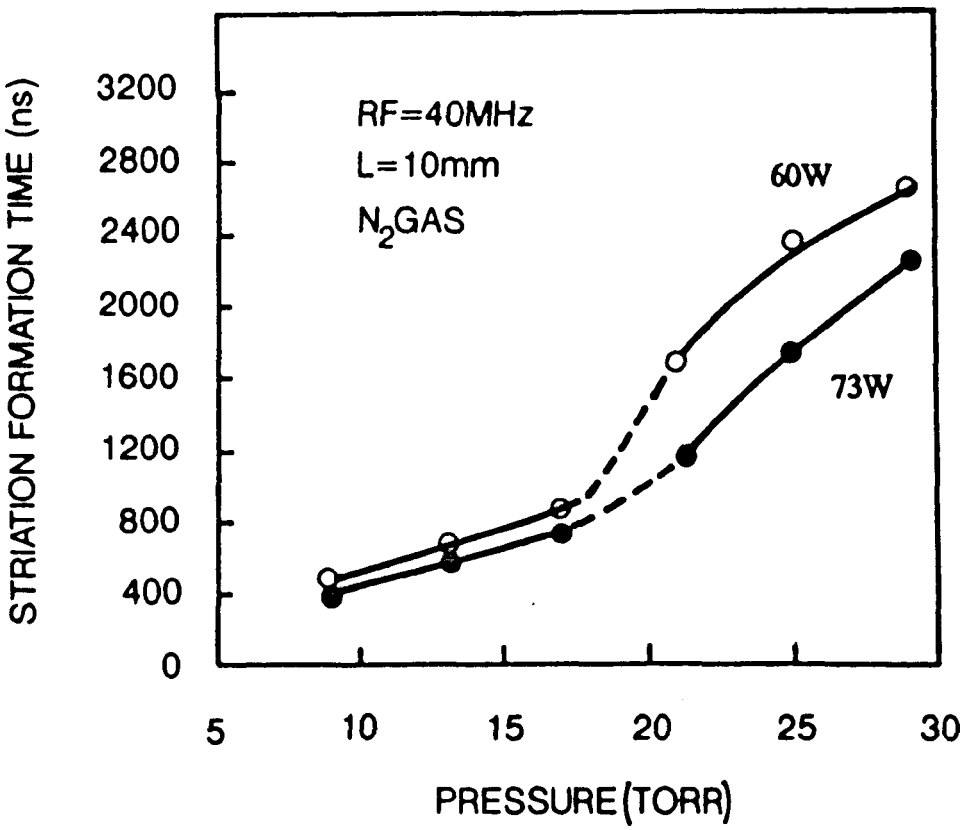

FIGURE 5.8 Striation Formation Time as a Function of Pressure for Different Input Powers.

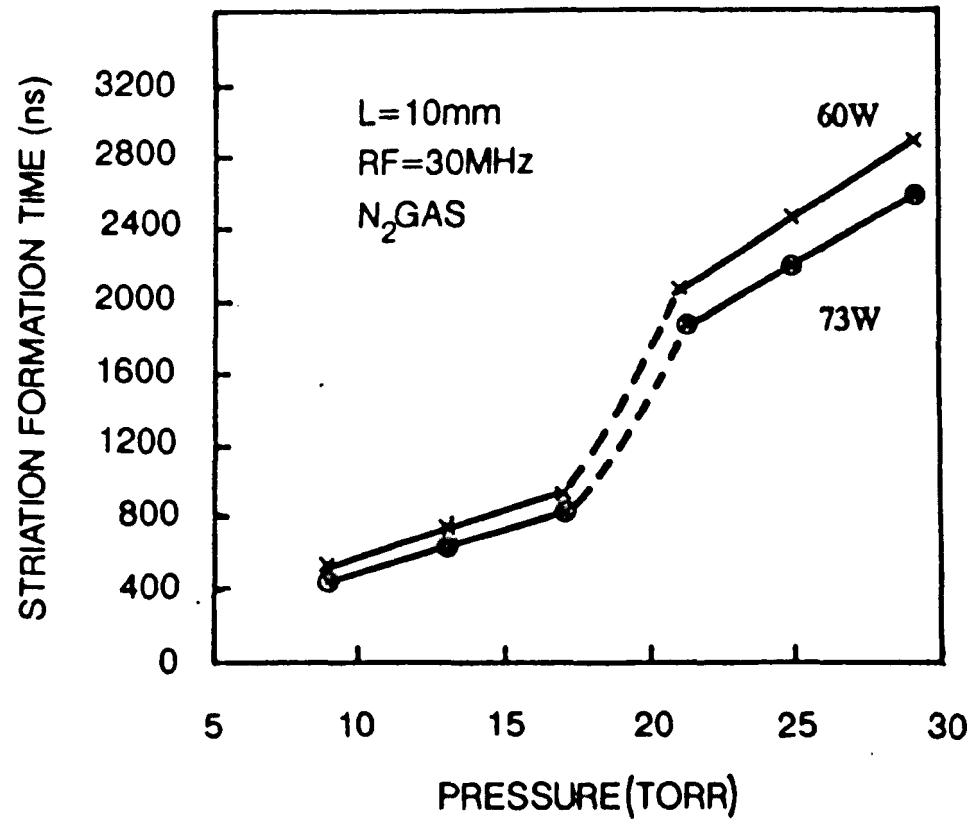

FIGURE 5.9 Striation Formation Time as a Function of Pressure for Different Input Powers.

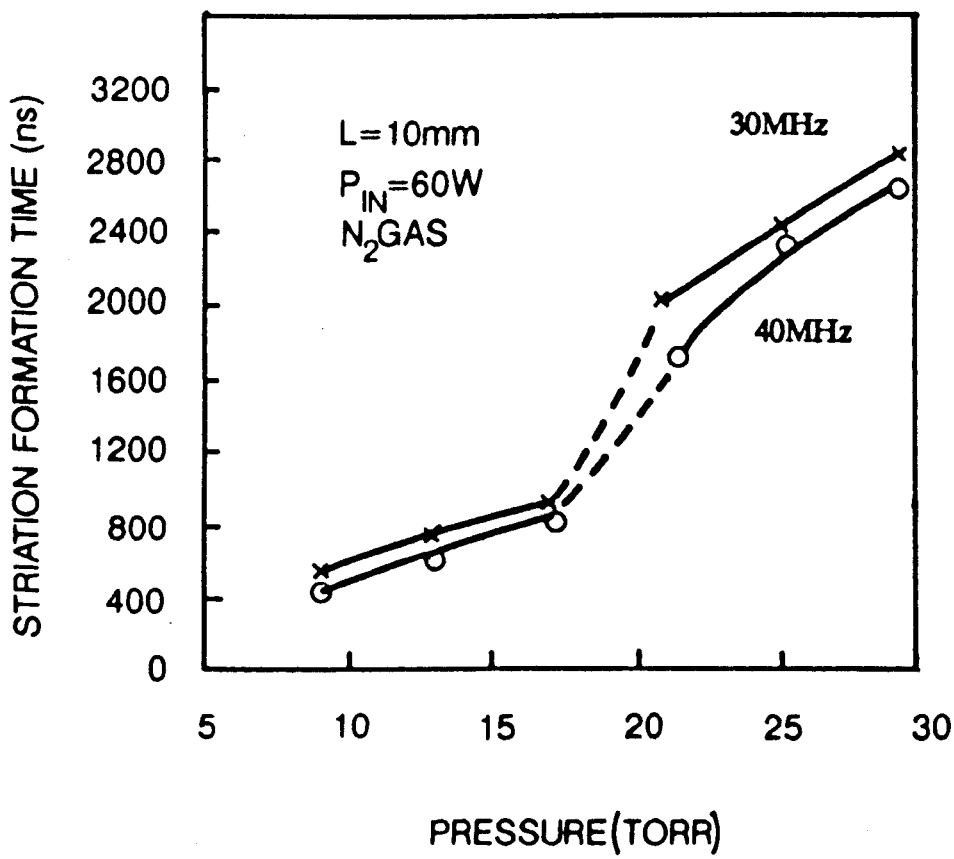

FIGURE 5.10 Striation Formation Time as a Function of Pressure for Different RF Frequencies.

will develop across the positive sheath zone where the electrons are cleared over one oscillation amplitude from the vicinity of the instantaneous cathode. Secondary electrons accelerated across this positive sheath produce the intensity wings or peaks of light called striations.

To find the critical value of the charge density n_s consider two infinite plane parallel electrodes as shown in Figure 5.11. Charge on the unit area of the plates due to applied electric field is $\epsilon\epsilon_0 E$ and the charge in the corresponding volume is $e\ n_s L$

When these fields are equal the space charge distortion becomes important. Setting the charges equal and solving for n_s gives

$$n_s = \epsilon\epsilon_0 E/e\ L = \epsilon\epsilon_0 V_0/eL^2 \qquad (5.1)$$

As an example, with $L = 2 \times 10^{-2}$m, $V_0 = 350$ volts and $\epsilon_0 = 8.8 \times 10^{-12}$ Farad/m,

$n_s = 4.84 \times 10^{13}/m^3 = 4.84 \times 10^7/cm^3$.

In order to develop an expression for the striation formation time or the time when the charge density reaches the critical value given by equation (5.1) above we proceed as follows.

Before the appearance of the sheaths and the consequent re-distribution of electric field in the discharge, the discharge reduced electric field is constant and uniform and can be written as

$$E/N = V_0 \sin\omega t/LN \qquad (5.2)$$

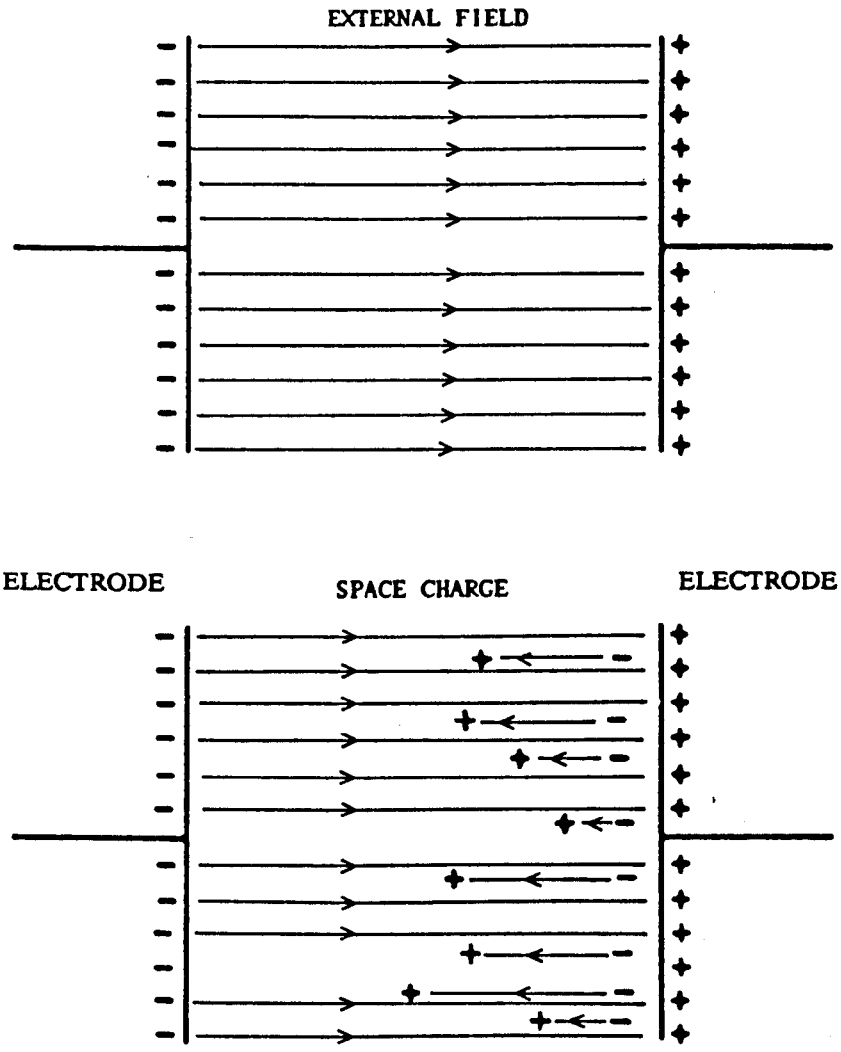

FIGURE 5.11 Schematic of the Effect of Space Charge on the Internal Electric Field.

Where V_0 is the interelectrode voltage.

For the electron energy we can write

$$\epsilon = B(E/N)^A, \qquad B = 7\times10^{4}, \quad A = 0.3 \tag{5.3}$$

Where B and A are constants.

The rate of ionization by electrons [13] can be written as

$$Z = pZ_1 = 9 \times 10^7 \, Ap\epsilon^{\frac{1}{2}} \, V_i \, e^{-eV_i/\epsilon} \tag{5.4}$$

Where Z_1 is the ionization rate at one torr and V_i is the ionization potential of N_2.

Hence by substituting the values of ϵ from (5.3) and E/N from (5.2) into (5.4), the rate of ionization can be written as

$$Z = 9 \times 10^7 ApV_i \left[B\left[\frac{V_0}{LN}\sin\omega t\right]^A\right]^{\frac{1}{2}} \exp - \left[\frac{eV_i}{B}\left[\frac{LN}{V_0 \sin\omega t}\right]^A\right] \tag{5.5}$$

Assuming volume recombination, then the rate of charge loss is σn where σ is volume recombination coefficient.

The continuity equation giving the rate of change of charge density can be written as

$$dn/dt = Zn - \sigma n^2 \tag{5.6}$$

With the boundary condition such that at t = 0 n = 500 electrons/cm^3 [14], the background charge density, Equation (5.6) is solved numerically to give the charge density as a function of time. In the calculations, the empirical experession 2.2.1 was used for σ and the constants A and B of Equation 5.3 were chosen to

give the best fit to the results of Dutton, [13].

5.5 DISCUSSION AND CONCLUSIONS

It has been found that fairly homogeneous or striationless pulses of duration up to about 5 μs can be generated provided the power input and RF frequency are low and the pressure high. The use of such pulses for RF lasers is limited by the power inputs. If the power input is too low, these striationless pulses are useless. More experiments on laser gas mixtures are needed.

Turning to the explanation of the times required for striation formation, the model outlined in Section 5.4 appears to give the right trends. In essence it is argued that the striations become important when space charge effects set in resulting in ambipolar diffusion and a large and rapid rise in the discharge charge density. The time, t_s, it takes for the critical charge density, n_s, to be achieved, depends on the discharge dimensions, neutral particle density and the interelectrode voltage V in the early portion of the discharge. From the voltage envelope trace shown in Figures 5.12 and 5.13 and drawn schematically in Figure 5.14, V is not constant until it reaches the value V_1 of the fully developed discharge. A comparison of the visible intensity traces and the V and i traces shows the appearance of the striated discharge to coincide with the collapse of the voltage as shown. This means that a quick and ready way of measuring t_s is to record the voltage envelope. To calculate t_s, E/N is needed. This was taken as $(V_2 + V_1)/2LN$ where N is the neutral gas density at room temperature. For the longer formation times where gas heating becomes important this value of N will be too high leading to low values of E/N and long calculated values of t_s. This effect is seen in Table 5.1 where for the larger values of t_s the calculated values are much longer than the observed values. The fact that for constant V, L and N, t_s is shorter for higher frequencies would appear to be due to the fact that the electron energy follows the applied field and that at low frequencies the times between field

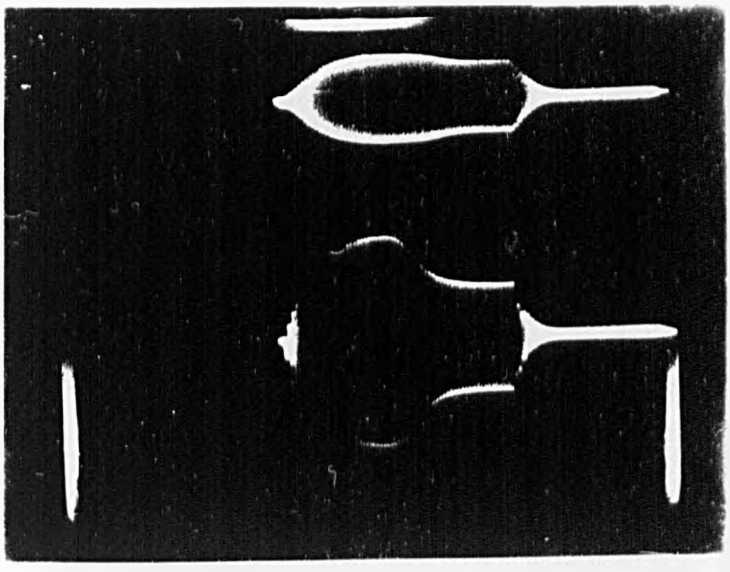

(a)

FIGURE 5.12a Pulse Duration = 2.05 μs, RF = 30 MHz, L = 10 mm, P = 21 torr and P_{IN} = 60 W.

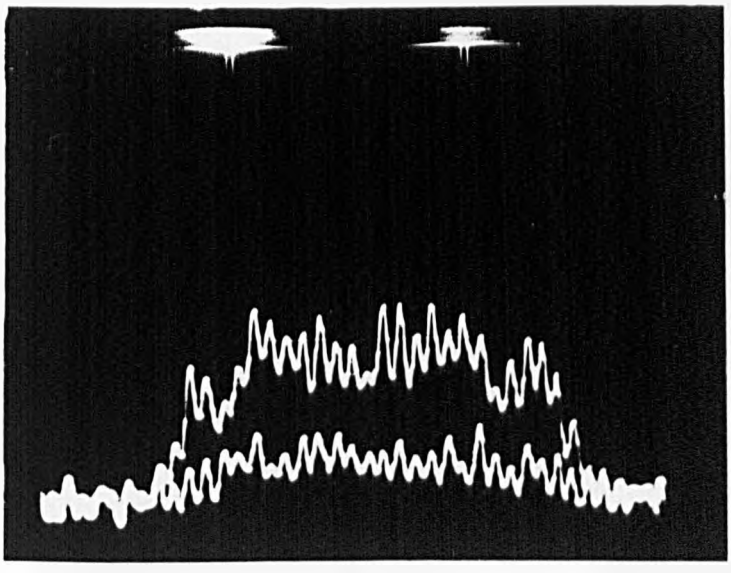

(b)

FIGURE 5.12 Oscilloscope photographs of the discharge (a) pulsed RF voltage and current (b) corresponding visible light emission profile, top discharge with striations, bottom, discharge without striations.

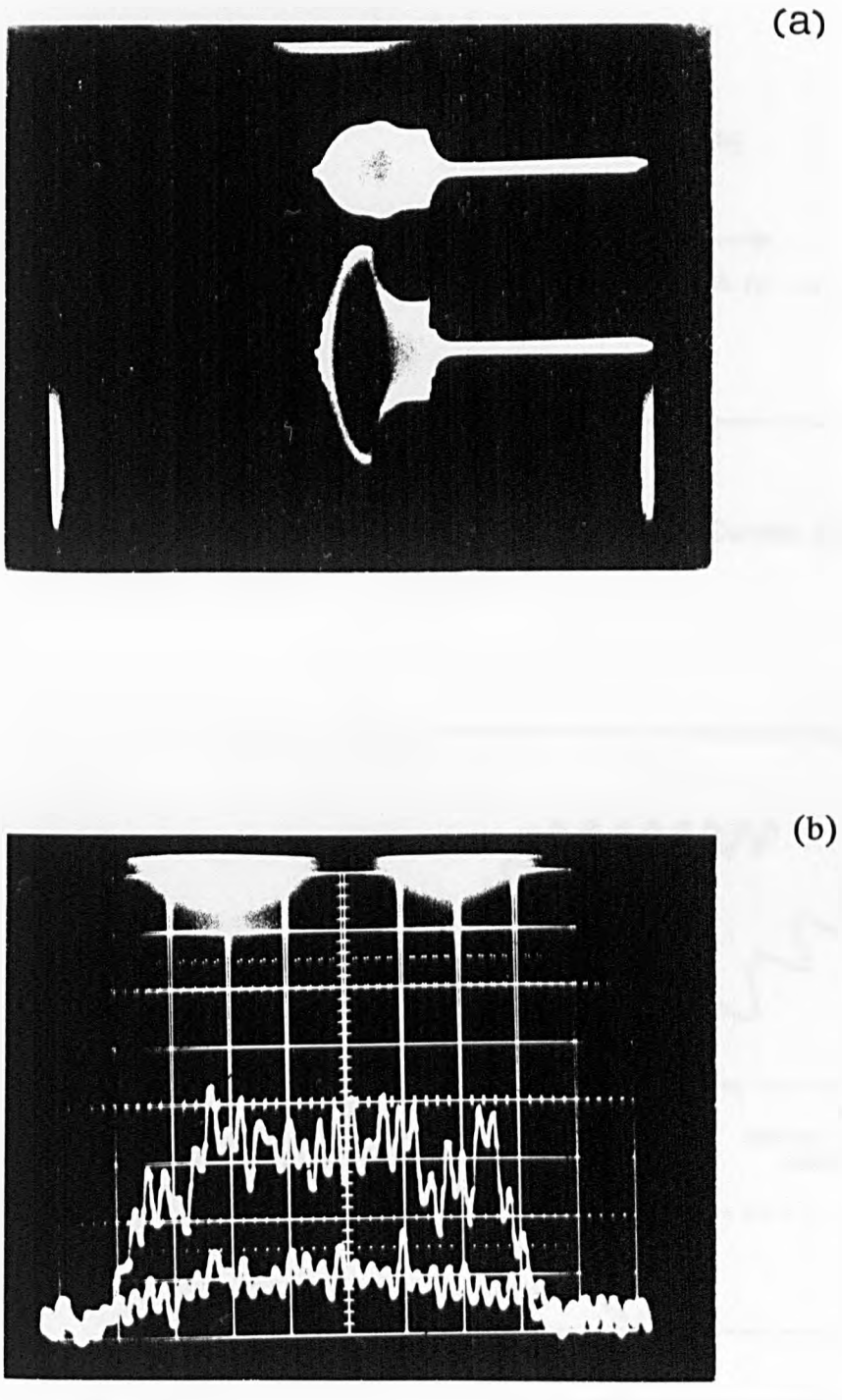

FIGURE 5.13 Oscilloscope photographs of the discharge (a) pulsed RF voltage and current (b) corresponding visible light emission profile, top discharge with striations, bottom, discharge without striations.

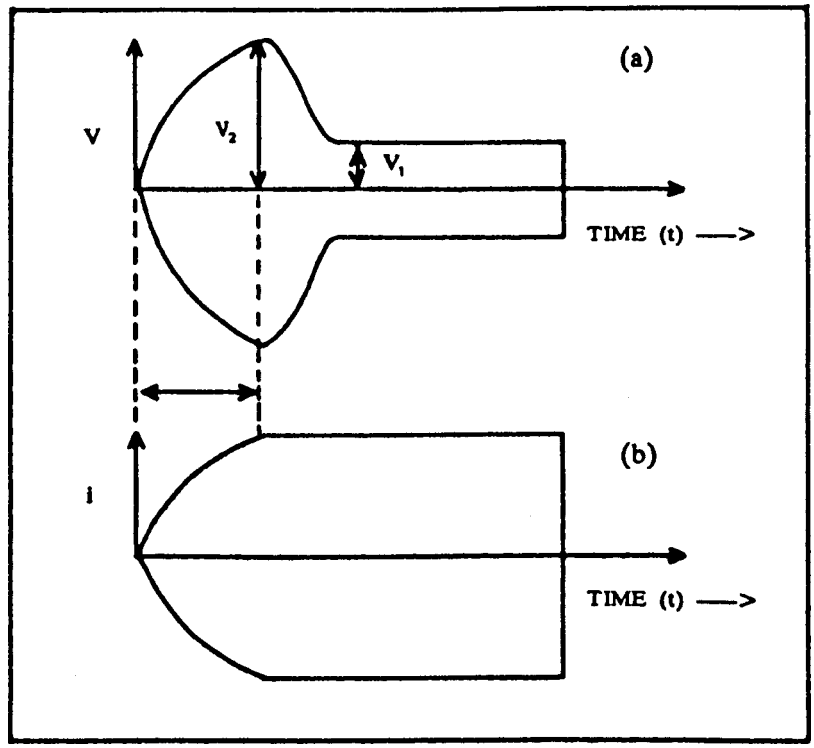

FIGURE 5.14 Oscillogram Trace Showing (a) Voltage and (b) Current for the RF Pulse.

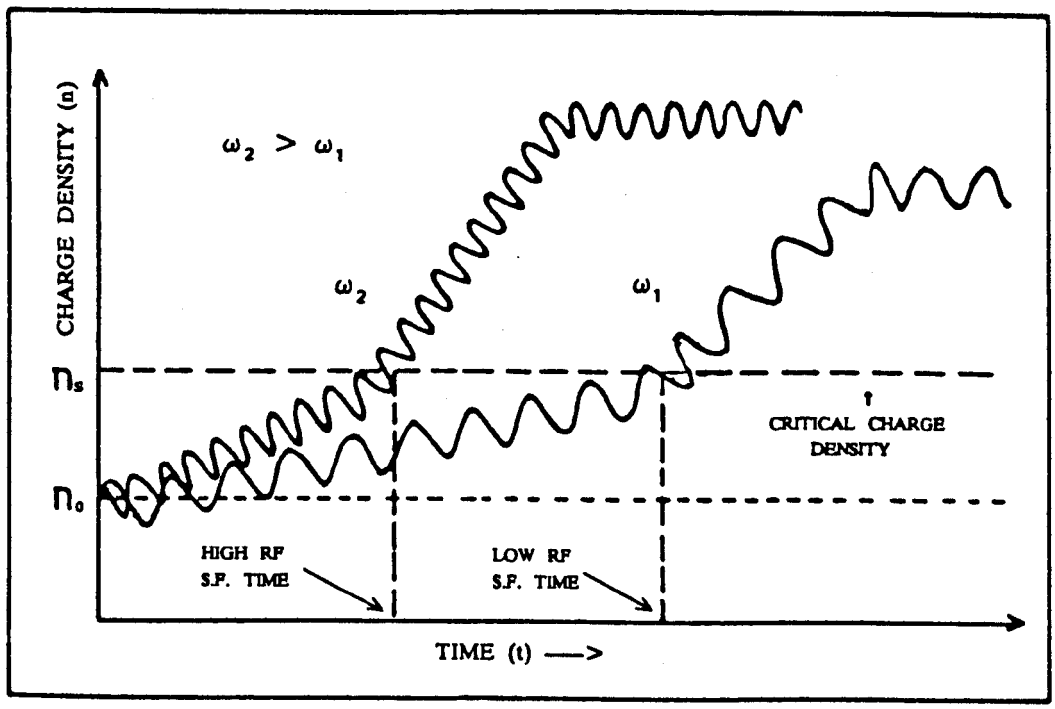

FIGURE 5.15 Theoretical Predictions of Plasma Charge Density as a Function of Pressure for Different RF Frequencies.

OBSERVED							CALCULATED			
f	ω	P	L	V_0	P_{IN}	t_s	V_0/LP	ϵ_0	n_s	t_s
MHz	rad s^{-1}	Torr	Meter	Volts (Peak)	W	sec	V/M-Torr	eV	M^3	sec
40	2.51×10^8	21	5×10^{-3}	432	60	0.94×10^{-6}	41.1	2.0	9.55×10^{14}	3×10^{-6}
40	2.51×10^8	21	5×10^{-3}	452	73	0.73×10^{-6}	43.0	2.2	1×10^{15}	1.4×10^{-6}
30	1.88×10^8	21	5×10^{-3}	562	60	1.05×10^{-6}	53.5	2.6	1.24×10^{15}	0.45×10^{-6}
30	1.88×10^8	21	5×10^{-3}	604	73	0.84×10^{-6}	57.5	2.8	1.33×10^{15}	0.28×10^{-6}
30	1.88×10^8	21	5×10^{-2}	752	60	2.06×10^{-6}	35.3	1.8	4.16×10^{15}	7×10^{-6}
30	1.88×10^8	21	5×10^{-2}	942	73	1.92×10^{-6}	44.8	2.4	5.21×10^{15}	4×10^{-6}
40	2.51×10^8	13	5×10^{-2}	729	73	0.6×10^{-6}	56.1	2.7	4.03×10^{14}	0.5×10^{-6}
30	1.88×10^8	13	5×10^{-2}	661	60	0.73×10^{-6}	50.8	2.5	3.65×10^{14}	0.84×10^{-6}
40	2.51×10^8	29	5×10^{-2}	877	73	2.24×10^{-6}	30.2	1.7	4.85×10^{14}	8.7×10^{-6}
40	2.51×10^8	21	5×10^{-2}	823	73	1.13×10^{-6}	39.2	1.9	4.55×10^{14}	4.3×10^{-6}

TABLE 5.1 Comparison of Observed and Calculated Striation Formation Time.

peaks with ionisations are longer allowing greater charge loss and consequently a slower build up of charge. The build up of charge in the system is shown schematically in Figure 5.15 for RF frequencies ω_1, and ω_2 where $\omega_2 > \omega_1$. The limited range of powers 60 and 70 W and RF frequencies 30 and 40 MHz was due to the fact that outside this range the pulses were too weak or transitions occurred to the gamma discharge.

REFERENCES

[1] S.P. McCallum and L. Klalzov, Phil.Mag., Vol.15, 829 (1933).

[2] W.P. Allis, S.C. Brown and E. Everhart, Phys.Rev., Vol.84, 519 (1951).

[3] H.S. Butler and G.S. Kino, Phys.Fluids, Vol.16, 1346 (1963).

[4] A.J. Hatch and I. Ehenkroth, J.Appl.Phys., Vol.41, 1701 (1971).

[5] D. He and D.R. Hall, IEEE J.Quant.Elec., Vol.QE-205, 509 (1984).

[6] N.A. Yatsenko, Sov.Phys.Tech.Phys., Vol.26, 678 (1981).

[7] V.A. Godyak and A.S. Khanneh, IEEE Plasma Sci., PS 14, 112 (1986).

[8] D.R. Hall and C.A. Hill, Handbook of Molecular Lasers, Marcel Dekker, Inc. (1987).

[9] J.D. Swift and M.J.R. Schwar, "Electrical Probes for Plasma Diagnostics", Ilffee Book Ltd., Chapter 7 (1970).

[10] B. Chapman, "Glow Discharge Processes", John Wiley and Sons, 153 (1980).

[11] S.M. Livitiskii, Sov.Phys.Tech.Phys., Vol.2, 913 (1958).

[12] V.A. Godyak and A.A. Kuzovnikov, Sov.J.Plasma Phys., Vol.1, 276 (1975).

[13] J. Dutton, J.Phys.Chem., Ref.Data 4, 64 (1975).

CHAPTER 6

THE STRIATED ALPHA DISCHARGE IN He

6.1 INTRODUCTION

Although moving and stationary stratifications of the positive columns of gas discharge are frequently observed [1-5], the phenomenon has not been given a generally accepted theoretical explanation. Waves that appear to be causing the stratification belong to a special class of waves perhaps involving changes in the ionization rate due to standing or travelling variations in the electric field [8]. Almost all the reports of striations deal with DC discharges where moving striations are divided into two classes, the positive and negative depending on whether they proceed from anode to cathode or vice versa. In RF discharges [6, 7] the striations are usually stationary but can be made to move when a d.c. field is superimposed on the RF field [8].

Experiments on DC discharges have shown that striations are observed within definite intervals of variation of the discharge conditions. In many cases, pure inert gases exhibit upper and lower limits of the current, gas pressure and tube radius in which the striations exist [9-11]. The upper limiting currents were first investigated by Pupp [10], who showed that the maximum current at which striations are still observed is inversely proportional to the pressure. He also showed that at constant pressure the upper limit current decreases with increasing atomic weight of the gas.

Striations were excited artificially by Zaitsev [12]. Zaitsev showed that external oscillations superimposed on a homogenous discharge can produce and

maintain moving striations.

The work presented here concerns observations on stationary striations in RF helium discharges that were observed in the course of the investigation of CO_2 gas laser mixture discharges. The phenomena was first noted in CO_2 gas laser mixtures richer in helium than $3He:1CO_2:1N_2$ for RF frequencies below 15 MHz, and was deemed to be sufficiently interesting for some time to be given to a closer look in pure helium where the effect was strongest.

The experimental arrangements here are the same as in Chapter 4, except that the electrode diameter here is 2.8 cm. Section 6.2 is based on the experimental results and the results are discussed in Section 6.3.

6.2 EXPERIMENTAL RESULTS

6.2.1 Striations as a Function of Pressure, Input Power, RF Frequency and Electrode Separation.

Figure 6.1 shows photodensitometer traces of the stationary striations as a function of pressure, for constant input power, RF frequency and electrode separation. It can be seen from these traces that the number of striations increases with pressure. The transition with increasing pressure, from n to n+1 striations (where n is the number of striations) occurred abruptly over a pressure change of about one torr with the central striation first dilating and compressing the striations to either side and then splitting itself into two new striations. Figures 6.2 and 6.3 show the photographs of striations and it can be seen from these photographs that each major striation consists of two sub striations separated from each other by a very thin dark layer, while two major striations are separated by a thick dark layer. We call these thicker dark layers the wavelength of the striations. Figure 6.4 shows striations as a function pressure for different

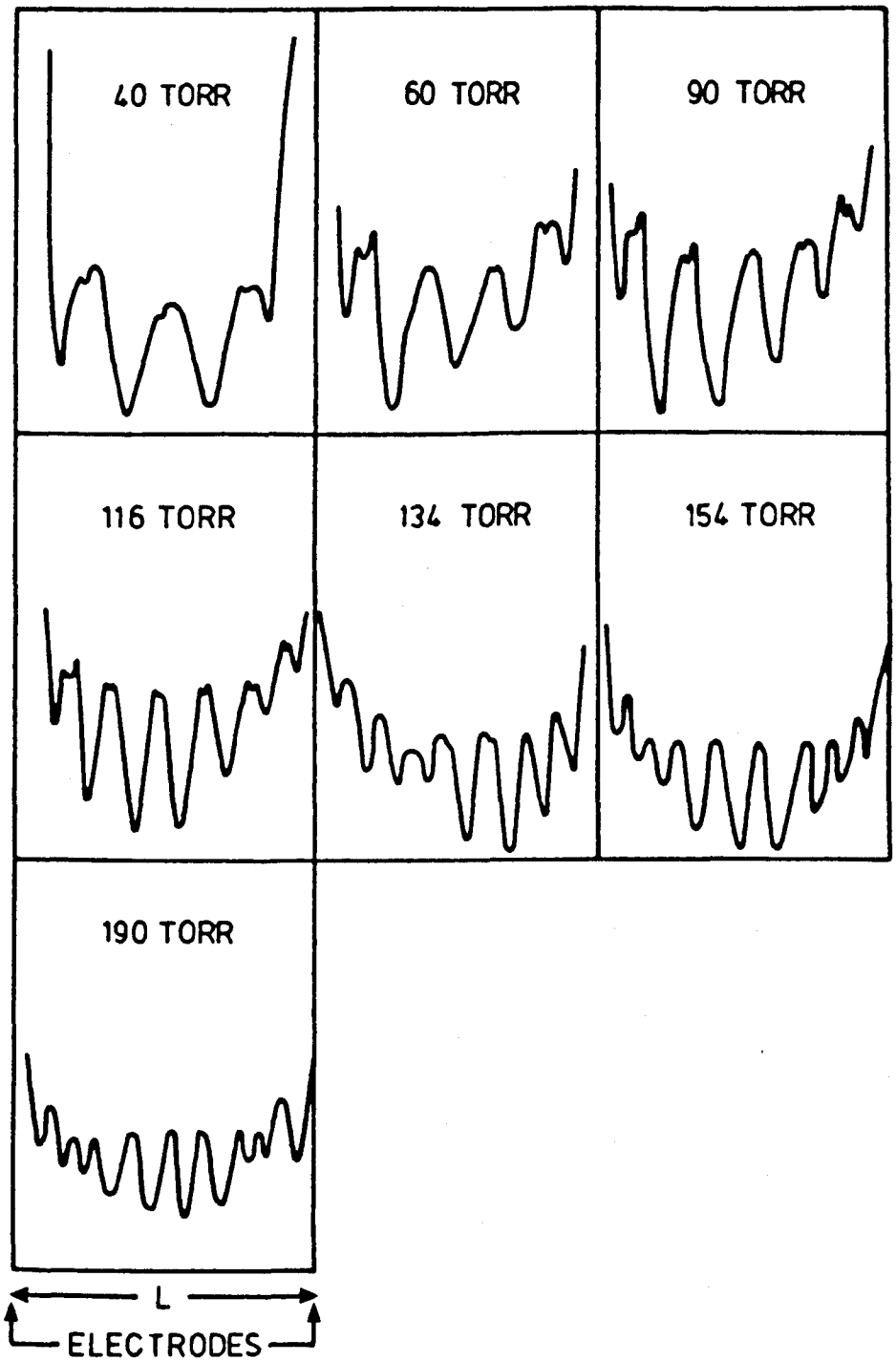

FIGURE 6.1 Densitometer Traces of Striations for Different Pressures RF = 15 MHz, L = 20 mm.

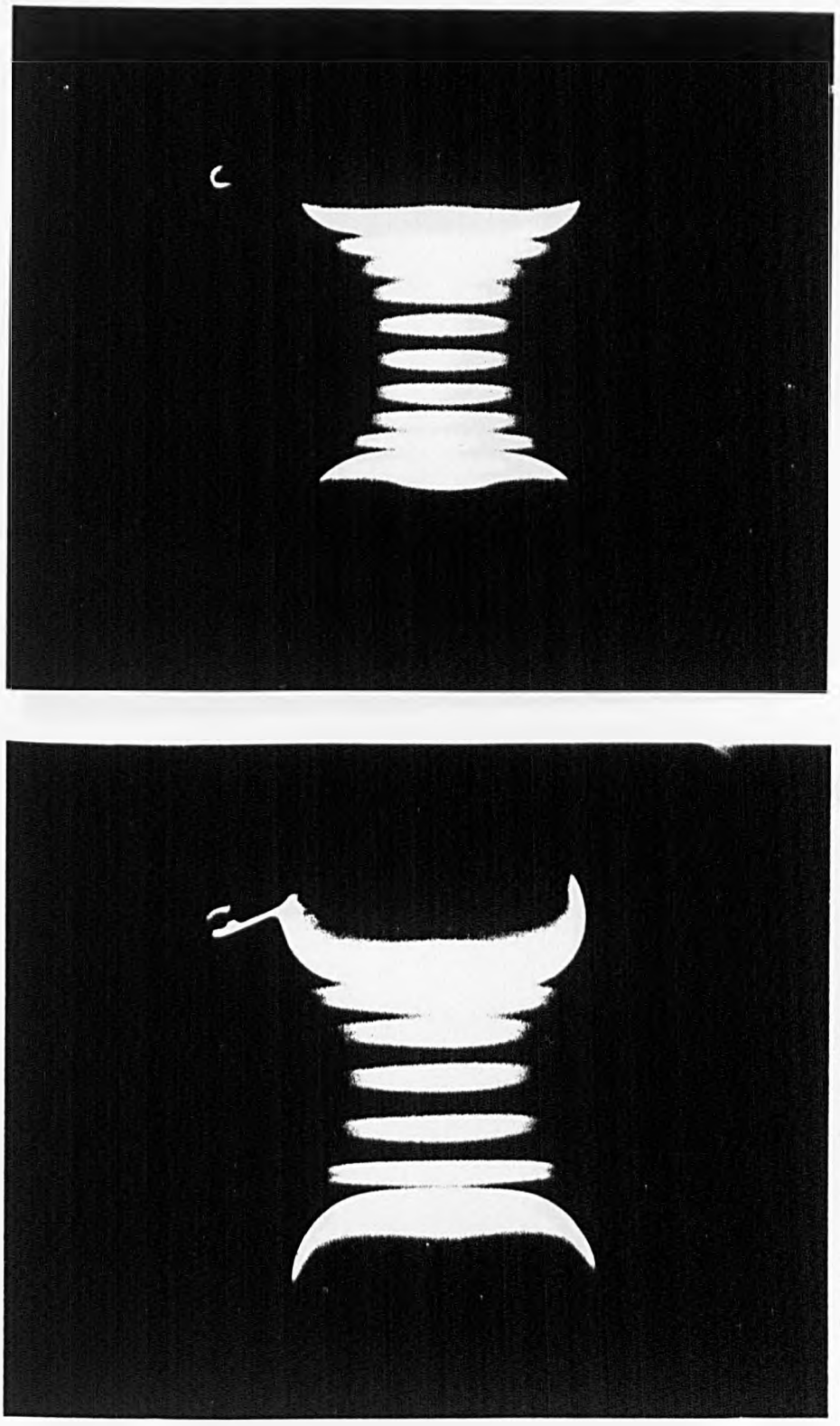

FIGURE 6.2 Striated He discharge L = 2.0 cm, RF = 15.5 MHz (a) P = 150 torr, (b) P = 90 torr.

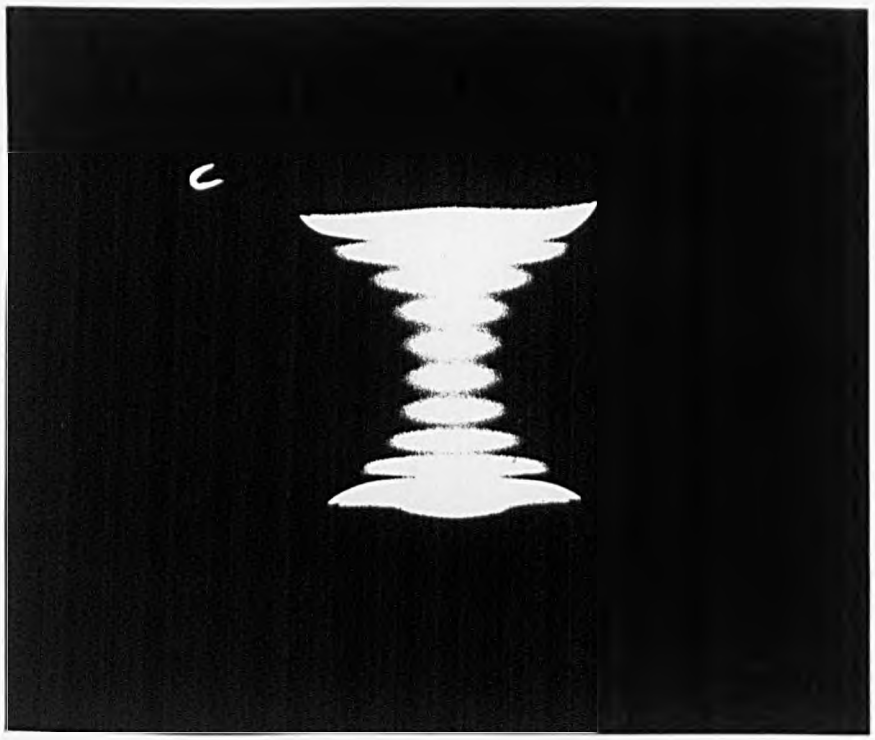

(a)

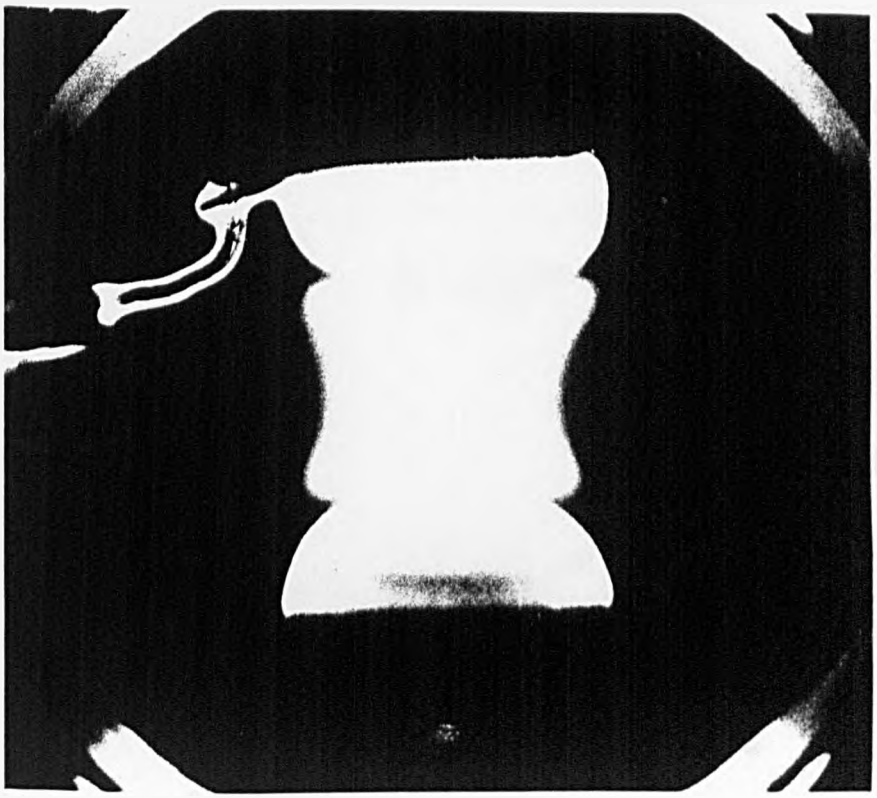

(b)

FIGURE 6.3 Striated He discharge L = 20 cm (a) RF = 25 MHz, P = 120 torr, (b) RF = 60 MHz, P = 300 torr.

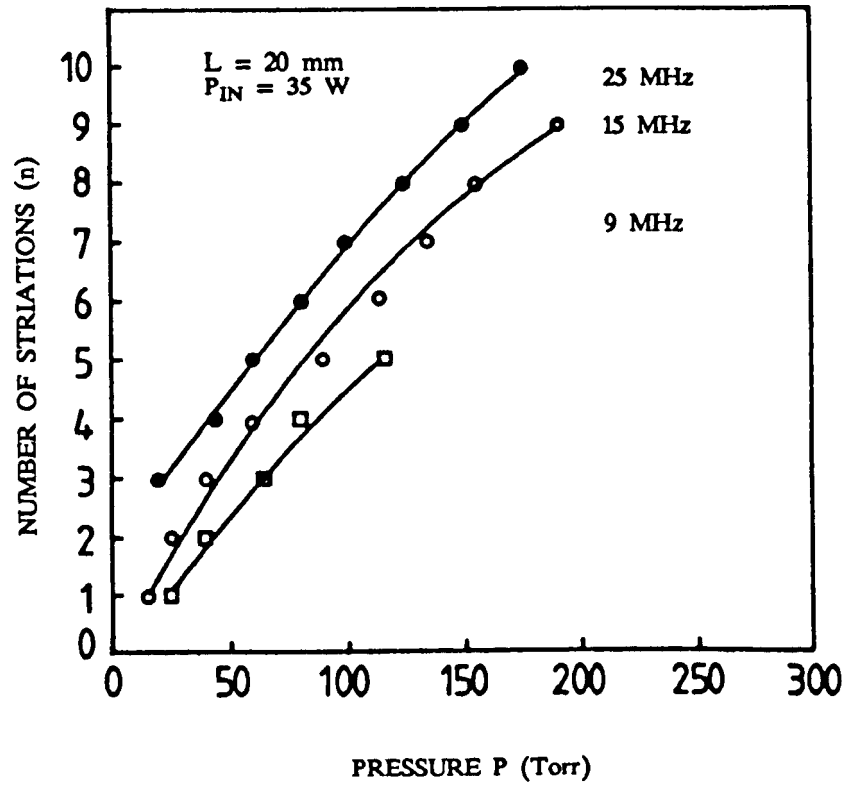

FIGURE 6.4 Number of Striations as a Function of Pressure for Different RF Frequencies.

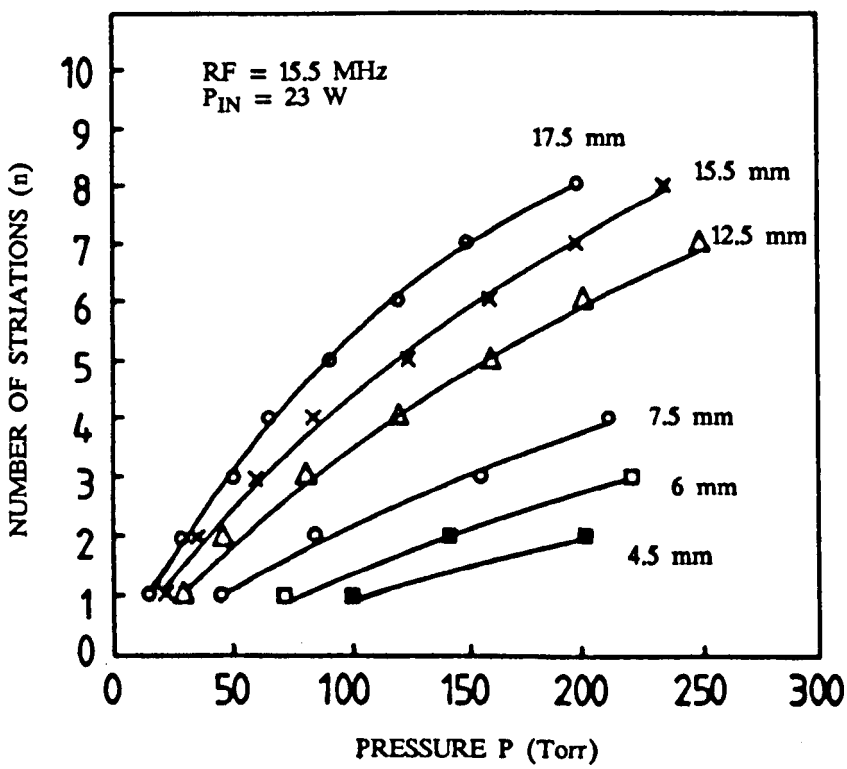

FIGURE 6.5 Number of Striations as a Function of Pressure for Different Electrode Separations.

RF frequencies at constant electrode separation and input power. This figure shows that at constant pressure, increasing RF frequency increase the number of striations e.g. for a pressure of 116 torr, n = 5, 6, 8 for 9 MHz, 15 MHz and 25 MHz respectively. For RF frequencies higher than about 60 MHz, the striations were so numerous and close together that they could not be resolved, Figure 6.3. A similar effect was observed for pressures above 200 torr. Figure 6.5 gives the number of striations as a function of pressure and electrode separation at constant input power and RF frequency. The number of striaitons, at constant pressure, is decreased by decreasing the electrode separation. Figure 6.6 shows the variation in wavelength of the striation with pressure for different RF frequencies at constant electrode separation and input power. The wavelength is decreased with increasing pressure and RF frequency. A similar trend for the wavelength was observed against the electrode separation, Figure 6.7.

For all the experiments here it was found that at constant pressure, RF frequency and electrode separation the number of striations did not vary as the power to the discharge was changed. Varying the power only changed the intensity of the striation profile.

Finally, when 15% nitrogen was introduced in the striated helium discharge, the striations disappeared and the discharge central zone become uniform.

6.2.2 Current and Voltage Characteristics

Figures 6.8 to 6.11 give the voltage and current characteristics of the discharge versus pressure for some of the conditions under which the striations were observed. These electrical measurements will be useful if a quantitative theory of these striations becomes available.

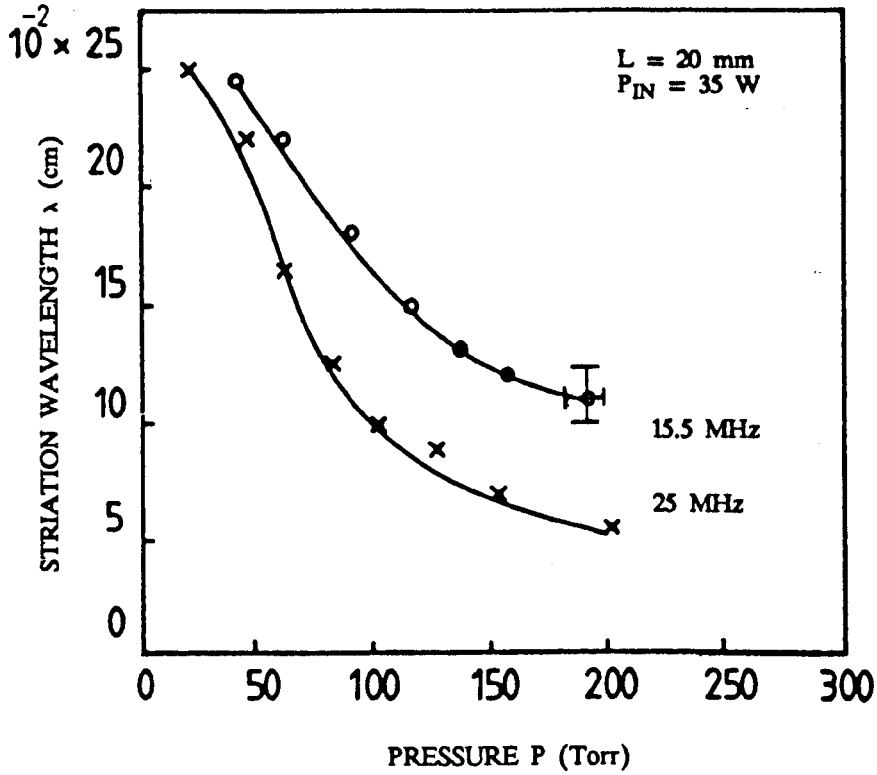

FIGURE 6.6 Striation Wavelength as a Function of Pressure for Different RF Frequencies.

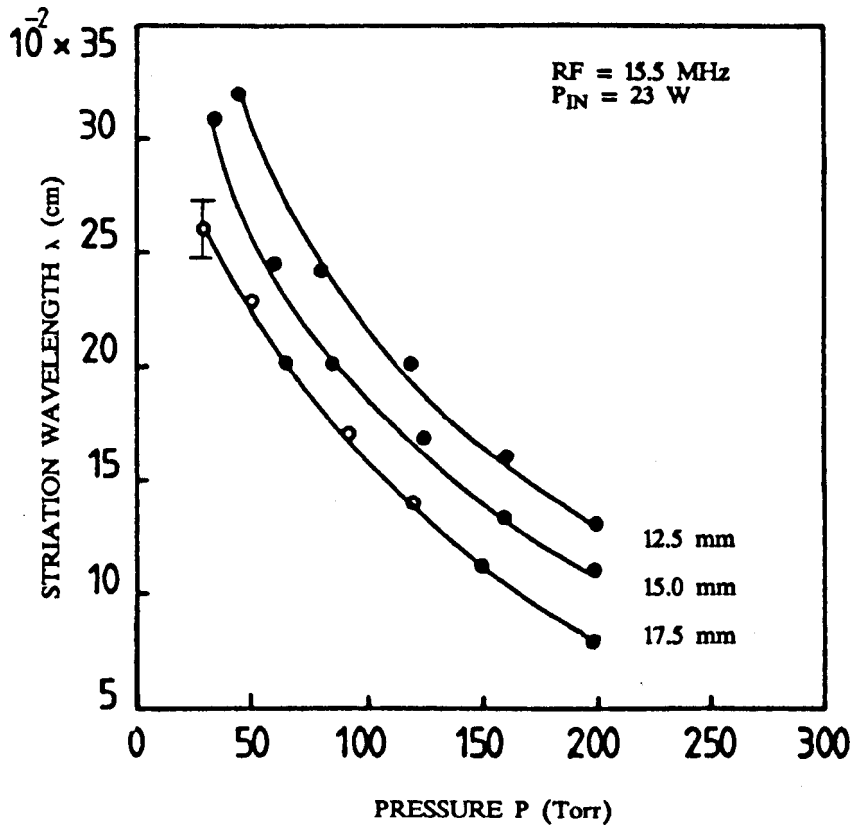

FIGURE 6.7 Striation Wavelength as a Function of Pressure for Different Electrode Separations.

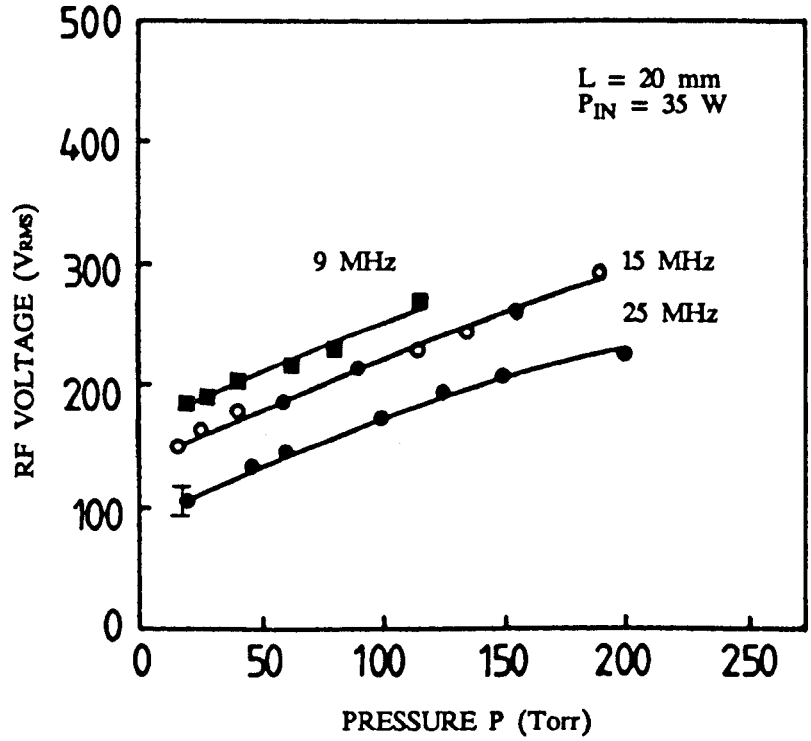

FIGURE 6.8 RF Voltage as a Function of Pressure for Different RF Frequencies.

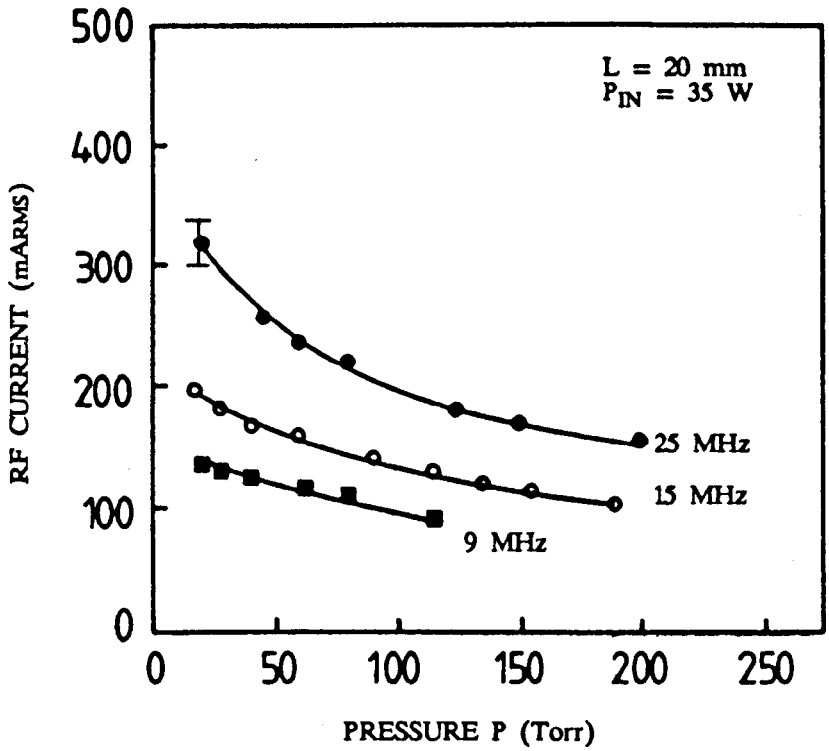

FIGURE 6.9 RF Current as a Function of Pressure for Different RF Frequencies.

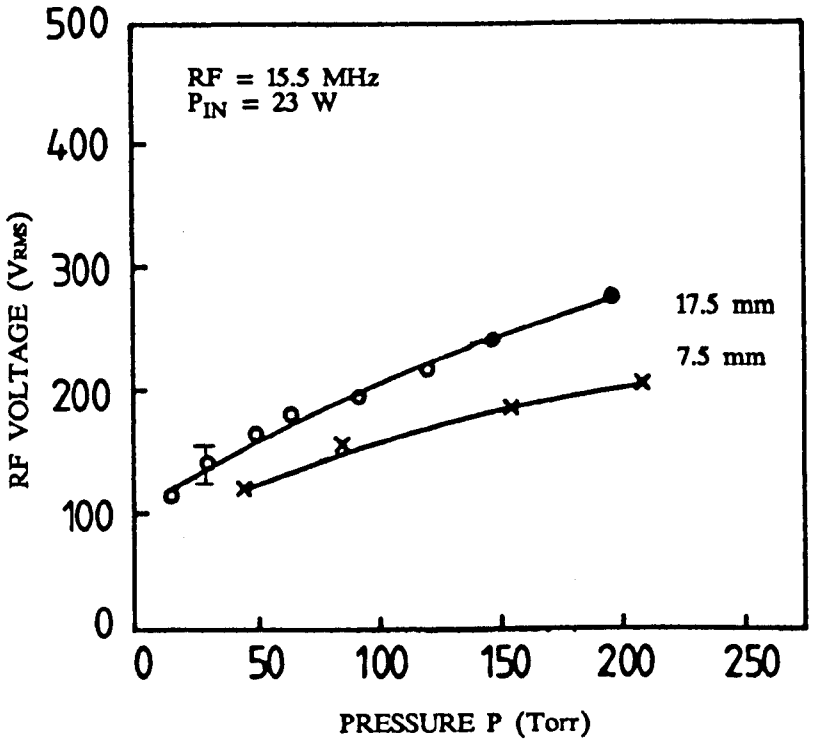

FIGURE 6.10 RF Voltage as a Function of Pressure for Different Electrode Separations.

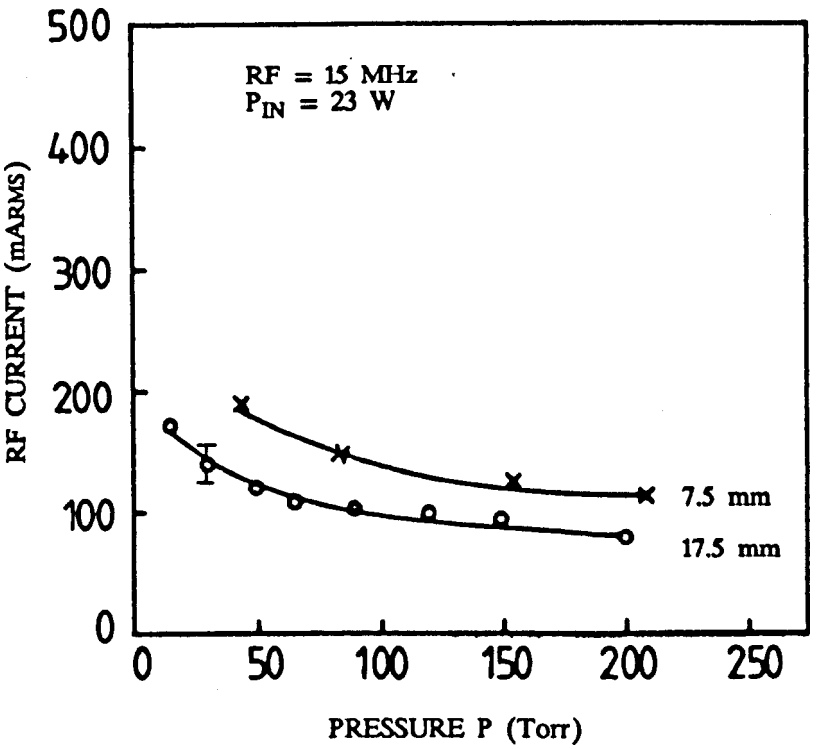

FIGURE 6.11 RF Current as a Function of Pressure for Different Electrode Separations.

6.2.3 Time Dependent Visible Emission

The time dependent visible emission from the striation zone of the discharge was found to be modulated at twice the frequency of the RF field. This phenomenon is explained and discussed in great detail in Chapter 4, Section 4.3.4.

6.3 DISCUSSION AND CONCLUSIONS

The apparently simple variation of the striation numbers with pressure, frequency and electrode separation suggests the phenomena has an easy explanation. This is not the case as far as the candidate can see. For example the increasing number of striations with pressure might be explained in terms of plasma parameters like the electron density or the electron temperature. But the reason for the RF frequency dependence of the striations is not clear.

Extra experimental results which would be useful to have are (i) the spatial distribution of the internal electric field and charge number density and (ii) the spatially and time resolved light emission. The material of this chapter cannot usefully be commented upon until these extra measurements are made.

REFERENCES

[1] L. Pekarek, Sov.Phys.USPEKHI, Vol.2, 188 (1968).

[2] D.A. Lee, A. Garscadden and P. Bletzinger proc. 7th Int.Con.Ion.Phen. in gas Belgrade, 22-27, 8 (1965).

[3] L. Pekarek and Kerjci, Proc. 5th Int.Con.Ion.Phen. in gas Munich, Vol.1, 573 (1961).

[4] M. Druyesteyn and F. Penning, Rev.Mod.Phys., Vol.12, 2 (1940).

[5] G. Francis, Handbook Phys. (1965).

[6] M. Klerk, Proc. 4th Int.Con.Ion.Phen. in gas, Vol.1, 293 (1959).

[7] N. Sato and Y. Hatta, Phys.Rev.Lett, Vol.16, 88 (1966).

[8] J. Nakata, E. Takenaka and J. Masutani, J.Phys.Soc. Japan, Vol.20, 9 (1965).

[9] W. Pupp, Phys. ZS., 33, 844 (1932).

[10] A.V. Nedospasov, Paper No.217, Con.On.Plasma Phys., Salsberg (1961).

[11] K. Rademacher and K. Wojaczek, Ann.Phys., Vol.2, No.7, 57 (1958).

[12] A.A. Zaitsev, Dokl, Akad, Nauk SSSR, Vol.79, 779 (1951).

CHAPTER 7

EXPERIMENTAL STUDY OF RF DISCHARGES IN THE CO_2 LASER GAS MIXTURE

7.1 INTRODUCTION

In spite of the rapid development of RF lasers, very little has been published on the experimentally observable properties of the discharge itself such as voltage and current characteristics and the spectroscopy of the visible and IR emissions [1]. Two of the areas are of particular interest, namely the mapping out of the parameter space which allow stable alpha discharges, and secondly the development of an understanding of the inhomogeneties or striations [2, 3] so important in those transverse excited discharges considered here where the interelectrode separation is small. In this chapter, experimental results are presented on the characteristics of the alpha discharges used in CO_2 lasers and the arc like gamma type discharge which results when the power loading of the alpha discharge exceeds a critical value. The experiments are for the laser mixture $3He:1CO_2:1N_2$ with and without 5% xenon. Section 7.2.1 gives the current, voltage and power characteristics of alpha and gamma type capacitative RF discharges, followed by a discussion of the stability region results in Section 7.2.2. In Section 7.2.3 experimental results on the electron and neutral gas temperatures are presented, while the effects due to xenon addition are discussed in Section 7.2.4. Section 7.2.5 is devoted to the spectroscopy of time averaged visible emissions, and finally the experimental results are further discussed with some conclusions in Section 7.3. For all the experiments reported in the present chapter, the same apparatus as described in Chapter 4 is used, except that the diameter of the electrodes for the present experiments was 2.8 cm.

7.2 EXPERIMENTAL RESULTS AND DISCUSSION

7.2.1 Current, Voltage and Power Characteristics

The current, voltage and power characteristics of alpha and gamma type RF capacitative discharge in the CO_2 gas laser mixture ($3He:1CO_2:1N_2$) have the same general features as those of N_2 described in Chapter 4, as illustrated in Figures 7.1 and 7.2. As the voltage is increased from $V\alpha_{MIN}$ the current increases fairly linearly to the $V\alpha_{MAX}$ point, where an abrupt alpha to gamma change occurs and the voltage falls to the $V\gamma_{TR}$ point. The dotted line shows the forward transition path. Further increase in input power from the $V\gamma_{TR}$ point results in a further, but much more gradual decrease in the RF voltage, as illustrated by the arrow pointing in the *forward path* of the input power. For discharges in the CO_2 gas laser mixture ($3He:1CO_2:1N_2$) it was found that the backward transition of gamma to alpha is possible. Considering Figures 7.1 and 7.2, we see that as the input power is reduced in the gamma regime *(backward path)* the RF voltage increases slowly to the $V\gamma_{MAX}$ point where a reverse transition i.e. (gamma to alpha) takes place. Unlike the forward transition (alpha to gamma), the reverse transition (gamma to alpha) was never an abrupt change and alpha and gamma discharges co-exist spatially in this region. For the path-ways $\gamma_{TR} \rightarrow \gamma_{MAX}$ and $\gamma_{MAX} \rightarrow \gamma_{TR}$ a pure gamma discharge is obtained. As the power to the gamma discharge is decreased below the γ_{TR} point, a mixture of gamma and alpha discharges occurs, with the portion of the discharge in the gamma regime decreasing until, at γ_{MIN}, the whole discharge is in the alpha regime. It is also observed that after the reverse transitions (gamma to alpha) Figure 7.2(b), the RF voltage was larger for the same input power at the α_{MIN} point. Thus, compared to the results with N_2, Chapter 4 there is considerable hysteresis in the power, current and voltage characteristics. Unlike the alpha discharge, it was found that there was no limit to the power loading of the gamma regime, up to the maximum available power from

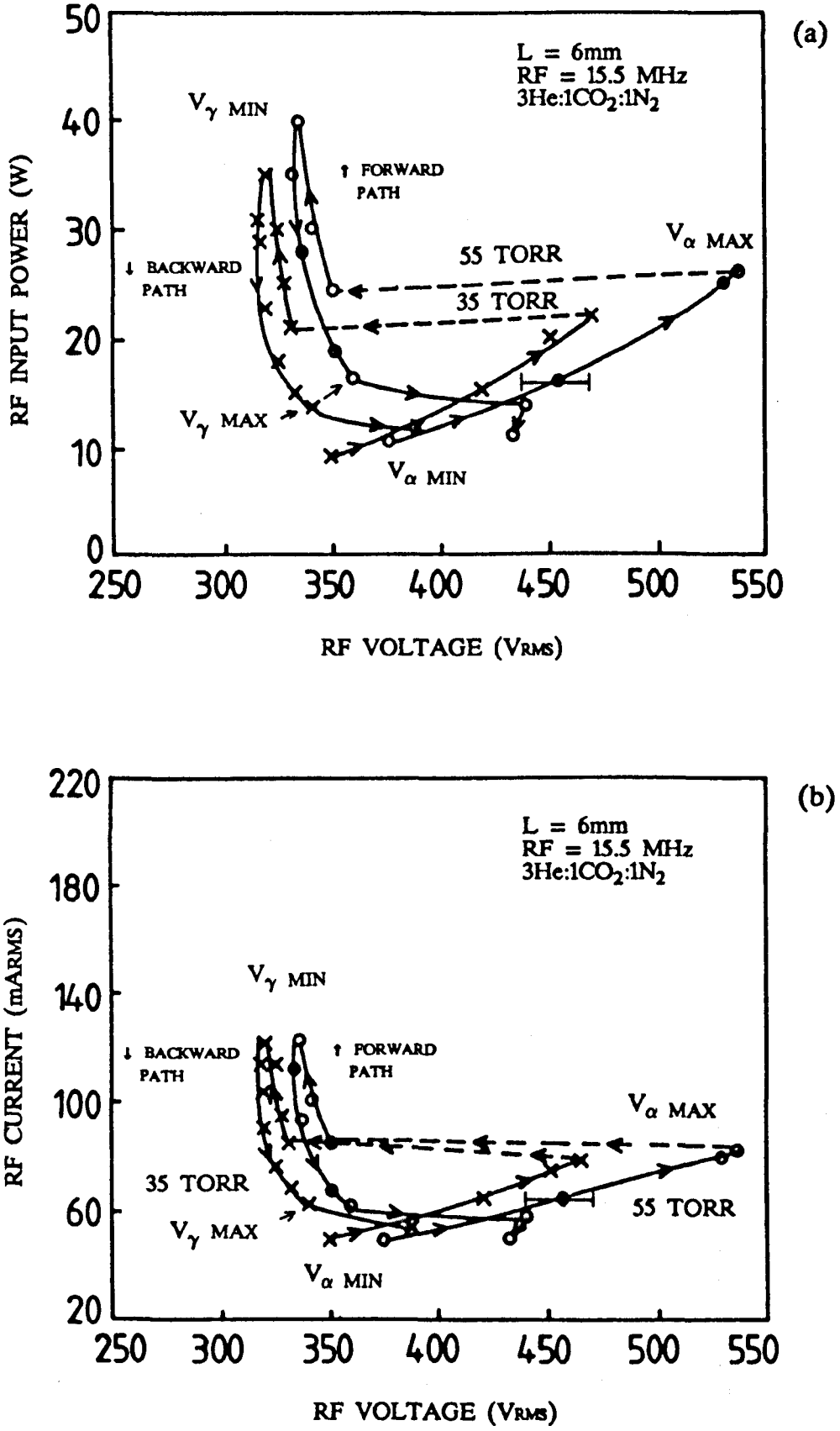

FIGURE 7.1 α and γ Total Discharge Power - Voltage and Current - Voltage Characteristics

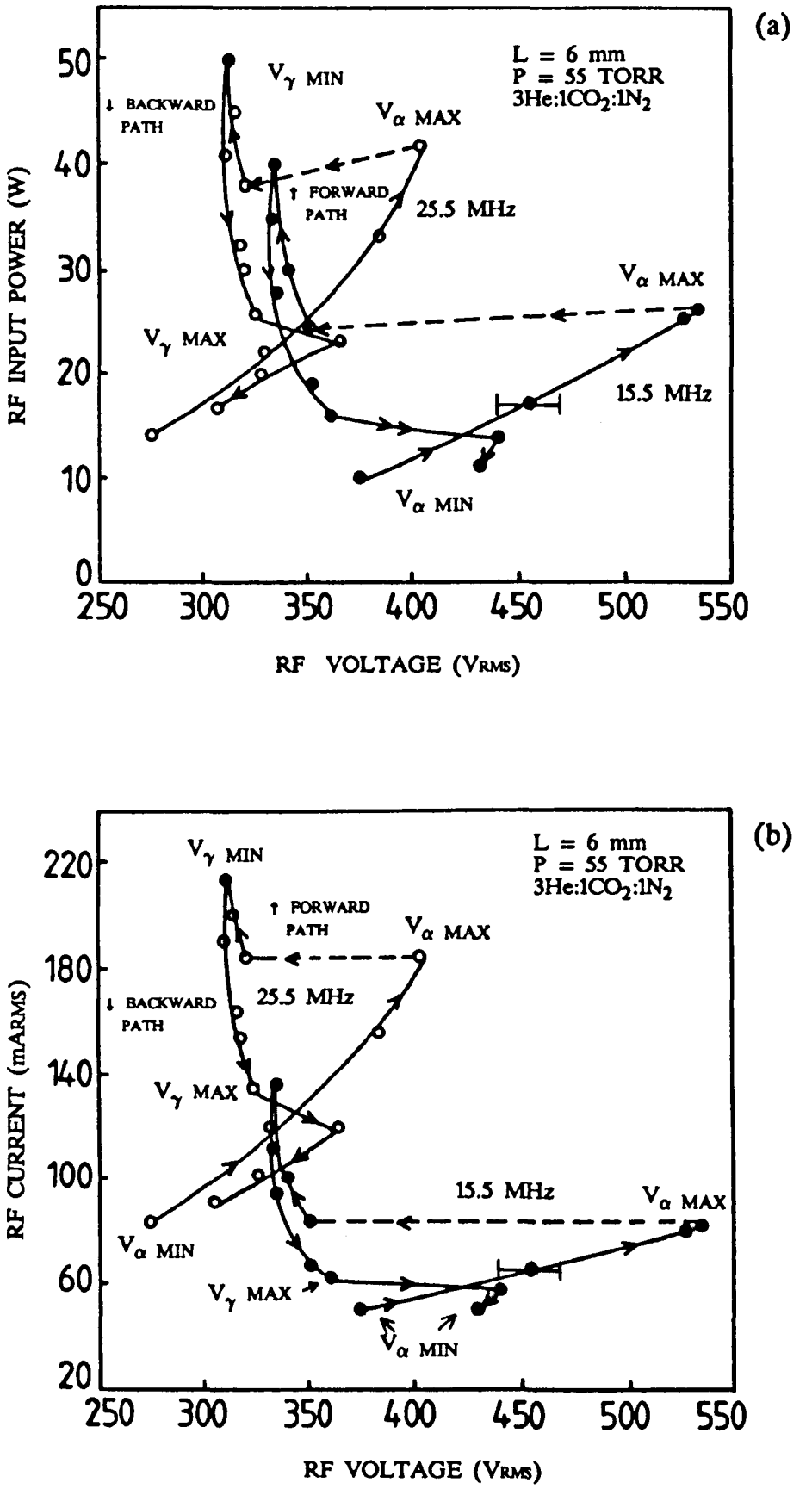

FIGURE 7.2 α and γ Total Discharge Power - Voltage and Current - Voltage Characteristics

the power generator (100 W) corresponding to 300 Watts/cm^3. As the power to the gamma discharge is increased, both the area of the discharge on the electrodes and the RF voltage decreased, Figure 7.1 and 7.2. In contrast to the situation for N_2, Section 4.3.1, where the area of the gamma discharge on the electrode increased with power. As with N_2, it was not possible to find exactly the variation of the discharge size with pressure, RF frequency and input power in the alpha and gamma regimes. In both pure N_2 and the laser mixture, the gamma discharge area decreases with increasing pressure. In Figure 7.1(b) for 35 and 55 torr, the area of the discharge was estimated as 1.76 cm^2 and 0.63 cm^2 respectively, which corresponds to current densities of 47.8 ma/cm^2 and 132 ma/cm^2 respectively. The minimum or maintenance voltages are also slightly different for the two different pressures as can be seen from Figure 7.1, which shows the maintenance voltage rising with pressure. The power density at which the transition (alpha to gamma) occurred is raised by nearly 60% for the ($3He:1CO_2:1N_2$) mix as compared with N_2 for otherwise similar discharge conditions, see Figure 4.5(b) and Figure 7.1(a). The current densities in the mixed gas is also slightly higher than N_2 for the same power density, frequency, pressure and electrode separations.

The current in the laser mixture is higher than in N_2 because the sheaths in the former are thinner. Figure 7.3 (iV). This results in a larger displacement current. The frequency dependency of current and voltage characteristics, is shown in Figure 7.2(a), 7.2(b). The RF voltage and the input power at the $V\alpha_{MIN}$ are quite different for the two different frequencies. At the lower RF frequency of 15.5 MHz for the same pressure conditions, the minimum maintenance power is 40% lower than it is for 25.5 MHz. Large differences are also observed at the $V\alpha_{MAX}$ points for the two frequencies. For 15.5 MHz frequency the transition occurs at an input power density of 3.49W/cm^2 while for a frequency of 25.5 MHz the power density at the transition point almost doubles to 6.8W/cm^2. Again, the RF voltages decrease and the currents increase with increasing

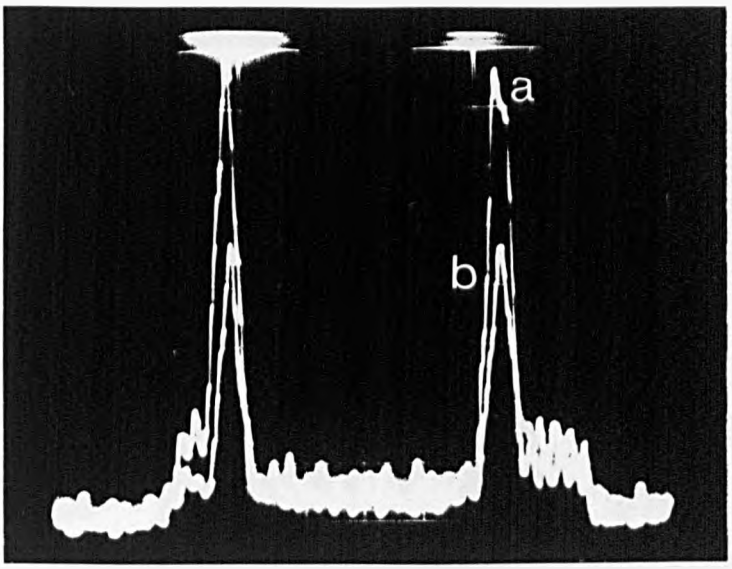

(i) P = 40 torr, RF = 40 MHz, L = 10 mm, 3He:1CO_2:1N_2 (a) P_{IN} = 25 W, (b) P_{IN} = 15 W

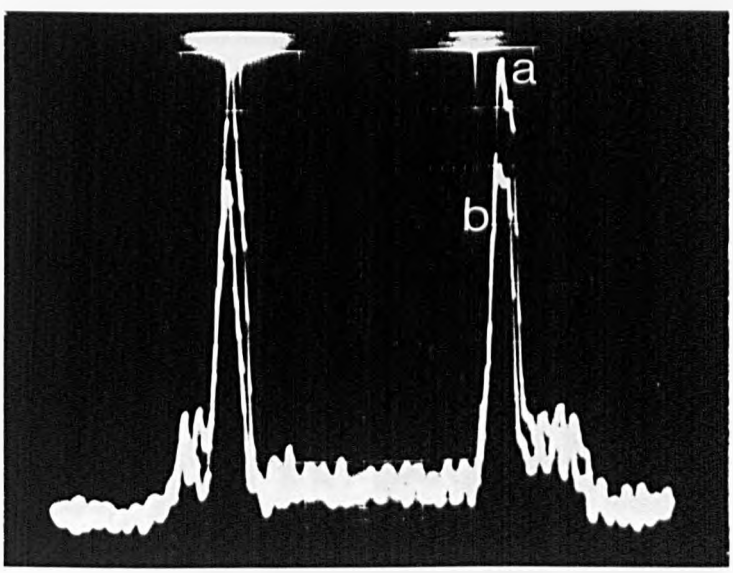

(ii) P_{IN} = 25 W, RF = 40 MHz, L = 10 mm, 3He:1CO_2:1N_2 (a) P = 40 torr, (b) P = 60 torr

FIGURE 7.3 Scope photographs showing the variation of sheath thickness with discharge parameters.

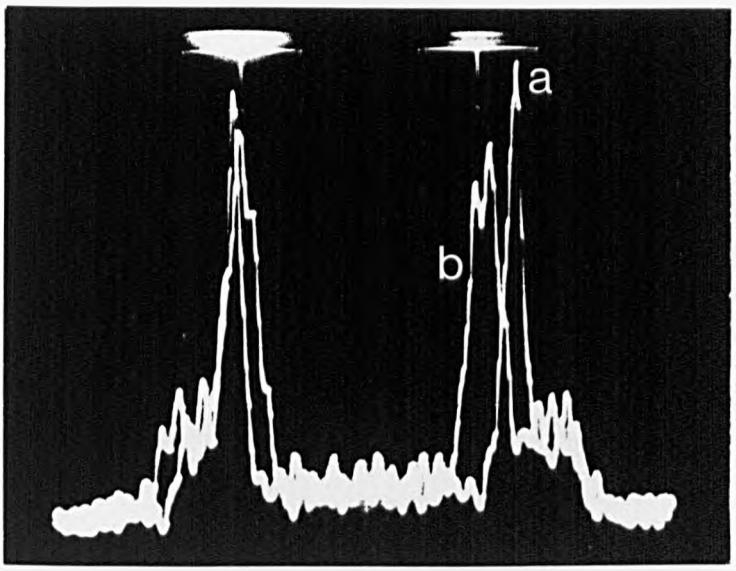

(iii) P = 40 torr, P_{IN} = 25 W, L = 10 mm, 3He:1CO_2:1N_2 (a) RF = 60 MHz, (b) RF = 20 MHz

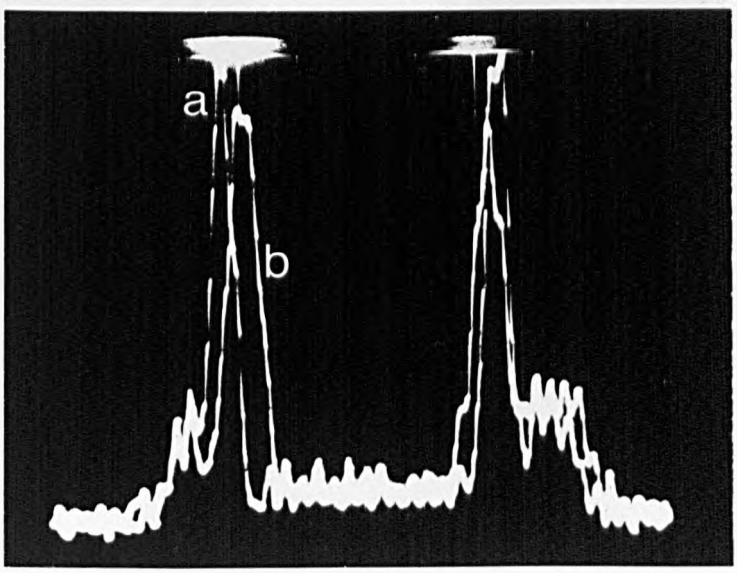

(iv) P = 40 torr, RF = 40 MHz, L = 10 mm, P_{IN} = 25 W (a) 3He:1CO_2:1N_2 (b) N_2

FIGURE 7.3 Scope photographs showing the variation of sheath thickness with discharge parameters.

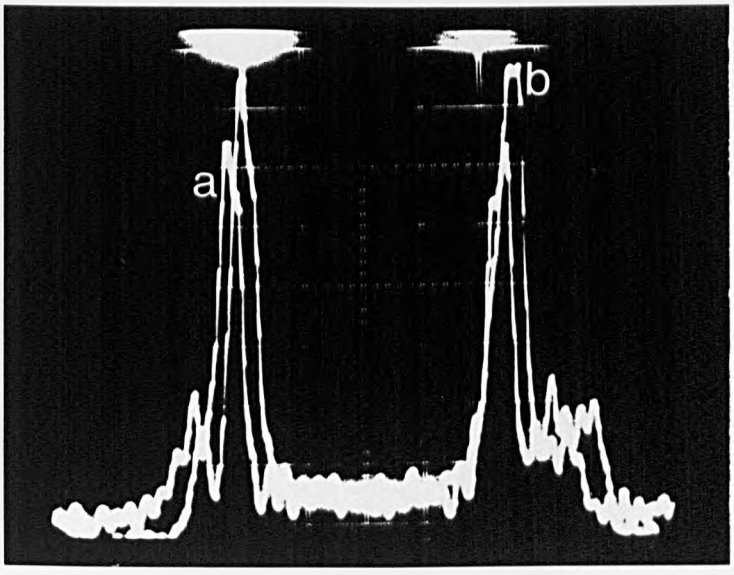

(v) P = 40 torr, RF = 40 MHz, L = 10 mm, P_{IN} = 25 W (a) He, (b) N_2

FIGURE 7.3 Scope photographs showing the variation of sheath thickness with discharge parameters.

frequency. In the gamma regime, the current differences are appreciable but the voltage was not so large. An explanation for the frequency effect in alpha discharges on voltage and current is given by the model described in Chapter 2. At high frequency the sheath is thin, its capacitance high, see Figure 7.3 and Equation 2.7, and the displacement current is large. The discharge displacement and conduction currents are equal so that the discharge current is large. With rising frequency, Equation 2.13, predicts a fall in the sheath voltage. As the interelectrode voltage measured is the sum of the voltage dropped across the sheath and the gain zone, the interelectrode voltage is lower at higher frequency. The effect of frequency on the alpha to gamma transition is covered in the next section. It is possible that the relatively large currents in the gamma discharge are due to their very thin sheaths and consequently large displacement currents.

7.2.2 The Functional Dependence of the Alpha to Gamma Transition

The lower power density alpha discharge, used in CO_2 lasers, has relatively poorly conducting and positively charged sheaths near each electrode boundary, has relatively low current densities, and is sustained largely by volume ionization. By contrast, the gamma discharge has been compared to the D.C. glow discharge [4]; it tolerates high current densities, is sustained mainly by wall ionization processes, and has relatively thin electrode boundary sheaths and high values of the displacement and conduction currents. It has been suggested [4] that the alpha to gamma transition occurs as a neutralization of the alpha discharge positive ion sheaths by electrons produced by secondary emission processes at the walls which increases with RF power. This neutralization leads to a substantial increase in conductivity of the sheaths and ultimately to their breakdown. The transition from the alpha to gamma type RF discharge is important in devices such as CO_2 and CO gas lasers as it places an upper limit on the power density that the alpha discharge used can accommodate.

In the present section we will discuss in detail the stability regions of alpha discharges in CO_2 gas laser mixtures with and without addition of Xe and then will compare the results with the stability regions of alpha discharge in N_2, Chapter 4. From Figure 7.1(b) and Figure 7.4 for the frequency of 15.5 MHz the RF transition voltage and power is seen to increase from 475V to 535V and from 22W to 25.5W for the pressures 35 and 55 torr respectively indicating a significant pressure dependence of the transition voltage and power. From Figure 7.2(a) again we can see that for constant pressure, the power loading to the discharge at the transition point is larger for the higher RF frequency as noted in the previous section. By comparison of Figure 7.4 with Figure 4.7(a), Chapter 4 it can be seen that for the same condition of 35 torr 15.5 MHz and 6 mm electrode separation, the RF transition voltage is increased significantly for the ($3He:1CO_2:1N_2$) alpha discharge, as compared to an N_2 alpha discharge. This higher transition voltage for $3He:1CO_2:1N_2$ discharge is due to the sheath voltage, which is higher in N_2, Table 4.2, Chapter 4, than ($3He:1CO_2:1N_2$) see Table 9.1, Chapter 9 for otherwise the same discharge condition of 35 torr, 52 MHz and 6 mm electrode separations. The transition power density for the above conditions was $1.9W/cm^2$ and $3.0W/cm^2$ for N_2 and $3He:1CO_2:1N_2$ discharges respectively. As was pointed out for the alpha to gamma transition in N_2, Chapter 4, the transition occurs more readily the greater the sheath mean reduced field V_s/ap where a is the electron oscillation amplitude and sheath thickness. V_s/ap decreases with increasing frequency. The alpha to gamma transition voltage and power is also increased with electrode separation Figures 7.4, 7.5 and 7.6. From Figure 7.6 it can be seen that as the electrode separation was changed from 6 mm to 10 mm the transition power is increased by 50%. The increase in transition power with electrode separation is due to the increased voltage drop across the gain zone.

The addition of Xe to the $3He:1CO_2:1N_2$ mixture decreases the RF transition voltage as shown by Figure 7.7. The change in transition voltage due to the Xe addition was smaller the lower the pressure but for the higher pressures, the drop

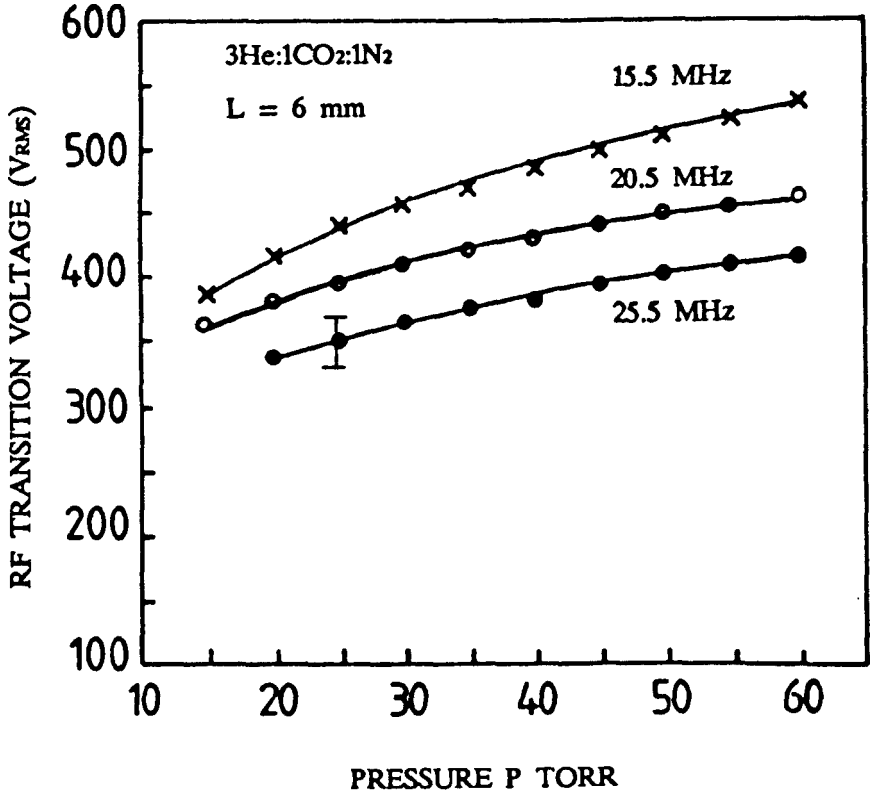

FIGURE 7.4 α to γ Transition Voltage as a Function of Pressure for Different RF Frequencies

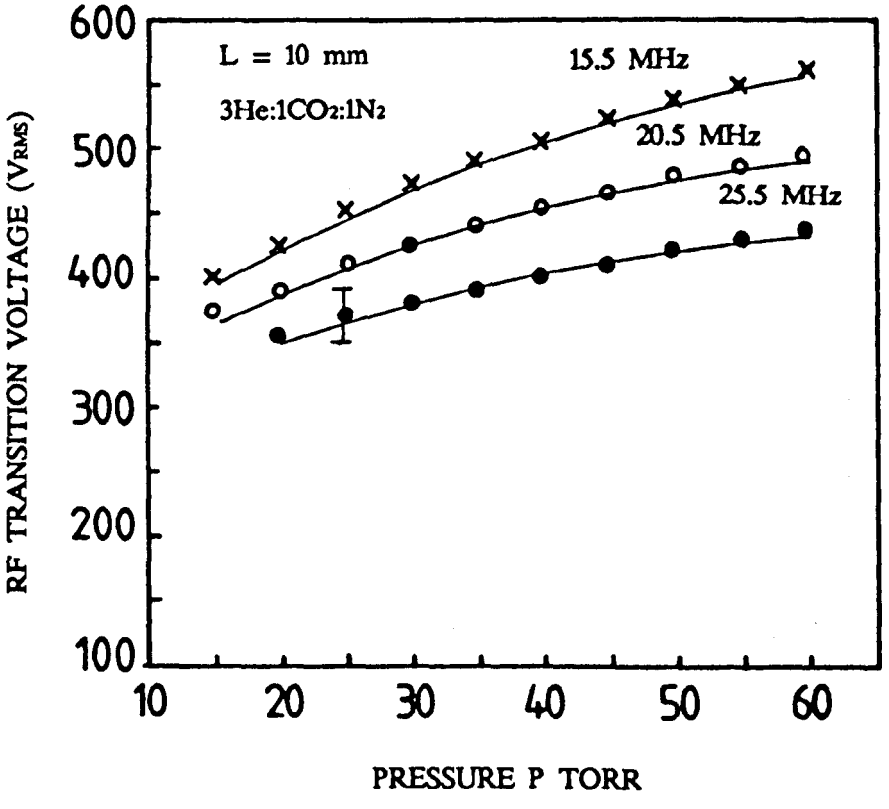

FIGURE 7.5 α to γ Transition Voltage as a Function of Pressure for Different RF Frequencies

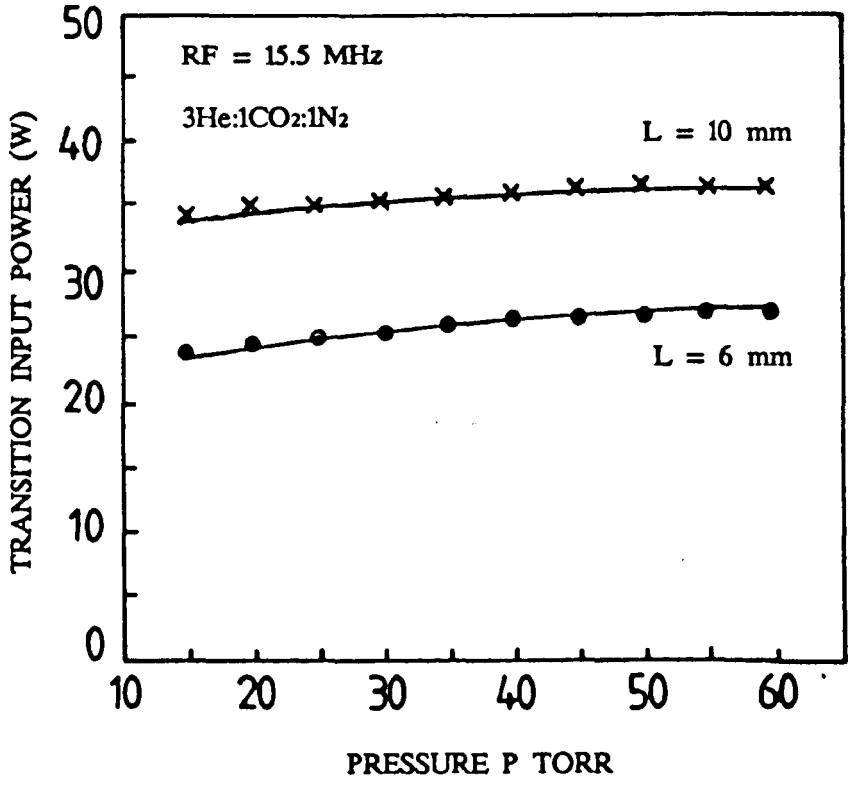

FIGURE 7.6 α to γ Transition Power as a Function of Pressure for Different Different Electrode Separations

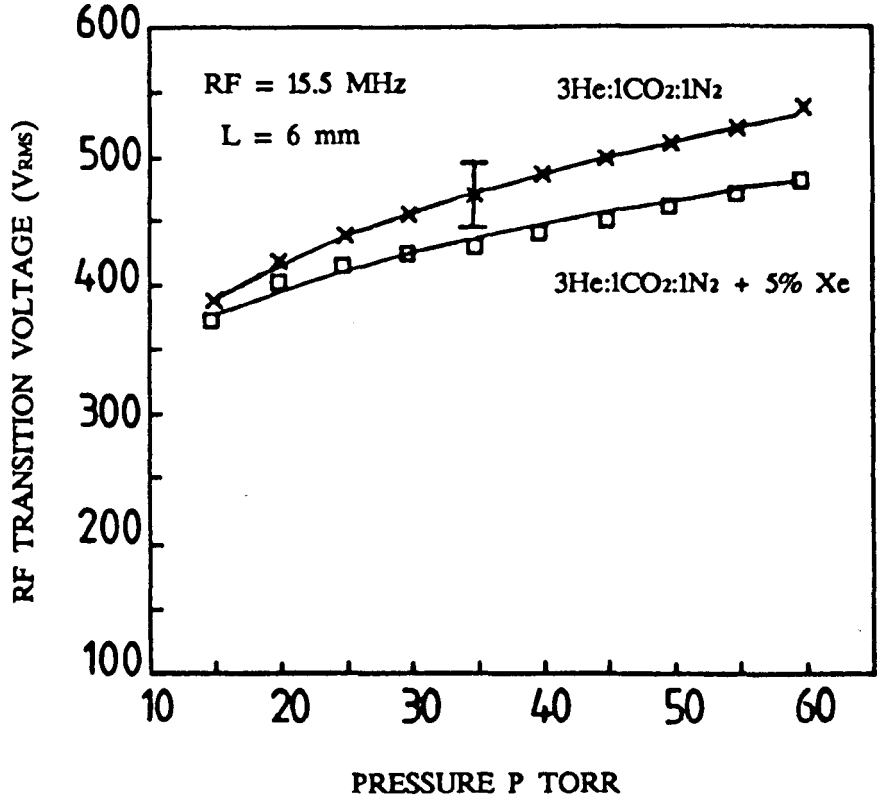

FIGURE 7.7 α to γ Transition Voltage as a Function of Pressure for Different Gas Mixtures

in the transition voltage was significant. Figure 7.8 shows that although the Xe addition reduces the RF transition voltage, the transition power is raised and the alpha discharge is more stable with the addition of Xe to the $3He:1CO_2:1N_2$ mix. The effect of Xe which is basically to reduce the gain zone electron energy and voltage drop is discussed in Section 7.2.4.

7.2.3 Electron and Neutral Gas Temperature Measurements

In this section some experimental results on the electron and neutral gas temperatures in alpha discharges in $3He:1CO_2:1N_2$ gas mix are presented and discussed. The knowledge of electron and neutral gas temperatures permits the calculation of the plasma gain zone reduced fields (E/N) in the positive column of the alpha type RF discharge which is significant in the assessment of the CO_2 laser gain medium. From Figure 7.9, it is seen that for an RF frequency of 15.5 MHz and a pressure of 25 torr, the neutral gas temperature increases both with RF power and with electrode separation. The increase in neutral gas temperature T_g with electrode separation is due to the fact that the discharge is cooled by the diffusion of molecules to the water cooled electrodes and this is less effective the further apart they are. Predictably, the effect of stopping the water cooling of the electrodes was to raise the discharge gas temperature. For constant power loading and at different pressures no change in the gas temperature was detectable. This is due to the fact that, to a first approximation, the thermal conductivity of a gas does not change with pressures in the range 1 to 150 torr [5]. Figure 7.10 shows the variation with pressure of mean electron energies in $3He:1CO_2:1N_2$, alpha type RF discharge for an input power of 26W, an RF frequency 20.5 MHz and an electrode separation of 17 mm. These observed mean electron energies are in the range of 4.25 eV to 3.75 eV for the pressures of 10 to 35 torr respectively, the decrease in mean electron energies with pressure being due to the fact that at constant input power the plasma zone reduced field (E/N) from which electrons gain energy, decreases with pressure.

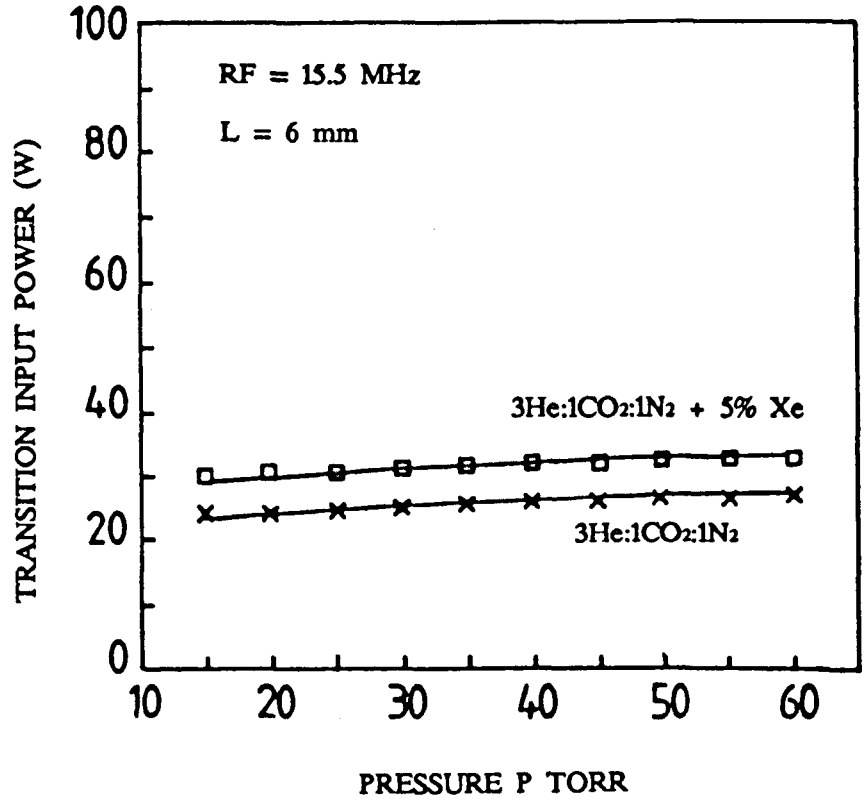

FIGURE 7.8 α to γ Transition Power as a Function of Pressure for Different Gas Mixtures

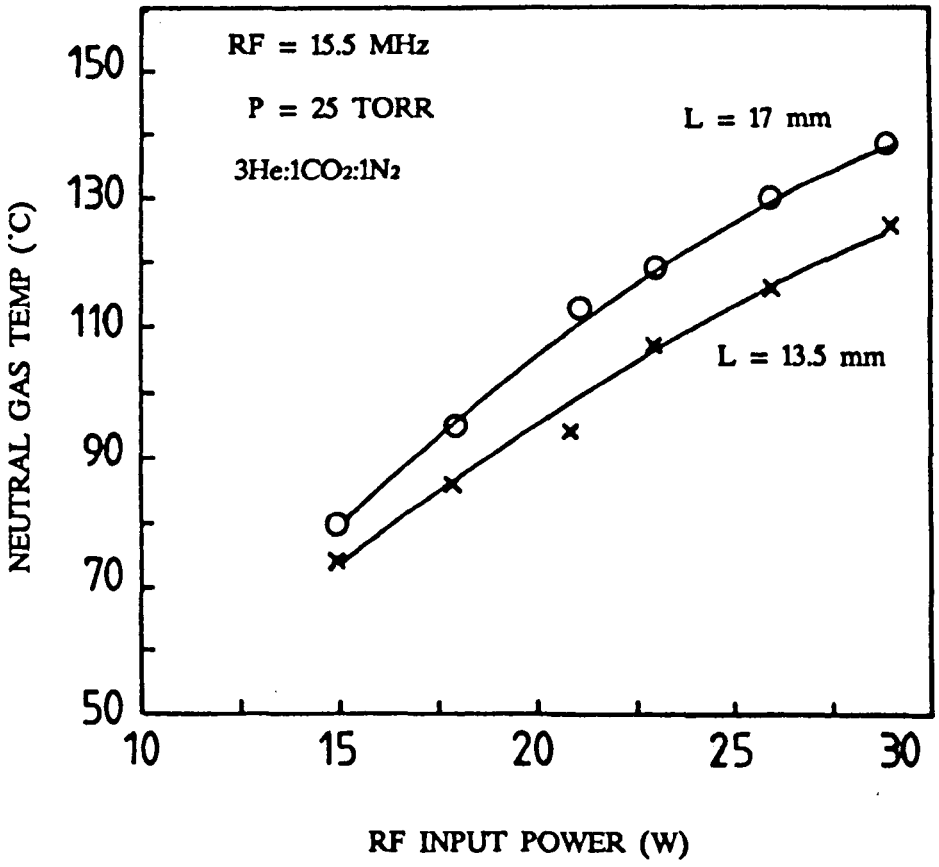

FIGURE 7.9 Neutral Gas Temperature as a Function of Discharge Input Power for Different Electrode Separations

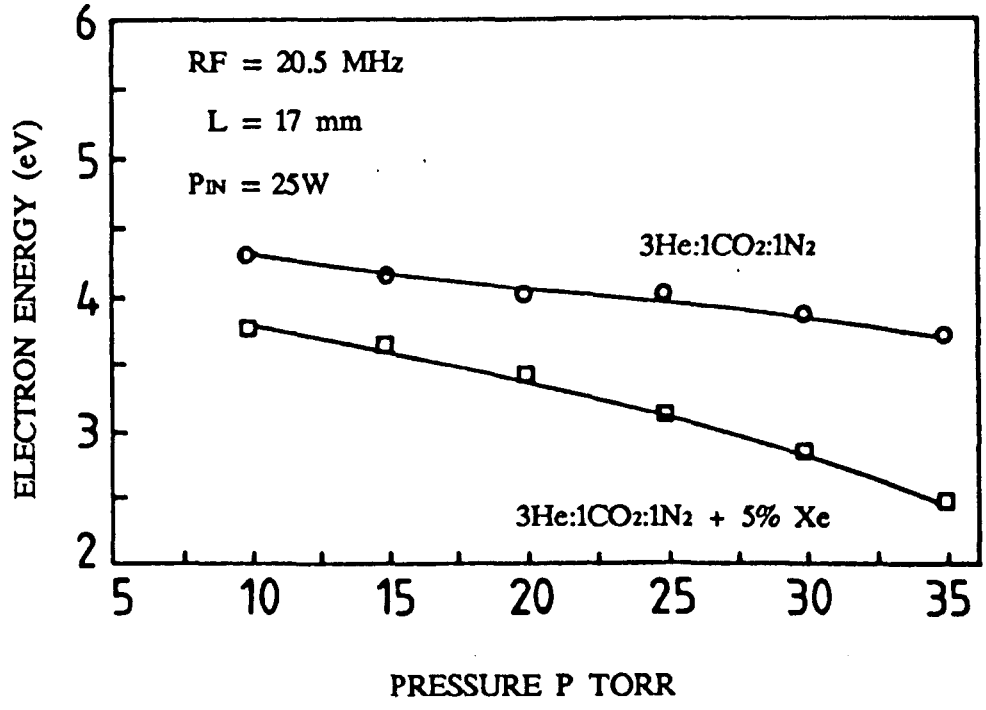

FIGURE 7.10 Electron Energy as a Function of Pressure for Different Gas Mixtures

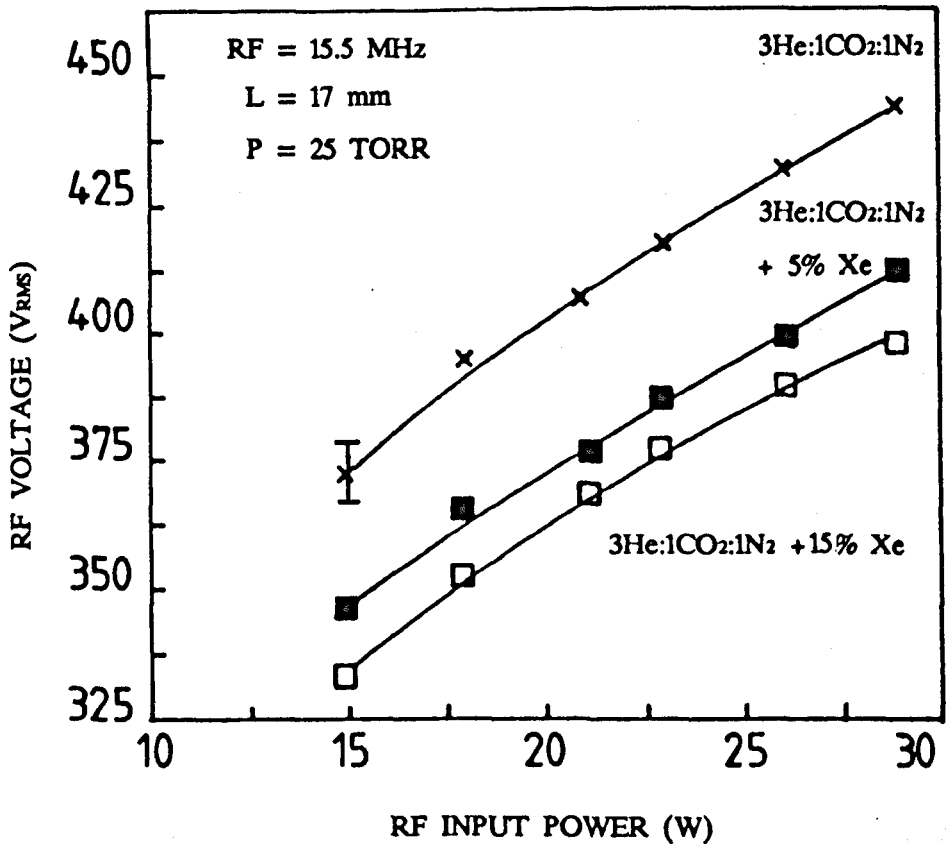

FIGURE 7.11 α Discharge RF Voltage as a Function of Input Power for Different Gas Mixtures

7.2.4 The Effects of Xenon Addition on the Electron and Neutral Gas Temperatures

It is well known that the addition of xenon to the CO_2 gas laser mixture commonly used in DC and RF excited lasers can produce significant improvement both in laser output power and efficiency, and can also lead to an extension of sealed-off life time [6-9]. The origin of these effects is attributed to the low ionization potential (12.1 eV) of xenon and its large momentum transfer collision cross-section, peaking at $\sim 4 \times 10^{-15} cm^2$ for 9eV electrons [10], which alter the discharge electron density and energy distribution in such a way as to improve the pumping of the upper laser bends by decreasing the electron energy needed to sustain the discharge. Moreover, reduction in the number of high energy electrons present leads to a decrease in the dissociation of CO_2 molecules with consequent extention of sealed-off operating life time. Working with constant input power, RF frequency and electrode separation it has been [11] found that the mean electron energies in CO_2 gas laser mixture discharge is decreased with the addition of 5% xenon in the centre of the discharge, but further increase in xenon concentration in $3He:1CO_2:1N_2$ discharge do not effect the mean electron energies to any great extent. Here, we have repeated some of the above experiments and have extended them in an effort to clarify further the xenon influence on CO_2 gas lasers. The details of the experimental techniques are given in Section 3.2.3. Figure 7.10 shows the variation in mean electron energies with total gas pressure for $3He:1CO_2:1N_2$ with and without added xenon at a fixed input power, RF frequency and electrode separation of 26W, 20.5 MHz and 17 mm respectively. It is clearly shown that when the Xe is added to the $3He:1CO_2:1N_2$ discharge, it has reduced the mean electron energies. Figure 7.11 shows the variation in RF voltage, with total input power for various amounts of added xenon at a fixed pressure, RF frequency and electrode separation. It is seen that increasing the xenon content decreases the voltage. Although, as shown by Figure 7.12,

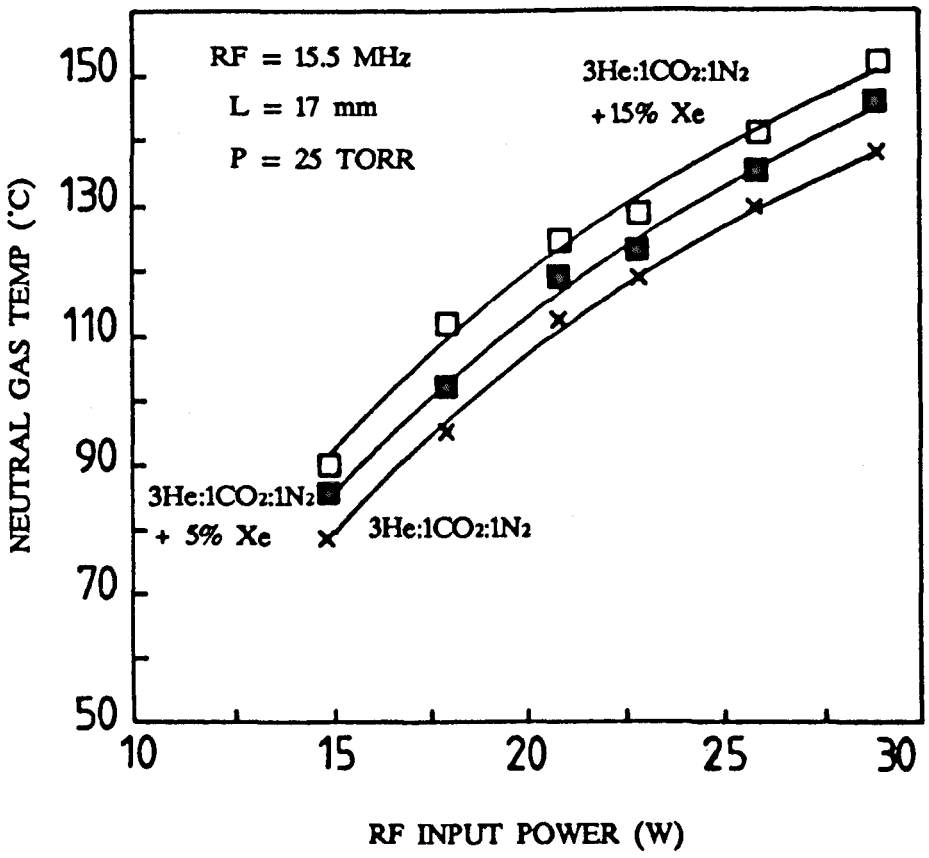

FIGURE 7.12 Neutral Gas Temperature as a Function of Input Power for Different Gas Mixtures

increasing the xenon content increases the neutral gas temperature and therefore decreases N, the net effect appears to be to reduce E/N and hence the electron energy as the electron temperature measurements discussed above show. If this assumption is true, then the question arises, why does the output power and efficiency of the CO_2 gas laser [9] not increase when the addition of xenon to the laser mixture discharge is increased above 5%? The answer to this question is probably that with a greater percentage of xenon, not only is the gas temperature rising but the amount of CO_2 available for excitation is decreasing. The increase in neutral gas temperature T_g with xenon is due to the decreasing percentage of helium in the mixture. Helium is included in CO_2 gas laser mixture because of its high thermal conductivity of 352 x 10^{-6} cal cm^{-1} Sec^{-1} $^0C^{-1}$ [12]. The thermal conductivity of xenon is 12 x 10^{-6} Cal Cm^{-1} Sec^{-1} $^0C^{-1}$, (due to its higher atomic weight), which is 25 times less than that of helium. Thus, the presence of xenon in CO_2 laser gas mixtures on the one hand will be beneficial in decreasing the mean electron energies, but on the other hand, due to its lower thermal conductivity it will increase the neutral gas temperature, which ultimately will degrade the laser performance [13].

7.2.5 The Spectroscopy of Time Averaged Visible Emission

The time averaged emission of an alpha and gamma discharge in $3He:1CO_2:1N_2$ between 3300Å and 6000Å and at resolutions of about 1Å emitted from the middle of the discharge is shown in Figure 7.13(a) and 7.12(b). In the range 3,300 to 4,400Å, the spectra for the two discharge types are the same as for pure N_2, see Section 4.3.6. Above 4000Å the CO_2 mixture spectrum differs considerably. The gamma spectrum, Figure 7.13(b), shows strong CO emission due to the $CO(B^1\sum \rightarrow A^1\Pi)$ system (4510.9, 4835, 5198Å) and the $NO(B^2\Pi \rightarrow X^2\Pi)$ β system (4574). Also found are a few atomic O (5018.2, 4924Å) and C (5889Å) lines. Comparison of Figure 7.13(a) with Figure 7.13(b) shows the presence of all the gamma discharge CO and NO lines in the alpha spectrum but at slightly

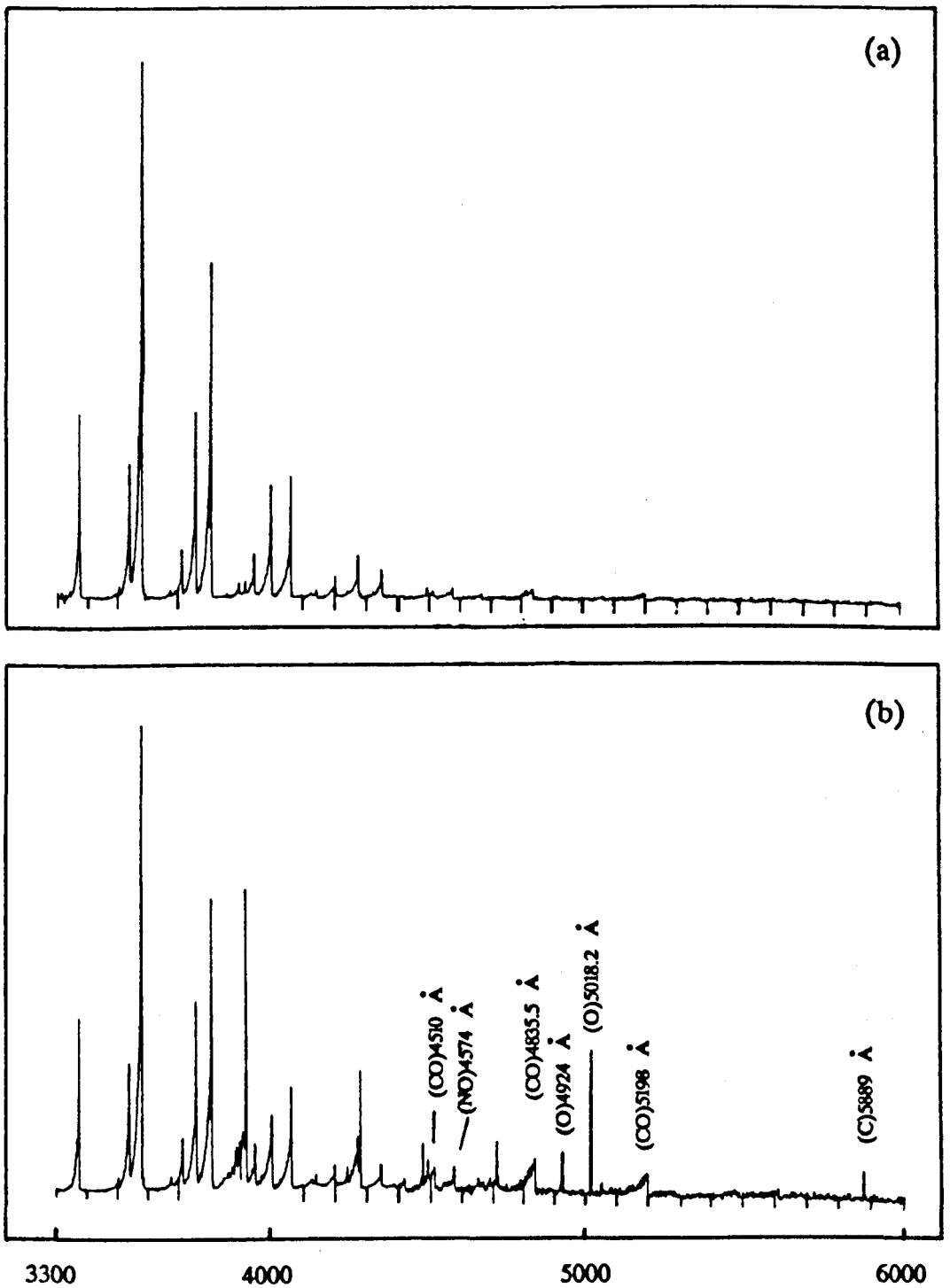

FIGURE 7.13 The 3He:1CO_2:1N_2 Emission Spectra 3300 to 6000 Å for (a) an α and (b) a γ Discharge

weaker intensities. The relatively strong emission of CO, NO and O and C in the gamma discharge is probably due to higher charge density in gamma discharge as compared to the alpha discharge. Again as in Section 4.3.6 we did not find any difference between the spectra for the middle and the electrode regions of the discharge.

The presence of CO in CO_2 lasers is extremely important as an indicator of dissociation, particularly in sealed-off CO_2 lasers, where up to 80% of the CO_2 can be dissociated [14]. Barton and von Engel [15] have shown that the maximum cross-section for the process $e + CO_2 \rightarrow CO + O + e$ is of order 10^{-21} m^2. Assuming that we have a resonable density of CO present, then the cross-section for electron impact pumping of CO is similar to that for N_2 except that it has a lower threshold and a higher peak. A sizeable fraction of the CO will be excited into vibrational levels and Nigham (25) has shown that upto 15% of the electron kinetic energy can go directly into the pumping of the vibrational levels of CO. The vibrationally excited CO is still in close energy agreement with the vibrational levels of CO_2, although the energy difference is greater than for N_2-CO_2 collisions. Although the allowed radiative decay of vibrationally excited CO reduces its effectiveness in transferring energy to CO_2, the large densities of vibrationally excited CO that are possible in the discharge ensure that this pumping process plays an important role. It is therefore of interest to monitor, if possible, the CO emission from the discharge.

7.3 DISCUSSION AND CONCLUSIONS

While the general behaviour of the CO_2 laser mixture discharge is similar to that of N_2 described in Chapter 4, there are several points of interest to be noted. The transition alpha and gamma is reversible. The reduction of the electron energy affected by the addition of xenon is confirmed by both direct measurement and voltage measurements. Again, the addition of xenon raises the

power loading at which the alpha and gamma transition occurs but also increases the gas temperature. The effect of xenon on the temperature will reduce its beneficial effect in lowering the electron energies. It has also been shown that the relative degree of dissociation in the discharges could be obtained by monitoring the CO visible emission and that the dissociation is higher in the gamma discharge than it is in the alpha. A reduction in the dissociation of CO_2 in discharges where the electrodes are covered with gold and an improvement in power output has been found [16]. The only work in this thesis on the effect of electrode material was for N_2, Chapter 4. The effect of different electrode materials on the laser mixture discharge should be studied in future work.

For the design of CO_2 lasers, the deductions to be made from the results of this chapter concern discharge stability at high power loadings and discharge gas temperature. High frequency, high gas pressure and the addition of xenon allows higher power loading. Higher frequency, because of its effect on the sheath capacitance, makes for higher currents and charge densities. Small electrode separations reduce the gas temperature. The value of designing lasers using these results cannot be judged until the corresponding laser output powers are measured. This comparison of discharge parameters and laser output power is made in Chapter 9.

REFERENCES

[1] C.G. Parazolli and K.R. Chien, IEEE J.Quant.Electron, QE-22, 479 (1986).

[2] A.J. Hatch and L.E. Henkroth, J.Appl.Physics, Vol.41, 1701 (1971)

[3] D. He, C.J. Baker and D.R. Hall, J.Appl.Phys., Vol.55, 4120 (1984).

[4] N.A. Yatsenko, Sov.Phys.Tech.Phys., Vol.26, 678 (1981).

[5] M.N. Saha and B.N. Srivastava, "A Treatise on Heat", The Indian Press Private Limited, Allahabad & Culcutta (1958).

[6] P.O. Clark and J.Y. Wada, IEEE J.Quant.Electron, QE-4, 263 (1968).

[7] K.J. Siemsen, Appl.Optics, Vol.19, 818 (1980).

[8] D. Souilhac and A. Gundjian, Appl.Opt. Vol.20, 3097 (1981).

[9] D. He and D.R. Hall, J.Appl.Phys., Vol.56, 856 (1984).

[10] B.R. Brode, Rev.Mod.Phys., Vol.5, 257 (1983).

[11] P. Vidaud and D.R. Hall, Appl.Phys., Vol.57, No. 5, 1757 (1985).

[12] Handbook of Chemistry and Physics, Weast 64th Edition, CRC Press, (1984).

[13] Taylor, Raymond L. and Bitterman, Rev.Mod.Phys., Vol.41, 26 (1969).

[14] B.E. Cherrington, "Gaseous Electronics and Gas Lasers", Pergamon Press (1980).

[15] M.J. Barton and A. Von Engel, Phys.Letts., Vol.32A, 173 (1970).

[16] J. Macken, H. Wrench and M. Samis, Paper FD3, Conference on Lasers and Electrooptics (CLEO) Anaheim, California (1988).

CHAPTER 8

EXPERIMENTAL STUDY OF PULSED RF DISCHARGES

8.1 INTRODUCTION

In the previous chapter, experimental results were presented on the stability with respect of the alpha to gamma transition of RF discharges in a typical CO_2 laser gas mixture under CW conditions. In this chapter, we present an analogous set of results on discharge stability for pulsed RF discharges in the CO_2 laser mixture. Pulsed excitation of CO_2 gas lasers allows high input power loadings and high laser power extraction if the pulse length and the repetition rate are such that the gas is prevented from over heating.

Transverse RF discharges have been used for excitaiton of both CW and pulsed CO_2 gas lasers [1-3]. For example Lachambre *et al* [2] reported both CW and pulsed operation of RF excited CO_2 waveguide lasers. For the CW mode Lachambre *et al* found an optimum pressure of 240 torr, while in the pulsed mode, the optimum pressure was around one atmosphere, with pulse durations greater than 20 μs repetition rates up to 300 MHz, and peak powers of a few watts.

Sutter [4] demonstrated improvement in amplitude and frequency stability, with a sealed off Al/BeO waveguide laser yielding peak powers up to 800 W at kilohertz repetition rates, with an RF frequency equal to 150 MHz.

Q-switching and cavity dumping techniques can also be applied to RF waveguide lasers. Miller and Ross [5] reported, peak powers of about 1 kW and

pulsed widths of about 100 ns, from a gain-switched device.

Lovold and Wang [6, 7] reported a pulsed RF CO_2 laser lasing at up to 10 atmospheres, where the pressure broadening allows continuous tunability over many gigahertz because the CO_2 lines overlap. Their three mirror transverse gas flow laser could be run quasi-CW with pulse lengths up to 10 ms.

In the following sections we present experimental results mapping out the regions of stability with respect to gamma discharges for pulsed RF discharges in the CO_2 laser mixture. For the present experimental work, the pulse duty cycle was kept constant at 2%. This ratio of pulse width to separation was used since for smaller pulse separations the results were a function of pulse separation. The arrangement of the following sections are such that Section 8.2 gives the current, voltage and power characteristics, the experimental results on the transition (alpha to gamma) is shown in Section 8.3, and finally the experimental results are discussed in Section 8.4.

For the experimental investigations of the present chapter, the same experimental set up as described in Chapter 5 is used, with exception that the visible light distribution measurements were not made.

8.2 THE TIME DEPENDENT CURRENT, VOLTAGE AND POWER CHARACTERISTICS

Figures 8.1 and 8.2 show the typical current, voltage and power characteristics of CW and pulsed RF discharges. For both the CW and pulsed RF discharges, current and voltage increases linearly from $V_{\alpha(MIN)}$ to $V_{\alpha(MAX)}$. At this point an abrupt change occurs with a corresponding increase in current and a reduction in RF voltage. This is qualitatively similar to the situation for CW discharges (Chapters 4 and 7). From Figure 8.1 it can be seen that for a particular value of

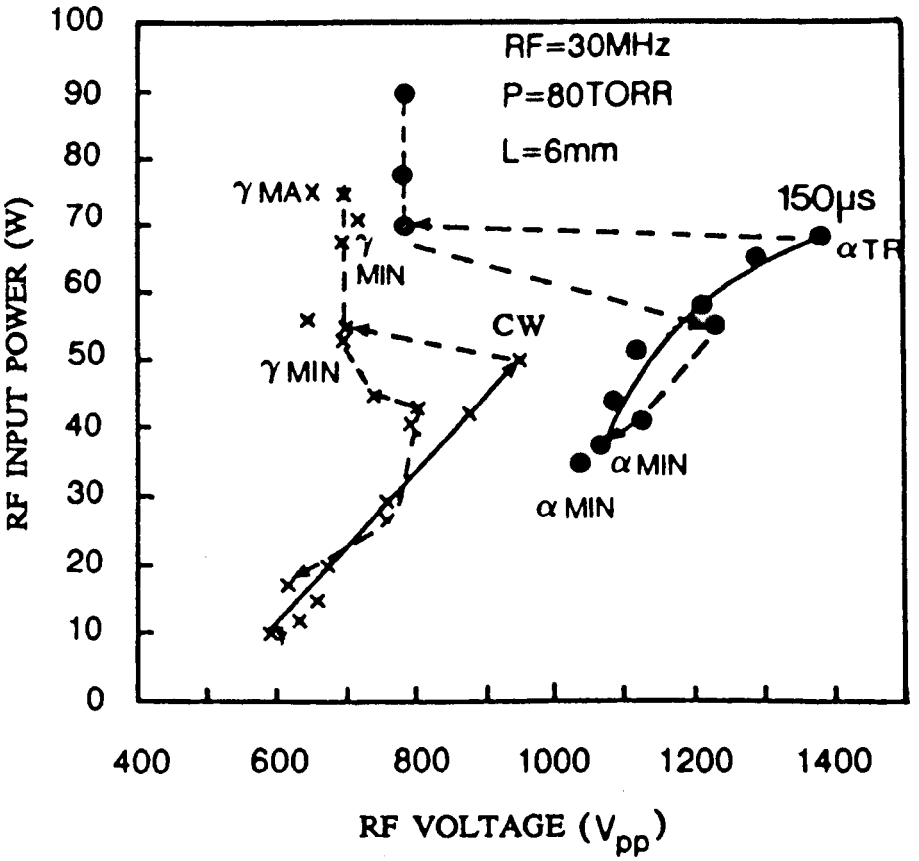

FIGURE 8.1 α and γ Total Discharge Power - Voltage Characteristic for Pulsed and CW RF Discharges.

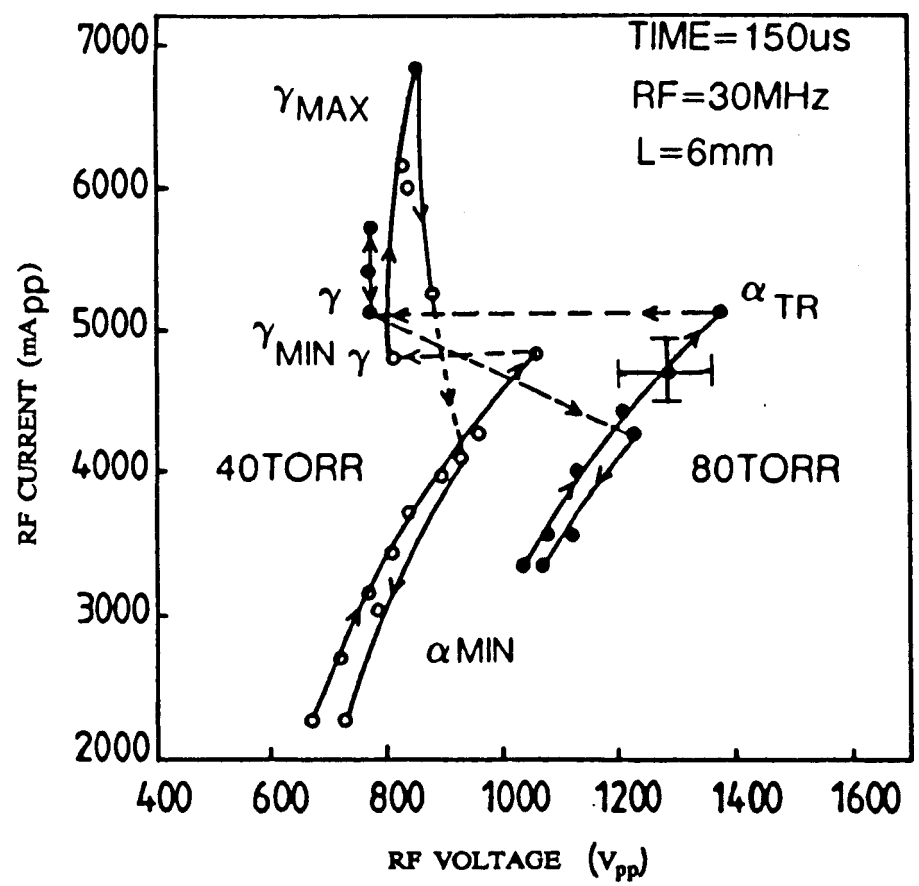

FIGURE 8.2 α and γ Current - Voltage Characteristic for Pulsed RF Discharge.

RF frequency, pressure and electrode separation, the transition occurs at different voltages for CW and pulsed (150 μs) discharges. The corresponding values of RF voltage are 950 Vpp (CW) and 1400 Vpp (pulsed). Comparison of CW and pulsed discharges, showed an increase of 50% in transition power for the 150 μs pulsed discharge over the CW discharge. The current and voltage characteristics of the pulsed and CW discharge had the same overall shape. As in Chapters 4 and 7, here it was not possible to find the exact electrode area covered by the discharge for either the alpha or the gamma regimes. Figure 8.3 shows the total discharge power and voltage characteristic of a 150 μs pulsed discharge, for constant electrode separation RF frequency and different pressures; as with the CW discharge the characteristics are shifted up to higher powers, currents and voltages when the pressure is raised. Again changing the RF frequency and electrode separation for a constant pressure and pulse width resulted as with the CW case, in higher currents and transitions point power as the frequency was raised and higher voltage when the electrode separation was raised.

8.3 THE DEPENDENCE OF ALPHA TO GAMMA TRANSITION CHARACTERISTICS ON THE RF TIME PULSE DURATION

Figure 8.4 shows the transition power for ($3He:1CO_2:1N_2$) pulse discharge as a function of pulse duration for different gas pressures at a constant RF frequency and electrode separation. The transition power is increased, both by increasing pressure (as Chapters 4 and 7) and a decrease in the pulse width. Changing the pressure from 40 to 100 torr, the transition power is increased by 40%, 50%, 77% and 113% for CW, 1010 μs, 200 μs and 100 μs respectively. These numbers clearly show the transition power dependence both on the time and pressure. For a constant pressure of 80 torr, the transition power is increased by almost 80%, by decreasing the time from CW to 16 μs pulse. Figure 8.5 shows the variation in transition power as a function of time for two different RF frequencies at a constant electrode separation and pressure. For a constant pulse width of 123 μs,

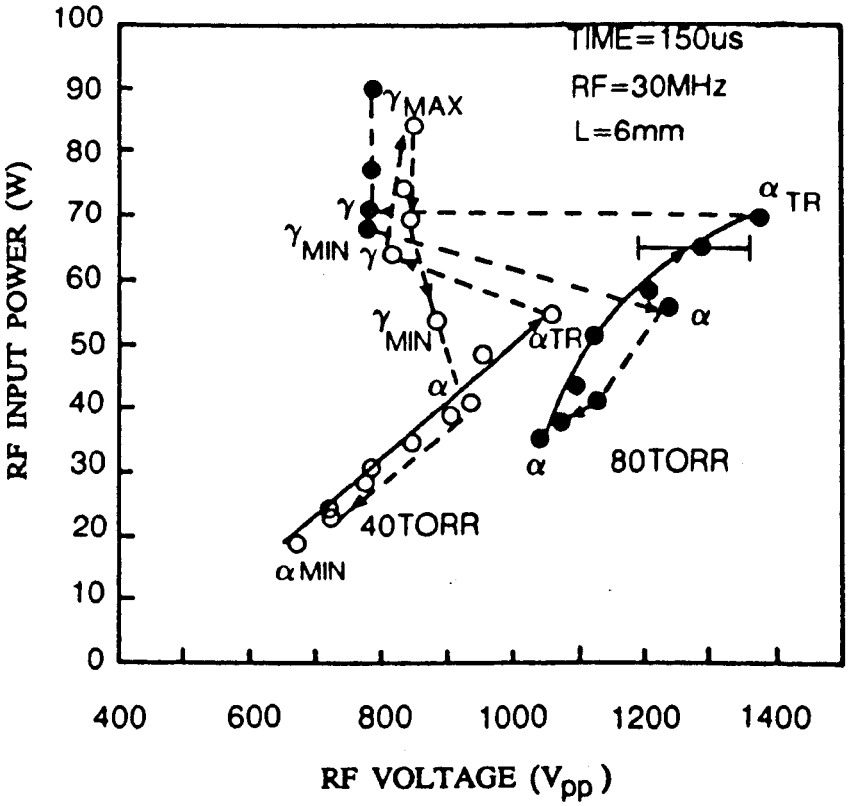

FIGURE 8.3 α and γ Total Discharge Power - Voltage Characteristic for Pulsed RF Discharge.

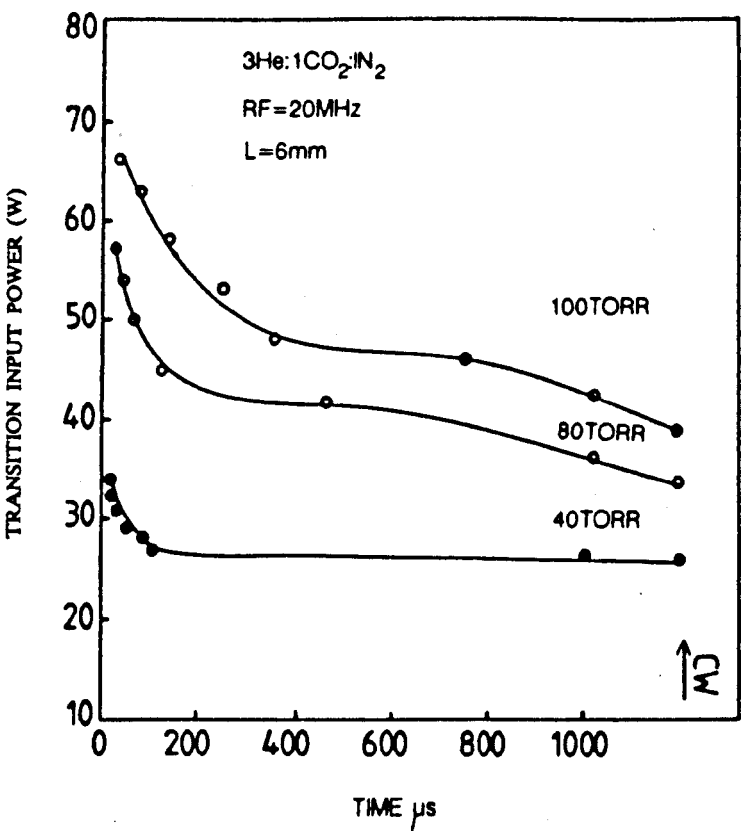

FIGURE 8.4 α to γ Transition Power as a Function of Time for Different Pressures.

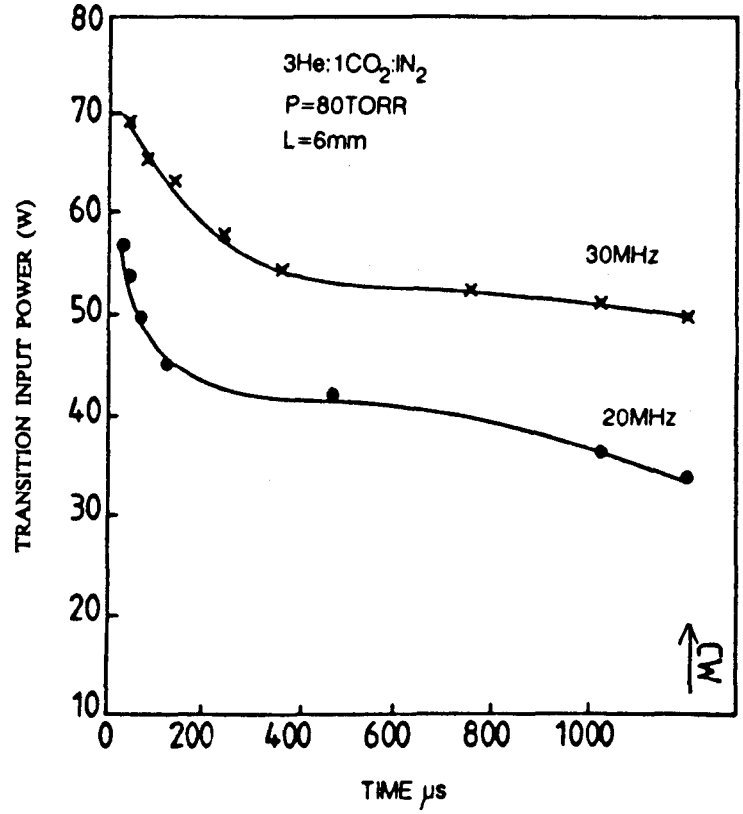

FIGURE 8.5 α to γ Transition Power as a Function of Time for Different RF Frequencies.

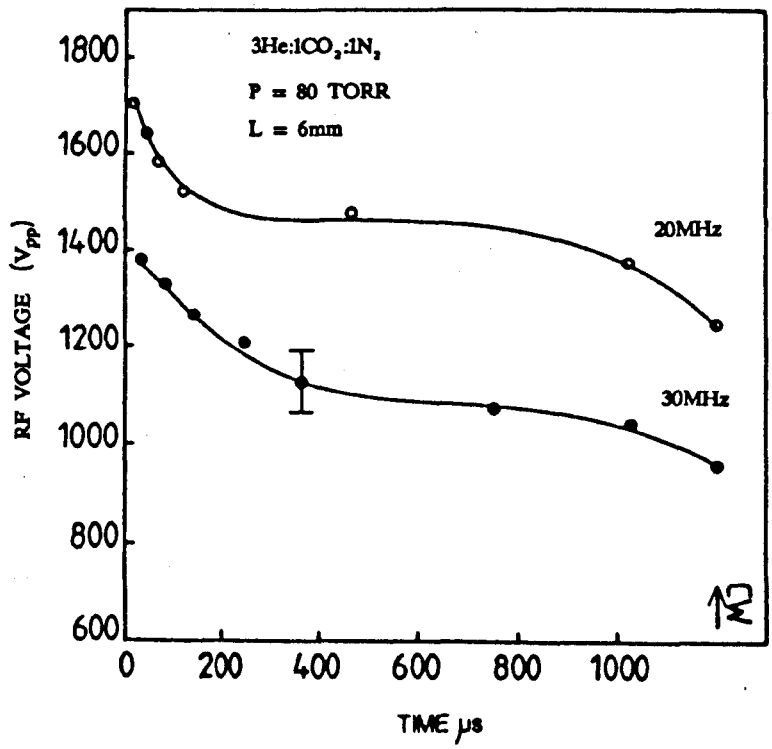

FIGURE 8.6 α to γ Transition Voltage as a Function of Time for Different RF Frequencies.

the power needed to cause a transition is increased by 40%, when the RF frequency is raised from 20 to 30 MHz. Figure 8.6 gives the transition RF voltages for the discharge conditions of Figure 8.5. It can be seen that the transition RF voltage is decreased with frequency as in the CW case. The transition power as a function of time, for the different CO_2 gas laser mixtures is shown in Figure 8.7. The results indicate that there is a significant increase in the power needed to cause a transition when the percentage of helium gas in the mixture is increased. For example, for a constant pulse width of 350 μs, the transition power is raised by 13%, by increasing the helium percentage, in the mixture from 60% to 80%. Figure 8.8 shows the transition RF voltages, corresponding to the discharge conditions of Figure 8.7. The transition RF voltages are decreased by increasing helium percentage.

Finally Figures 8.9 and 8.10 show the scope traces, of RF voltages, currents and reflected powers, for the alpha and gamma pulsed RF discharges. An interesting illustration of the alpha to gamma transition is given by the traces of RF voltage, current and reflected power when the gamma discharge occurred, see Figures 8.9(c), 8.9(d) and 8.10. The current trace shows an initial level portion for an alpha discharge followed by a jump corresponding to the establishment of the gamma discharge. The voltage trace passes from the higher alpha voltage through to the lower gamma one. This means that the alpha to gamma transition times can be obtained from the current and voltage trace. Changes in the reflected power with the alpha to gamma transition is perhaps due to the discharge impedance which changed with the transition.

8.4 DISCUSSION AND CONCLUSIONS

It has been shown that the power loading of the discharge at the alpha to gamma transition point can be considerably increased if the power to the discharge is pulsed. For a 50 μs pulse, the transition point power is raised by 11 and 62%

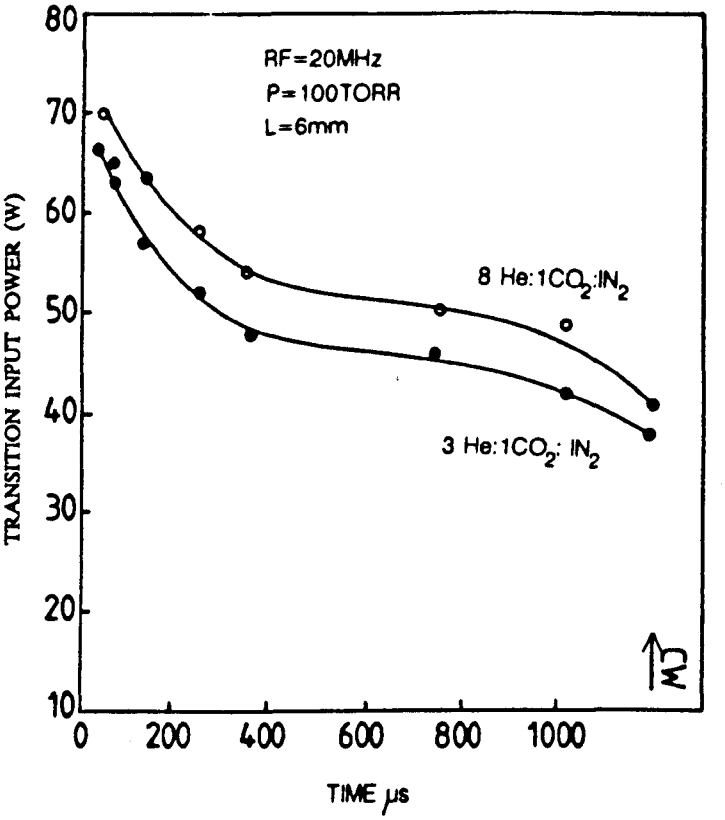

FIGURE 8.7 α to γ Transition Power as a Function of Time for Different Gas Mixtures.

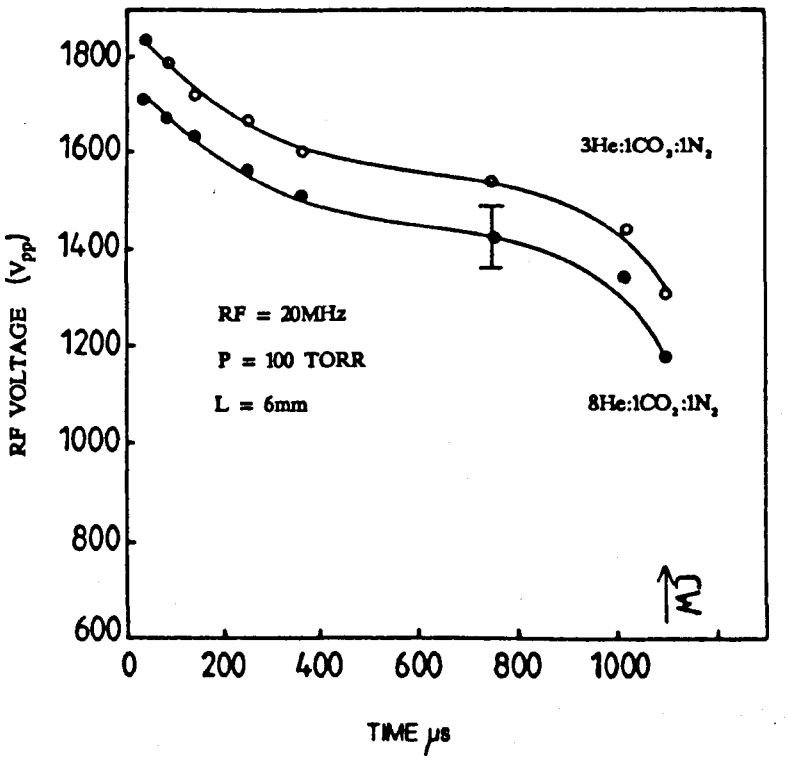

FIGURE 8.8 α to γ Transition Voltage as a Function of Time for Different Gas Mixtures.

(a)

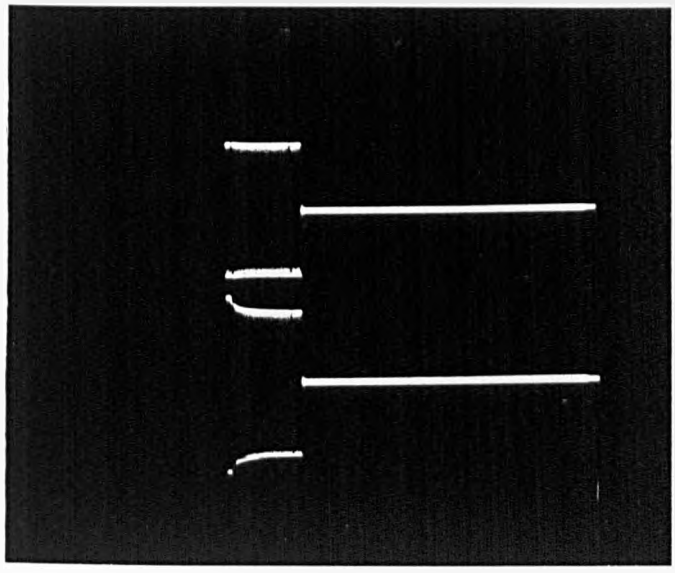

(b)

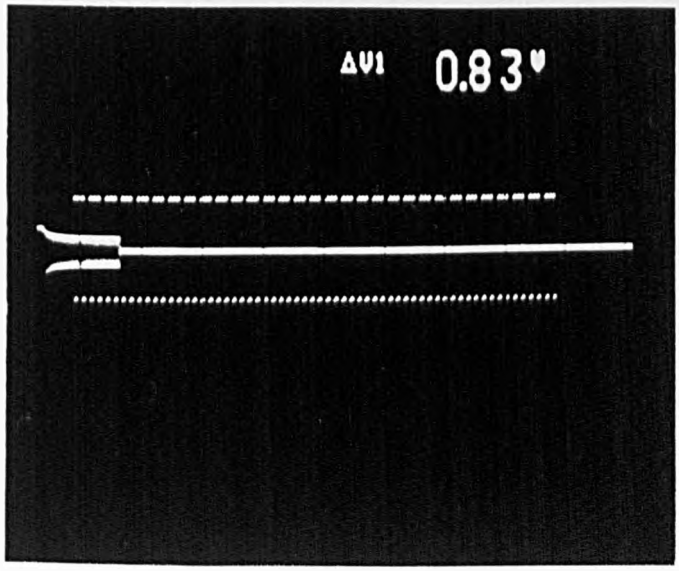

FIGURE 8.9 Oscilloscope traces of pulsed RF voltage, current and reflected powers, α discharge, $3He:1CO_2:1N_2$, RF = 20 MHz, L = 6 mm, P_{IN} = 58 W, P = 100 torr, (a) top current, bottom voltage, (b) RF reflected power. Pulse Duration 90 μs

(c)

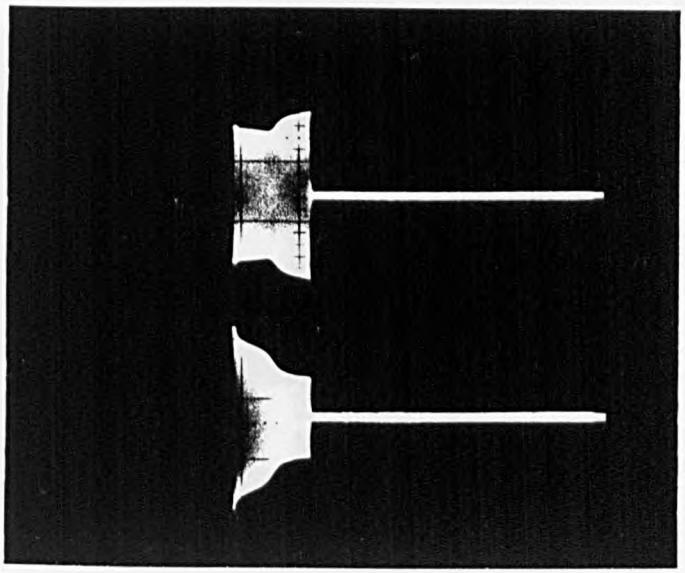

(d)

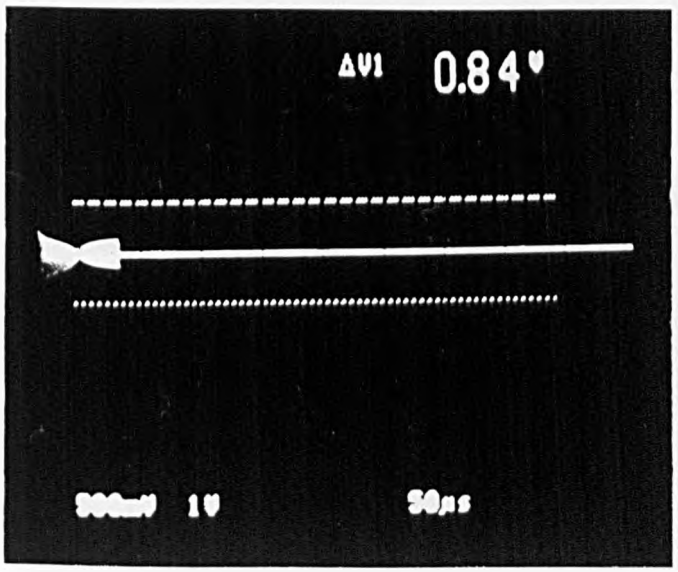

FIGURE 8.9 Oscilloscope traces of pulsed RF voltage, current and reflected powers, γ discharge, 3He:1CO_2:1N_2, RF = 20 MHz, L = 6 mm, P_{IN} = 60.5 W, P = 100 torr, (c) top current, bottom RF voltage, (d) RF reflected power.

(a)

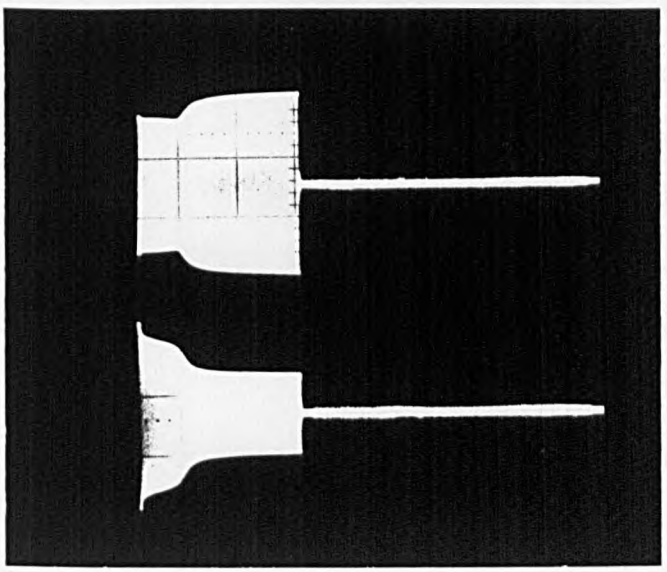

(b)

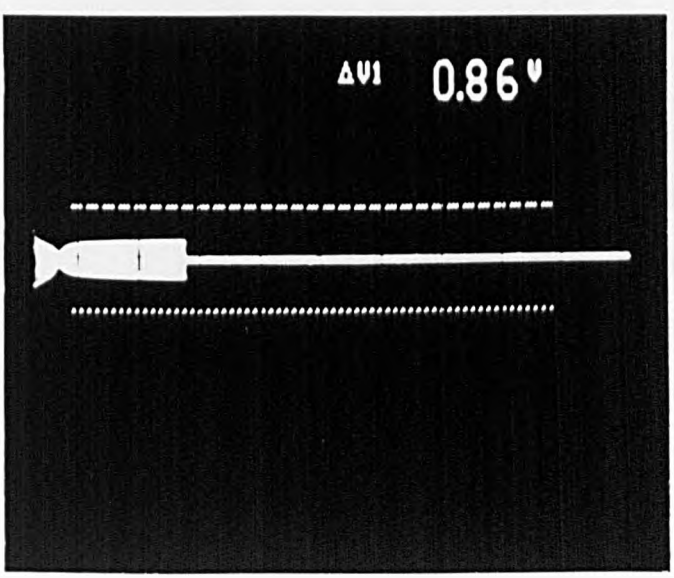

FIGURE 8.10 Oscilloscope traces of pulsed RF voltage current and reflected power, γ discharge 8He:1CO_2:1N_2, RF = 20 MHz, P = 100 torr, P_{IN} = 65 W, L = 6 mm, (a) top current, bottom voltage, (b) RF reflected power.
Pulse Duration 140 μs

at 40 and 100 torr respectively compared to the CW values. The fact that the critical power loading at the transition point increases with rising pressure and decreasing pulse duration suggests a heating effect where the neutral gas density N is reduced so that E/N reaches some critical value. Ignoring heat losses and taking the gas's specific heat at constant pressure as being proportional to pressure [8], the time taken to raise the gas's temperature to the critical value is proportional to p/W where W is the pulse power. This is seen to be roughly the case in Figure 8.4. Again, as helium improves gas cooling, it is not surprising, see Figure 8.8, to find that a helium rich pulse can take higher power loadings.

It has already been suggested in Chapters 2, 4 and 7, how the transition from alpha to gamma occurs with the breakdown of the alpha discharge positive ion sheaths. Now it is seen from the work on N_2 (Chapter 5) that the striation formation times are all less than 2.8 μs. For the same RF discharge conditions, here the transition alpha to gamma times were greater than 10 μs, which is to be expected, due to the fact that first the striations form in the discharge and then their breakdown occurs.

In conclusion the alpha discharge is more stable, the lower the RF discharge excitation pulse width and the higher the pressure and frequency. Higher helium concentration in CO_2 gas laser mixture also increased the stability of alpha discharge. For the practical RF pulsed CO_2 lasers, the transition of an alpha to gamma regime can easily be identified from the shapes of the pulsed RF voltage and current traces. It can also be detected in the traces of the reflected power Figures 8.9(d) and 8.10(b).

REFERENCES

[1] C.K.N. Patel, Phys.Rev., Vol.33, 6A, 1187 (1964).

[2] J.L. Lachambre, J. MacFarlane, G. Otis and P. Lavigne, Appl.Phys.Lett., Vol.32, 652 (1978).

[3] K.D. Laakmann, Paper Tukk3 presented at CLEO, San Diego, California (1980).

[4] L.V. Sutter, Proceedings of SPIR Meeting, Washington D.C., Vol.227 (1980).

[5] G. Meller and I.E. Ross, Proceedings of the Third Topical Meeting on Coherent Laser Radar, Malvern, 69 (1985).

[6] S. Lovold and G. Wang, Appl.Phys.Lett., Vol.40, 18 (1982).

[7] S. Lovold and G. Wang, Paper ThLI, CLEO, Anaheim, California (1984).

[8] M.N. Saha and B.N. Strivastava, "A Treatise on Heat", Indian Press, Private Limited, Allahabad (1958).

CHAPTER 9

DISCHARGE PARAMETER SCALING AND LASER POWER OUTPUT OPTIMIZATION

9.1 INTRODUCTION

The last decade has seen a considerable increase in the use of transverse radiofrequency gas discharges for laser excitation. Such discharges have found particular application for CO_2 lasers. They have been used with small cross section waveguide lasers [1-3] and larger bore gaussian beam, diffusion cooled devices [4], and also for very high power fast axial gas flow lasers [5]. For diffusion cooled, sealed lasers, the use of RF discharge pumping has brought with it a number of important practical advantages. Among these are low voltages in transverse operation, avoidance of internal metallic electrodes and overall flexibility in design. In addition several more fundamental benefits have been noted including increased discharge stability under high power loading, high power extraction and efficiency as well as increased capacity for discharge switching and hence laser modulation.

The optimisation of RF discharge lasers is made more complex, but at the same time potentially more efficacious, by the availability of an additional parameter - the frequency, f of the power generator - which can be selected to facilitate the achievement of optimum discharge conditions for laser excitation. During the past ten years, various workers have employed a whole range of different frequencies and discharge geometries with a range of results in terms of laser performance. The optimum choice of generator frequency has received some attention for carbon dioxide waveguide lasers [6], [7], and experiments indicate that

for a given transverse electrode separation, L, laser output power reaches a peak at a particular frequency and pressure (for example 125 MHz and 125 torr for L = 2.25 mm). Moreover, it has been observed that the estimated value of interelectrode reduced field (V_L/NL) has a minimum value at this frequency. In [6] V_L is the interelectrode voltage, deduced from measurements of RF input power and discharge resistance, (determined by an indirect substitution technique [8]) and N is the neutral gas density. Griffiths [9], using f = 145 MHz and a waveguide laser of 1.5 mm bore, measured laser power and interelectrode voltage as a function of gas pressure. In both of these investigations, the authors have calculated the interelectrode reduced field from interelectrode voltage measurements and assumed a field which is uniform in the transverse direction. However, as pointed out in Chapters 1, 2 and 4 it is well known that RF discharges operated under conditions appropriate to CO_2 laser action are characterised by transverse non-uniformities [10], and that considerable voltages are dropped across the sheath zones near each electrode [11, 12]. Using Godyak's RF discharge model [13], Parazolli and Chien [14] have described some of the behaviour of RF excited CO_2 waveguide lasers allowing for the neutral gas temperature but having to assume a uniform energy deposition and charge distribution. Like Baker [15] and the authors of [14], Sharp [16], working with a 5 x 5 mm^2 cross-section discharge, observed somewhat higher small signal gain near the electrode. Ignoring sheath effects and displacement currents, Sharp ascribes this gain profile to the effect of relatively high electric field and cooler gas close to the electrodes.

In this chapter results are presented from a systematic study of the dependence of laser output power on the discharge drive frequency and gas pressure for a representative range of square gain cell cross sections. This investigation differs from previous studies in two important respects. First, it refers to discharge cross sections which are characteristic of non-waveguide, free space gaussian resonators, and secondly, the analysis used takes account of the distribution of the electric field between the sheath zones near the electrodes and the central

positive column or gain zone allowing the calculation of the molecular excitation rates in the gain zone. Section 9.2 shows how with an adaptation of the theory for N_2 of Chapter 2, the electron mean energy in the gain zone is calculated. Using the results of Section 9.2, Section 9.3 gives the calculation required to estimate the densities of CO_2 in the upper lasing level. These last results are compared to the experimental results in Section 9.5, with some conclusions in Section 9.6.

9.2 CALCULATION OF GAIN ZONE MEAN ELECTRON ENERGY

Using electron swarm data, the discharge model of Chapter 2 and measured discharge parameters, the average electron energy, ϵ, in the discharge gain zone can be calculated. Once ϵ is determined, estimates can be made of the discharge densities of excited CO_2 lasing levels for comparison with observed laser output powers.

9.2.1 Average electron energy functions

These functions, most of which are empirical, give expressions for various electron volume collision processes and transport characteristics in terms of the average electron energy ϵ. Unless otherwise stated, the data used is all for the CO_2 gas laser mixture of $3He:1N_2:1CO_2$.

The minimum reduced field, E/N, for the discharge (ignoring the contribution made to the charge balance by electrons generated in the sheaths) is $E/N \approx 5 \times 10^{-20}$ volts $-m^2$ [21] where the ionisation and electron attachment coefficients are equal. Since the optimum values of E/N for pumping of the $N_2(X^1\Sigma_g^+, v = 1)$ and upper lasing CO_2 (001) levels lie between about 2×10^{-21} and 2×10^{-19} volts - m^2 [24], a reasonable range of E/N for laser operation is $5 \times 10^{-20} < E/N < 2 \times 10^{-19}$ volts - m^2. The corresponding range for the average electron energy is

2.3 $\leq \epsilon \leq$6.0 eV [21] and this is taken as the range of validity for the following expressions:-

Reduced field [21]

$$E/N = 2.12 \times 10^{-20}\ \epsilon^{1.15} \qquad \text{volts rms m}^2 \qquad (9.1)$$

Electron ionisation coefficient [21]

$$\alpha/N = 5.65 \times 10^{-20}\ \exp^{-(24/\epsilon^{1.15})} \qquad \text{m}^2 \qquad (9.2)$$

Electron drift velocity [19]

$$v = 3.18 \times 10^{3}\ \epsilon^{1.15} \qquad \text{ms}^{-1} \qquad (9.3)$$

Excitation coefficient for the CO_2 001 upper lasing level [21]

$$(\eta/N) = 6.4 \times 10^{-19}\ \epsilon^{-3.45} \qquad \text{m}^2 \qquad (9.4)$$

Volume rate of dissociative recombination for CO_2 [18]

$$\sigma = 6.54 \times 10^{-14}\ \epsilon^{-0.5} \qquad \text{m}^3\ \text{s}^{-1} \qquad (9.5)$$

The ambipolar diffusion coefficient for CO_2^+ at 1.0 torr and 273^{0}K [23]

$$D = 0.073\ \epsilon \qquad \text{m}^2\ \text{s}^{-1} \qquad (9.6)$$

The electron attachment coefficient which has a small variation from 6 to 8 x 10^{-24} m^2 in the range of ϵ considered is taken to be constant with a value of a/N = 7 x 10^{-24} m^2 [21].

9.2.2 The Discharge Model

The only difference between the model used here and that described for N_2 in Chapter 2 arises from the different discharge processes that occur in the laser mixture $3He:1N_2:1CO_2$. The principle difference is that in the laser mixture dissociative attachment

$$e^- + CO_2 \rightarrow CO^- + O$$

is an important loss process for the electrons. For the gain zone to have a constant charge density n, the loss of charge by ambipolar diffusion to the walls must be negligible compared to the volume attachment and recombination losses. To establish this, we assume the discharge is maintained between two infinite parallel electrodes a distance L apart and consider the charge losses from a volume extending a distance L/2 from unit area of one electrode. To a first approximation, the ambipolar diffusion loss in unit time is

$$\Phi^D = \frac{D}{p}\frac{dn}{dx} = \frac{D2n}{pL} \qquad m^{-2}s^{-1} \qquad (9.7)$$

and the attachment and recombination losses respectively

$$\Phi^a = n\left[\frac{a}{N}\right] NvL/2 \text{ and } \Phi^R = n^2\sigma L/2 \qquad m^{-2}s^{-1} \qquad (9.8)$$

If we assume the conditions that most favour ambipolar loss, low pressure and electrode separation, for p = 10 torr, L = 4×10^{-3} m and taking from Table 9.2. ϵ = 2.59 eV and n = 7×10^{17} m^{-3} we have with expressions (9.3), (9.5) and (9.7) that $\Phi^D/(\Phi^a + \Phi^R) = 8.8 \times 10^{18}/(2.5 \times 10^{19} + 3.9 \times 10^{19})$. From this, we take volume attachment and recombination to be the dominant charge loss processes.

9.2.3 Gain Zone Mean Electron Energy, Reduced Field and Charge Density

Following Denes and Lowke [29], the reduced current density, j/N, and the charge density, n, are respectively

$$j/N = -\frac{(\alpha-a)}{N\sigma} e\ v^2 \qquad \text{amps-(rms)-m} \qquad (9.9)$$

and

$$n = (\alpha/N - a/N)\ Nv/\sigma \qquad m^{-3} \qquad (9.10)$$

substituting the expressions of Section 9.2.1 for α, a, v and σ into the R.H.S. of (9.9) and the measured reduced current on the L.H.S., yields

$$\frac{i_0 T}{Ap} = 2.36 \times 10^3\ [8.1 \times 10^3\ \exp^{-(24/\epsilon^{1.15})} 1]\epsilon^{2.8} \qquad (9.11)$$

i_0, T and A are respectively the peak discharge current, the discharge gas temperature and the electrode area. The solution of (9.11) gives the mean electron energy which in turn, with expressions (9.10) and (9.1), can be used to obtain the gain zone charge density and reduced field.

9.3. CALCULATION OF THE GAIN ZONE VIBRATIONALLY EXCITED CO_2 (001) DENSITY

Using the calculated values of ϵ and n from the previous section, an estimate can be made of the absolute density of CO_2 molecules in the upper laser (001) level. For a given set of fixed discharge conditions, this density of excited CO_2 molecules will be compared to the laser output power. It would be reasonable to expect that to a first approximation power and excited state density would be proportional. To justify this assumption, it must be shown that the population

inversion, $[CO_2(001)]-[CO_2(100)]$, for the main 10.6 μm transition is equal to $[CO_2(001)]$ where the square brackets denote the concentrations of the two states. Ignoring wall collisions, and assuming volume collisional relaxation, the density of both states is proportional to the ratio of the excitation over the relaxation rates. In $3He:1CO_2:1N_2$ [21], for the whole of the range of reduced fields considered here, the excitation coefficient for CO_2 (001) is ten times that for CO_2 (100). The rate constants of volume deactivation of the CO_2 (001) and CO_2 (100) levels are respectively 6×10^{-21} and 7×10^{-19} m^3s^{-1} at 300 ^{0}K [18, 25]. This gives $[CO_2(001)]/[CO_2(100)] \approx 150$.

9.3.1 Comparison of CO_2 (001) Lifetime for Volume and Wall De-excitation

In $3He:1CO_2:1N_2$, the combined rate constant R for de-excitation of CO_2 (001) by collision with ground state molecules of the mixture varies from about R = 6×10^{-21} at 300 ^{0}K to R = 10^{-19} m^3 s^{-1} at 600 ^{0}K [25]. Let N* be the excited CO_2 density, then

$\frac{dN^*}{dt} = -NN^*R$ and the half life for volume de-excitation is $t_R = 0.69/NR$.

If the excited molecules are assumed to be de-activated with 100% efficiency at the boundary wall of the discharge, the diffusion lifetime for molecules at the discharge centre is $t_{DIFF} = (L/2)^2/2D^*$. Taking D* the diffusion coefficient of the molecule in its excited to be the same as that of the ground state, and taking the lowest gas pressure of 10 torr and lowest gas temperature of about 300 ^{0}K, with L = 4×10^{-3}m and D* = $2 \times 10^{-4}m^2$ s^{-1}, $t_{DIFF} = 10^{-2}$secs. For the same conditions with R = $2 \times 10^{-20}m^3$ s^{-1}, $t_R = 10^{-4}$secs. From this it is concluded that the dominant loss mechanism for the excited CO_2 is by collisions in the volume of the discharge.

9.3.2 CO_2 (001) Density in Gain Zone

Ignoring diffusion to the walls and balancing the volume rates of excitation and relaxation.

$$nN(\eta/N)v = N^*NR \qquad m^{-3}s^{-1} \qquad (9.12)$$

where N* is the density of CO_2 (001) molecules, re-arranging

$$N^* = n(\eta/N)v/R \qquad m^{-3} \qquad (9.13)$$

From equations (9.3) and (9.4) and with R taken to be constant at 2×10^{-20} m^3 s^{-1} in the gas temperature range 300 to 380°K

$$N^* = 10^5 n\epsilon^{-2.3} \qquad m^{-3} \qquad (9.14)$$

9.4 LASER SCALING MEASUREMENTS

The objective of the experiments described here was to investigate the manner in which laser output power and RF discharge characteristics varied with RF drive frequency and gas pressure, for discharge cross sections in the range 4-10 mm. Two separate discharge modules were employed, one of length 20 cm for the laser power and some electrical measurements, and the other of length 4 cm which was used for most of the electrical measurements. Both discharge electrode assembly modules could be used interchangeably in the same vacuum vessel. Each was square in cross section (4, 6, 8, 10 mm on a side) and constructed with a pair of water-cooled aluminium electrodes separated by aluminium oxide side wall spacers. Figure 9.1(a) shows the 20 cm discharge module sealed at each end with an anti-reflection coated zinc selenide window. The resonator consisted of a plane 95% reflectivity output coupler with a high reflectivity, ~ 99.6%, spherical mirror whose radius of curvature was selected, so that for each square cross section used, the lowest order TEM_{oo} gaussian beam mode "fitted" the available cross section. Thus, comparisons between the results at different cross sections could be made on the basis of a normalised mode volume. Laser power measurements were made with a calibrated power meter. Figure 9.1(b) shows the short 4 cm discharge

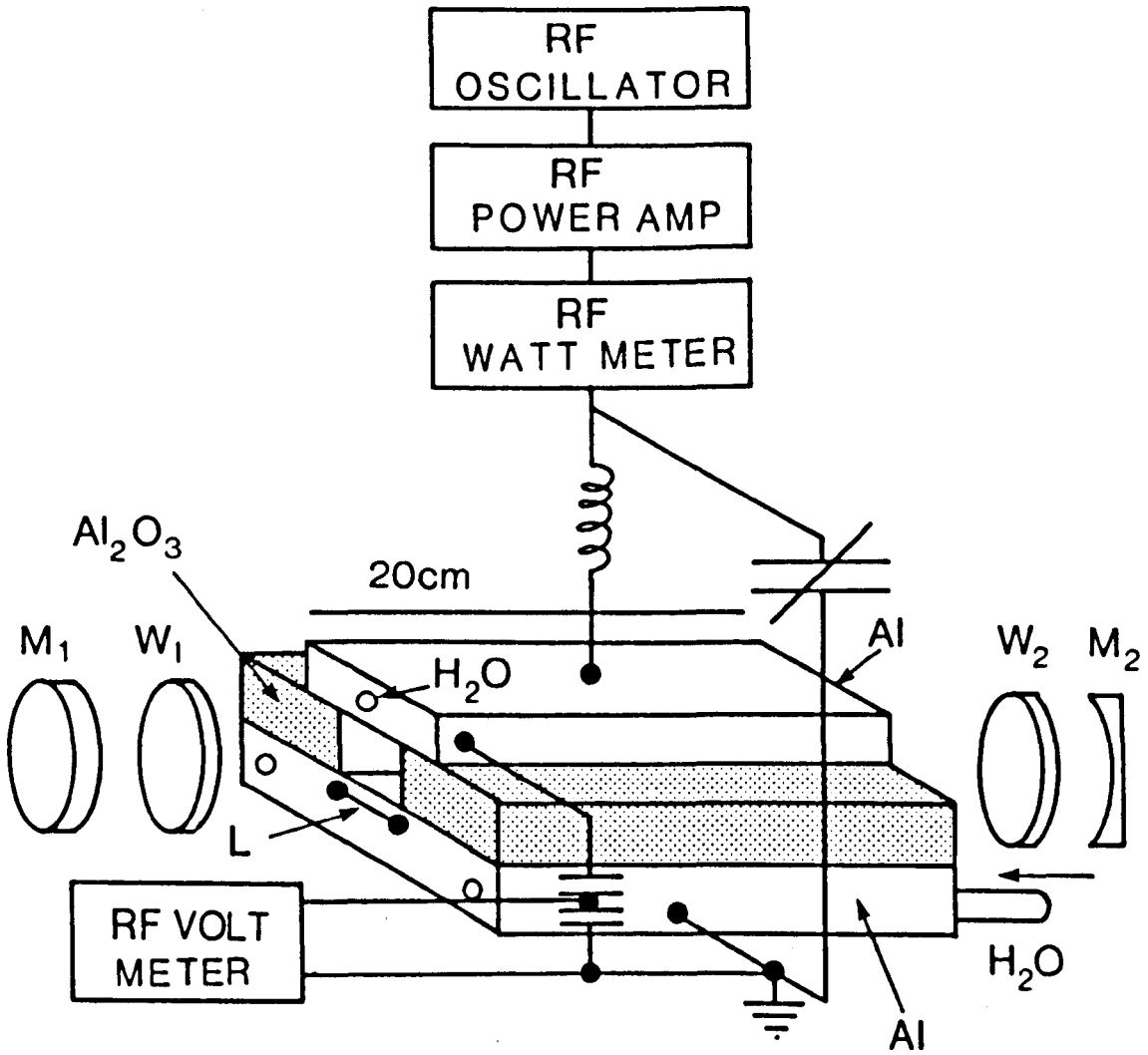

FIGURE 9.1(a) The Apparatus, Electrode Assembly and Resonator for Laser Power and Some Discharge Electrical Measurements. W_1 and W_2 are Plane ZnSe Windows. M_1 is the Plane Output Coupler Mirror and M_2 the Curved High Reflectivity End Mirror.

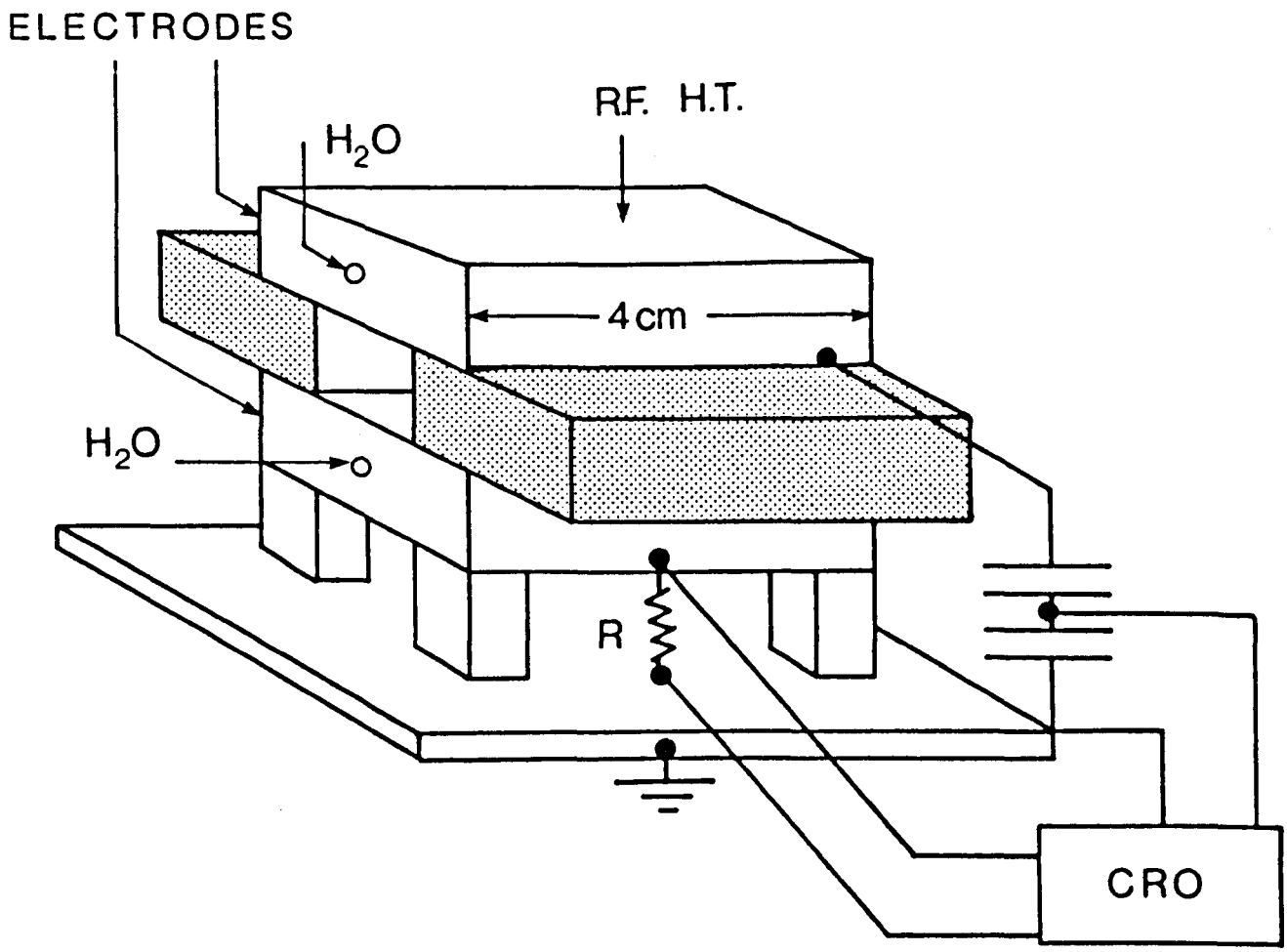

FIGURE 9.1(b) Electrode Assembly for Discharge Power, Current, Voltage and Gas Temperature Measurements.

assembly. The voltage, current and neutral gas temperature measurements were made using techniques described in Chapter 3. The gas used was a research grade CO_2 laser mixture of $3He:1N_2:1CO_2$ for which the swarm data and CO_2 vibrational excitation efficiency as a function of reduced field (E/N) are known. Experiments were conducted with a pressure range of 10–70 torr and for generator frequencies in the range 25–88 MHz, within which range, the optimum conditions were achieved for each cross section studied. RF input power loading to the discharge was in the range 5–50 Watts/cm^3.

The method of taking measurements was to select a particular electrode separation and measure laser output power as a function of gas pressure and input RF power at a particular frequency. These experiments were then conducted for a range of frequencies spanning the optimum value. The process was repeated for a total of four values of electrode separation. Current, voltage and discharge temperature were then recorded on the short electrode assembly for the corresponding RF frequency, electrode separation, pressure and power loading density.

9.5 RESULTS AND DISCUSSION

Data is presented in Figure 9.2 of the pressure dependence of laser output power for a range of input RF power loadings at a fixed frequency of 46 MHz and for an electrode separation of 0.8 cm, while Figure 9.3 shows a similar set of results except that here the input power is maintained constant at 75 Watts while the generator RF frequency is varied. It was found that 75W was the best power loading for all the electrode separations studied. The constants chosen in these two graphs, 46 MHz and 75 Watts, correspond to the optimum conditions for this cross section. While the optimum gas pressure is independent of the input RF drive power over the range studied, it falls significantly as the generator frequency rises. A plot of the dependence of laser power on the generator frequency is

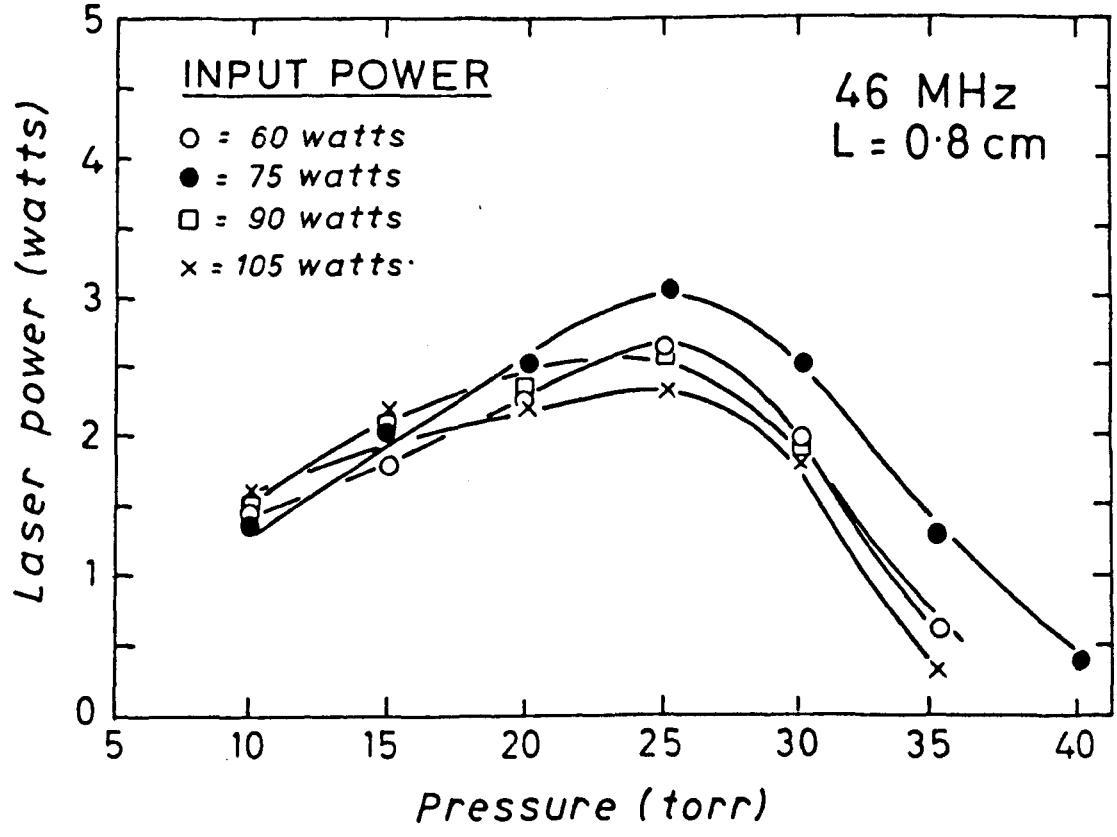

FIGURE 9.2 Laser Output Power Versus Gas Pressure for Varying Input Power.

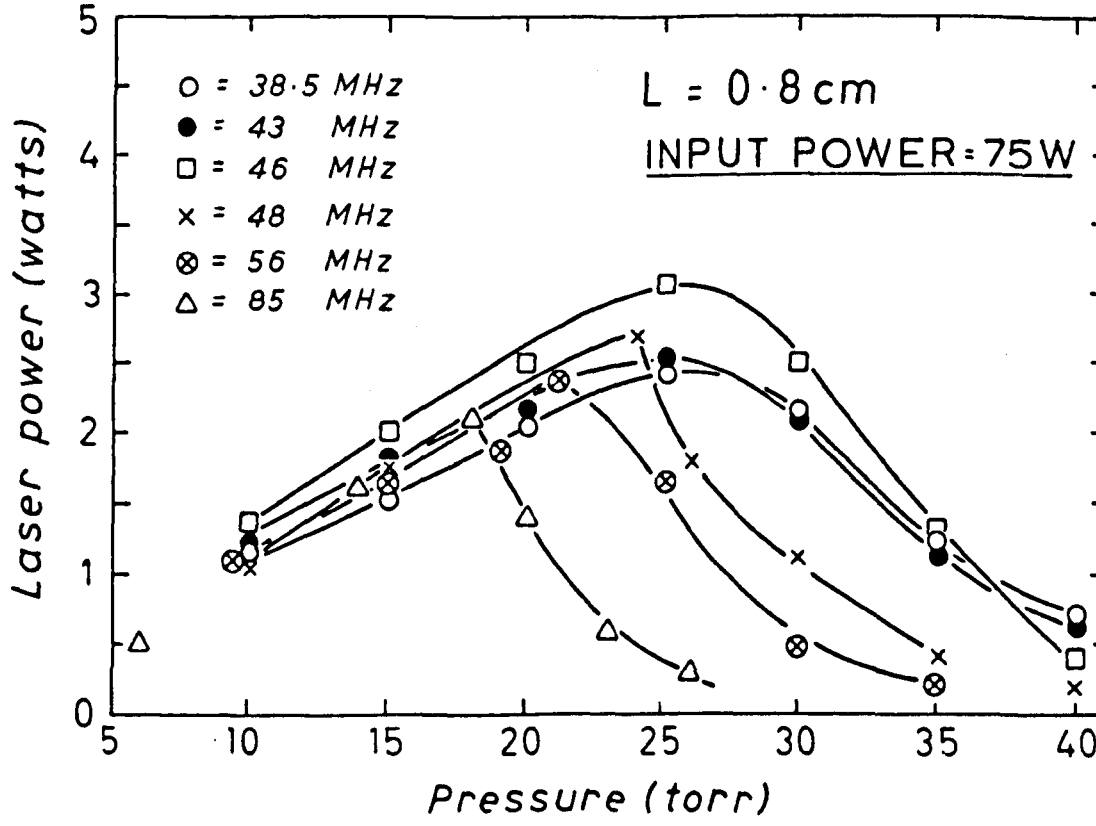

FIGURE 9.3 Laser Output Power Versus Gas Pressure for Varying RF Frequency.

shown for L = 0.8 cm in Figure 9.4. This is typical of the curves obtained for other values of L except that the optimum frequency is seen to fall off significantly at larger electrode separations, while the maximum laser power obtained increases slightly with larger values of L. Figure 9.5 shows more clearly the pressure dependence of laser power at the optimum frequency for each of the discharge cross sections. Predictably, the neutral gas temperature, Tg in the discharge rises with L for constant RF power density loading as illustrated in Figure 9.6. The graph shows the gas temperature for each value of L under optimum laser power conditions. Figure 9.7 and 9.8 show the typical discharge electrical measurements. RMS interelectrode voltage, V_L and peak discharge current, i_0 are plotted as function of electrode separation, L (Figure 9.7) for a constant input power of 75 Watts and for the generator frequency and gas pressure corresponding to highest laser power. The pressure dependences of V_L and i_0 for a particular input power level and frequency are shown for L = 0.8 cm in Figure 9.8. Figure 9.9 shows a plot of the optimum generator frequency at the optimum pressure for each of the electrode separations chosen. The results show a smooth fall-off in the preferred frequency as the discharge cross section increases. Also plotted on this graph is data from Reference [6] which lie reasonably well on the same smooth curve. The penalty for detuning or moving away from these optimum frequencies in terms of laser output power is illustrated by Figure 9.3. A shift of ~ 5 MHz either side of the optimum frequency of 46 MHz results in a 20% drop in output power. Figure 9.10 gives laser power and calculated vibrationally excited CO_2 densities N* for fixed electrode separation, RF frequency and input power with varying pressure. It is seen that the maximum in observed power output coincides with the maximum in the calculated N* for the gain zone.

Lowke, Phelps and Irwin [24] have calculated that for the laser gas mixture $3He:1CO_2:1N_2$ the most efficient value of E/N for pumping the upper lasing levels of CO_2 is ~ 2.0×10^{-20} volts m^2. It is seen from Table 9.1 (which tabulates other observed and calculated discharge parameters) that the calculated value of

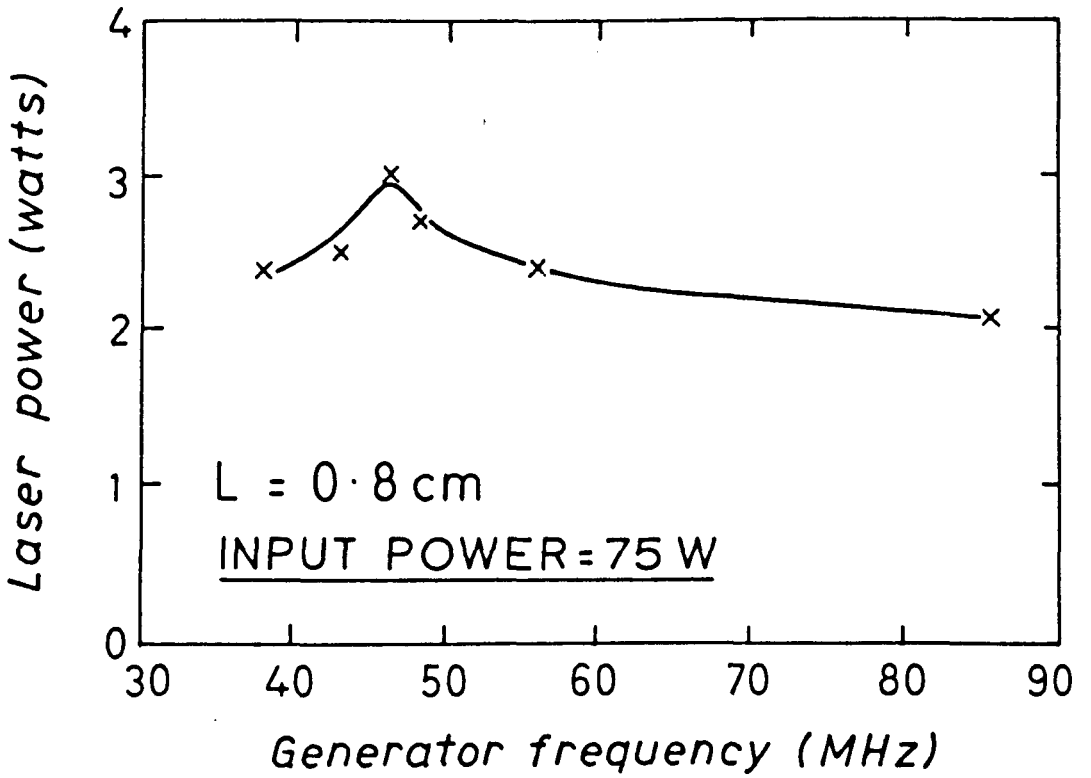

FIGURE 9.4 Laser Output Power Versus RF Frequency for Constant Electrode Separation L = 0.8 cm and Input Power.

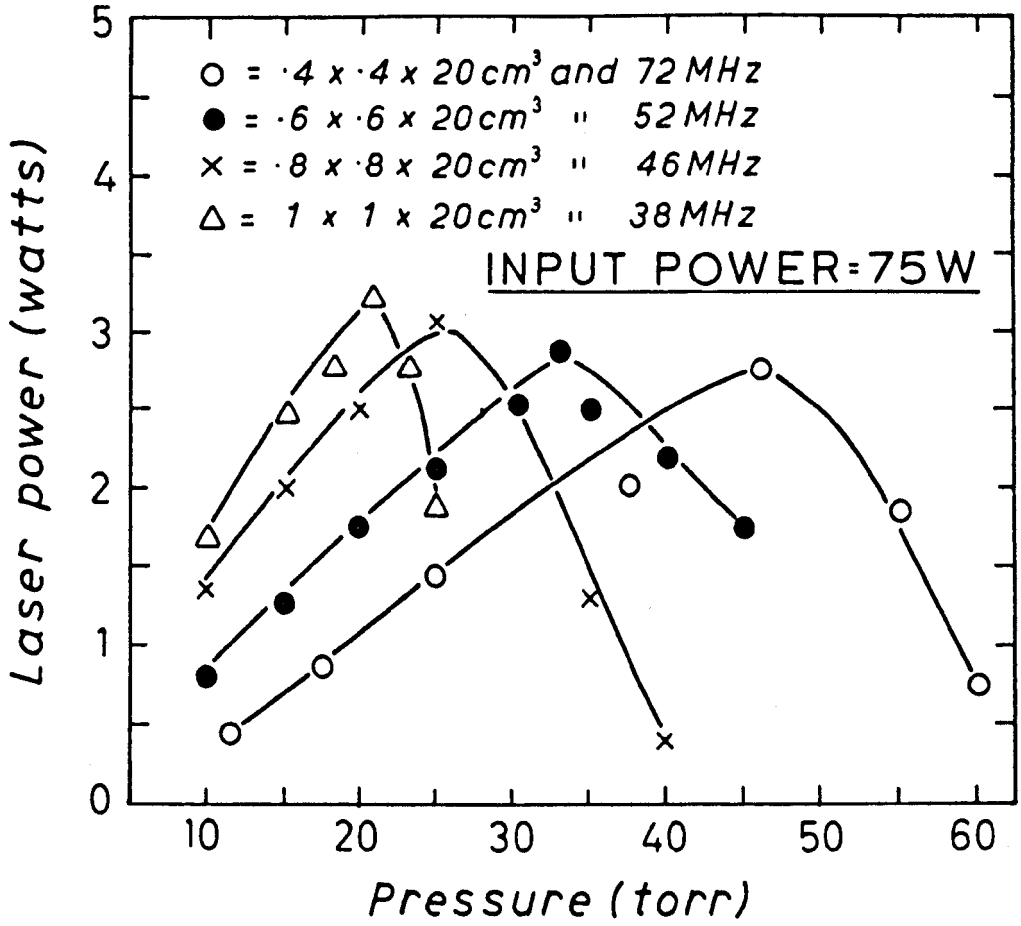

FIGURE 9.5 Laser Output Power Versus Gas Pressure for the Optimum RF Frequency of Each Electrode Separation at the Constant Best Input Power.

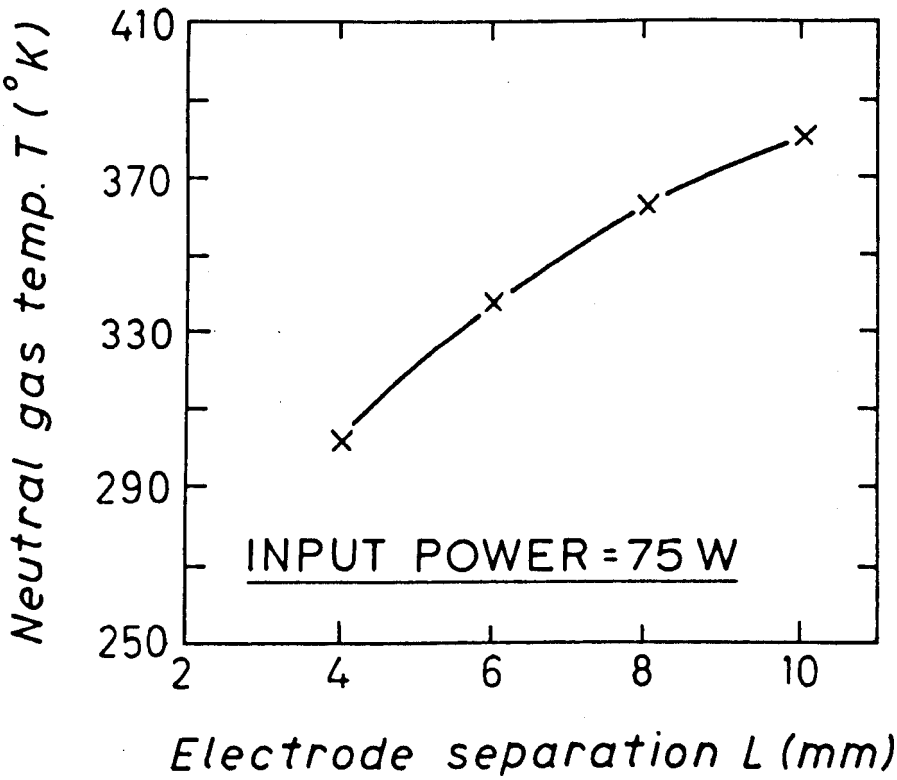

FIGURE 9.6 Average Neutral Gas Temperature Versus Electrode Separation for Discharge Conditions of Maximum Laser Power Output.

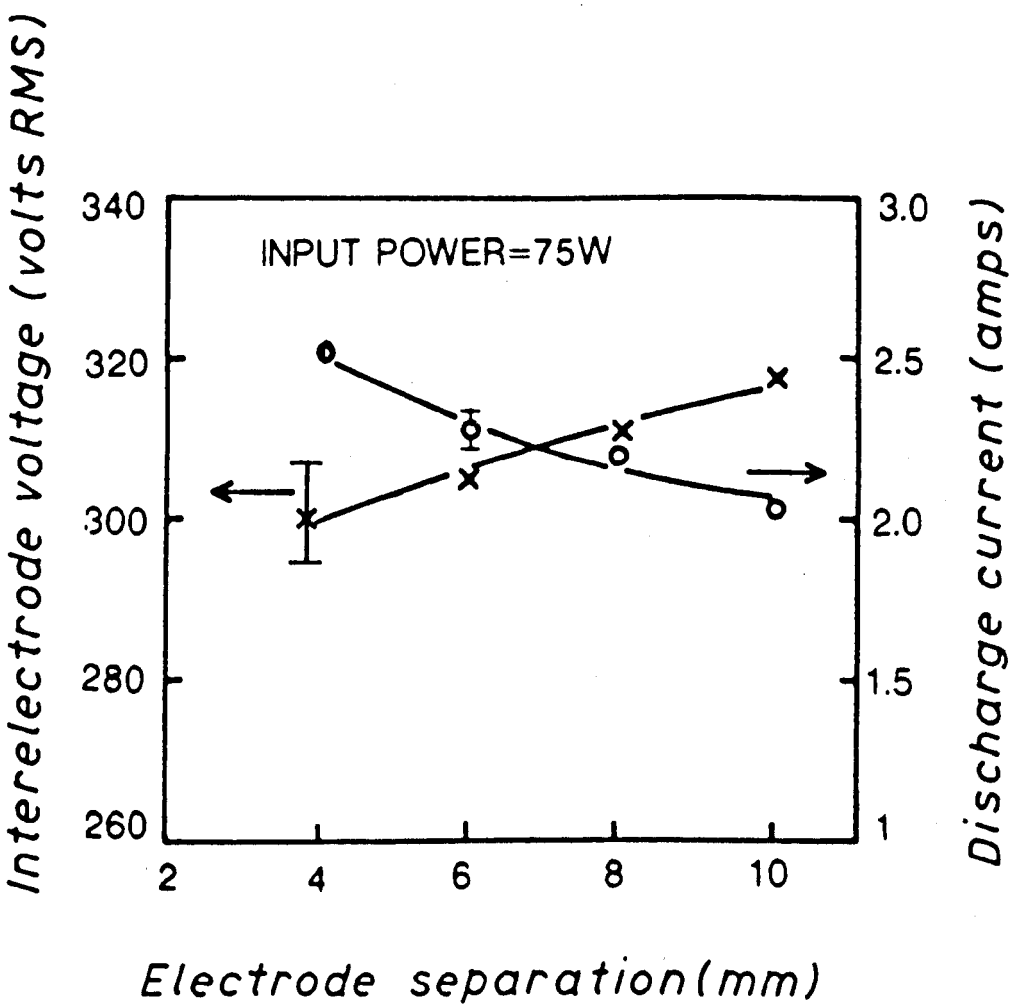

FIGURE 9.7 Discharge RMS Interelectrode Voltage and Peak Current at Each Interelectrode Separation for Discharge Conditions of Maximum Laser Power Output.

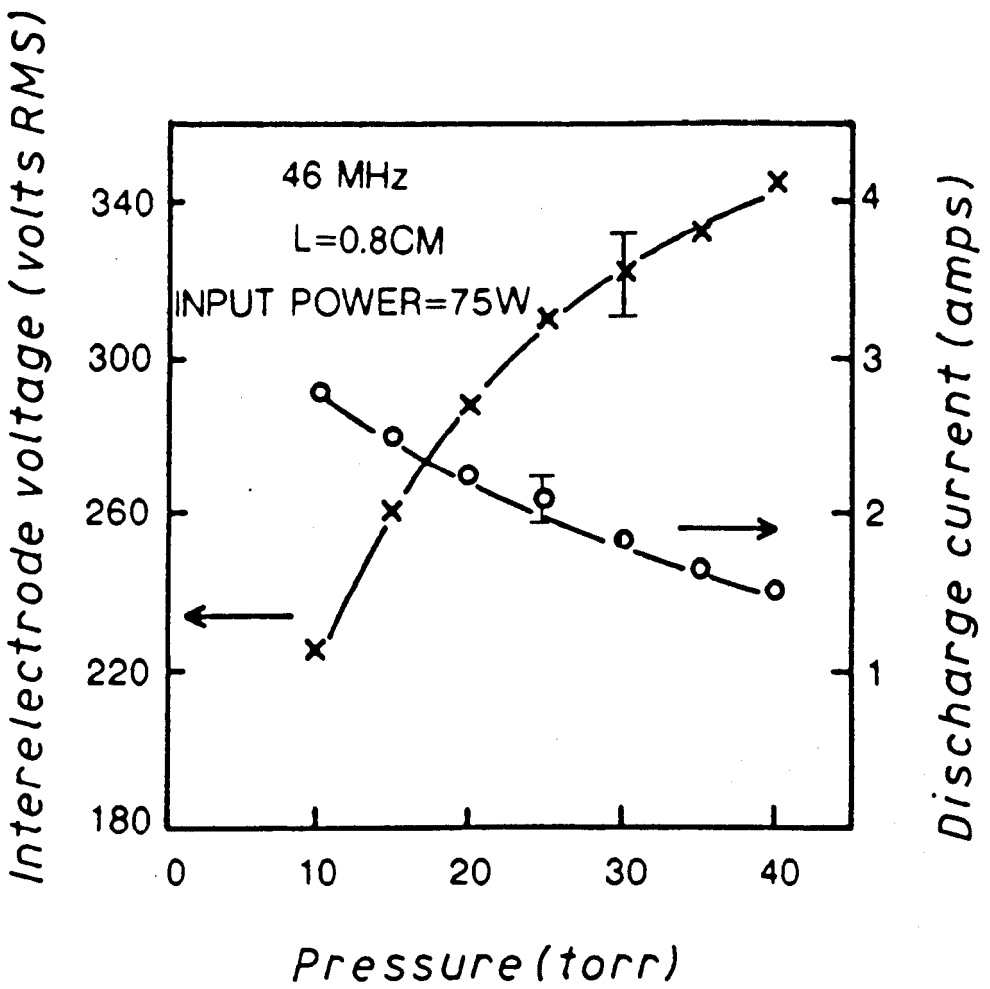

FIGURE 9.8 Interelectrode Voltage and Discharge Current Versus Gas Pressure for Constant Electrode Separation, Input Power and RF Frequency.

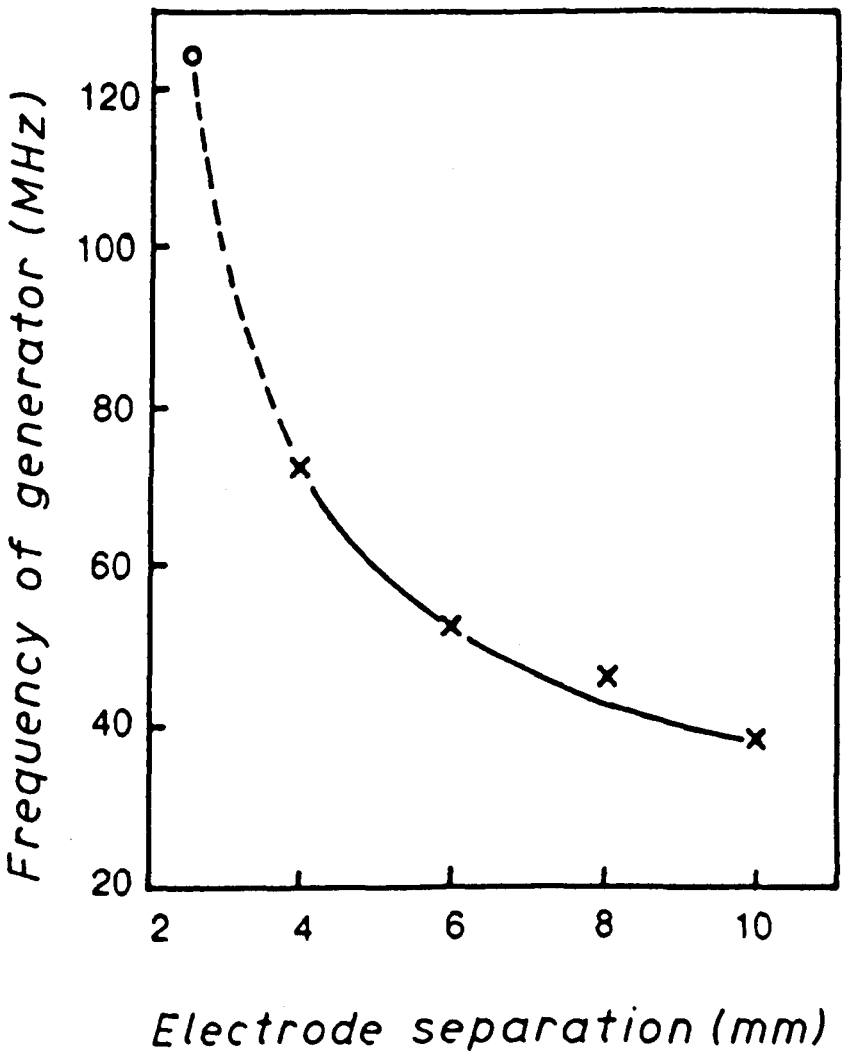

FIGURE 9.9 Optimum RF Frequency and Calculated Plasma or Gain Zone Reduced Field Versus Electrode Separation. Full Circle Denotes Optimum Frequency for a Waveguide Laser of Electrode Separation 2.25 mm [6].

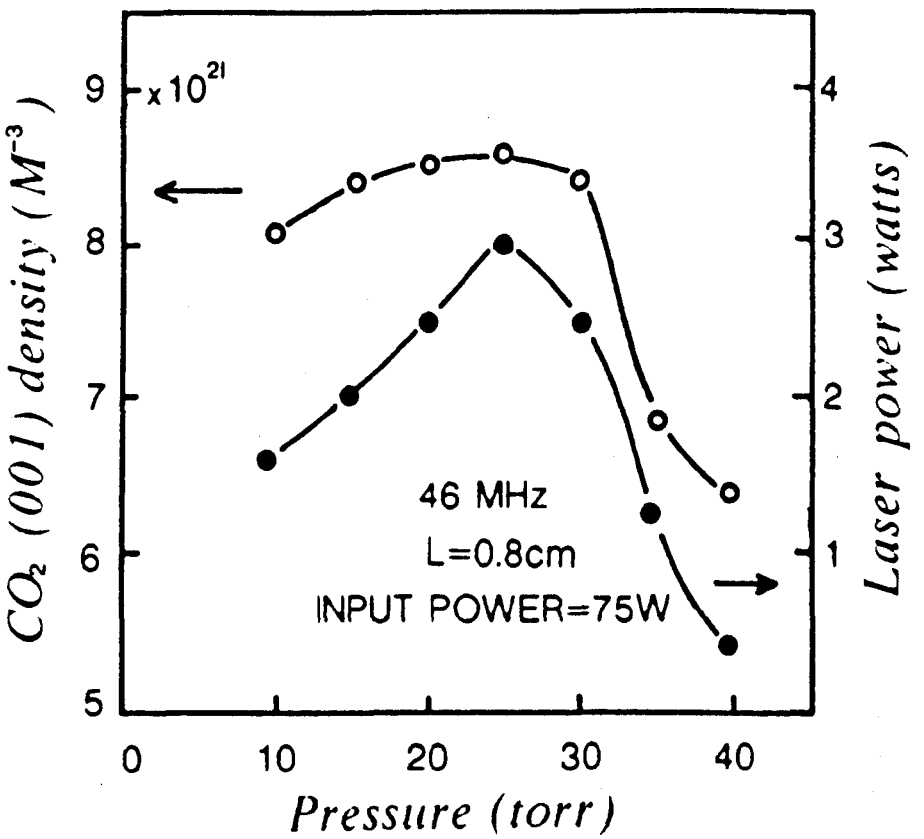

FIGURE 9.10 Laser Output Power and Calculated Gain Zone CO_2 (001) Density Versus Pressure for Constant RF Frequency, Electrode Separation and Input Power.

OBSERVED						CALCULATED					
L	P	f	V_L	$i_0=\frac{\sqrt{2W}}{V_L}$	T	V_P	V_S	ϵ	E/N	n	N*
M	TORR	MHz	VOLTS RMS	AMPS PEAK	^0K	VOLTS RMS	VOLTS RMS	eV	VOLTS RMS-M^2	M^{-3}	M^{-3}
4×10^{-3}	46	72	300	0.353	302	332	44	2.34	5.65×10^{-20}	1.07×10^{16}	1.5×10^{20}
6×10^{-3}	33	52	305	0.346	339	318	57	2.34	5.65×10^{-20}	6.8×10^{15}	9.6×10^{19}
8×10^{-3}	25	46	311	0.340	363	300	53	2.34	5.65×10^{-20}	4.8×10^{15}	6.8×10^{19}
10×10^{-3}	21	38	318	0.332	380	301	62	2.34	5.65×10^{-20}	3.8×10^{15}	5.4×10^{19}

TABLE 9.1 Observed and Calculated Discharge Characteristics for Each Electrode Separation L Under Conditions of Maximum Laser Power Output.

E/N for best laser output power is constant at 6×10^{-20} volts m^2. As pointed out in Section 9.2.1, this is close to the cross-over point at which the attachment coefficient becomes greater than the ionisation coefficient and reflects the fact that the electron energy has to be a compromise between what is optimum for ionisation and laser level excitation. Table 9.2 gives observed and calculated discharge parameters for the same discharge conditions as in Figure 9.10. V_S and V_P, the sheath and gain zone voltages respectively were calculated using the expressions of Chapter 2. In both Table 9.1 and 9.2 the calculated V_S is small and the calculated and measured values of the interelectrode voltage V_L are in only approximate agreement. These results are probably due to the fact that the measured values of the gas temperature Tg underestimates the true values. Scrutiny of the appropriate equations in Sections 9.2 and Chapter 2 shows that the net effect of increasing the measured values of Tg by about 100 ^{0}K is to increase V_S and decrease V_P. This would give a better fit to the measured value of interelectrode voltage and a more plausible value to the sheath voltage. The fact, see Figure 9.5, that for the different electrode separations, the optimum laser output power is roughly constant at 3 watts suggests that the total number of excited CO_2 molecules in the discharge under these conditions is constant. In agreement with this, it is found from Table 9.1 that the product of discharge volume times N^* is constant for all L and equal to $\sim 3 \times 10^{18}$ molecules.

Concerning the stability of the alpha type RF discharge discussed here against a transition to the arc like gamma type discharge [26] [27], it is generally agreed [28] that the transition, which occurs as the power or interelectrode voltage in an alpha discharge reach a critical value, depends on the size of the ratio V_s /ap where V_s is the sheath voltage, a is the sheath thickness and p the pressure. Experiments carried out in Chapter 4 have shown that the transition occurs for lower power loadings for lower values of the RF frequency and the gas pressure [17]. The alpha discharge theory, Chapter 2, gives V_s /a being inversely proportional to the RF frequency, while V_s itself rises with decreasing gas pressure,

NOTE

The calculations in Table 9.1 and 9.2 are based on values of current that were deduced from the power and voltage measurements assuming current and voltage to be in phase. The currents plotted in figures 9.7 and 9.8 are observed values using the technique described in Chapter 3. This technique has been found to overestimate the currents by about one order of magnitude. This is due to the fact that the displacement current in the ceramic side walls, see figure 9.1b, was overlooked.

Concerning the excited state densities tabulated in Table 9.2 we see a monotonic decline in N^* with increasing pressure. If, however allowance is made for the higher diffusive loss of excited states to the wall at low presures and the larger striations zone at low pressures, the effective excited state concentration would be expected to pass through a maximum at the middle pressures of arround 25–30 Torr. This would give a maximum in N^* under the conditions where laser output power is also a maximum as indicated in figure 9.10. The plot of N^* in figure 9.10 whilst giving the expected trend is not quantitatively accurate as it was based on the erroneous current measurements mentioned above.

OBSERVED			CALCULATED					
P	$i_0=\frac{\sqrt{2}W}{V_L}$	V_L	ϵ	E/N	n	V_S	V_P	N*
TORR	PEAK AMPS	VOLTS RMS	eV	VOLTS RMS-M^2	M^{-3}	VOLTS RMS	VOLTS RMS	M^{-3}
10	0.472	224	2.34	5.65×10^{-20}	6.95×10^{15}	75	119	9.92×10^{19}
15	0.406	260	2.34	5.65×10^{-20}	6.12×10^{15}	64	180	8.60×10^{19}
20	0.367	288	2.34	5.65×10^{-20}	5.29×10^{15}	60	240	7.44×10^{19}
25	0.340	311	2.34	5.65×10^{-20}	5.00×10^{15}	55	300	7.00×10^{19}
30	0.328	322	2.34	5.65×10^{-20}	4.92×10^{15}	52	360	6.90×10^{19}
35	0.319	332	2.34	5.65×10^{-20}	4.61×10^{15}	52	420	6.48×10^{19}
40	0.306	346	2.34	5.65×10^{-20}	4.55×10^{15}	49	480	6.39×10^{19}

TABLE 9.2 Observed and Calculated Discharge Characteristics Versus Pressure for L = 0.8 cm at the Optimum Frequency of 46 MHz and Input Power of 75 W. Constant Gas Temperature, T = 363°K.

see Table 9.2 (see also Table 4.2). It follows that the advantages in terms of laser power of operating diffusively cooled lasers at larger electrode separation where the optimum pressure and frequency are lower will be offset not only by rising neutral gas temperature but also by the increasing tendency at higher power loadings for an alpha to gamma transition to occur.

The effect of relatively high small signal gain observed [14] [15] [16] near electrode boundaries would appear to be due to a combination of two effects. Firstly, the gas is denser and cooler near the electrodes and this itself explains the differences found [16] between the near electrode profiles of gain with metal and ceramic boundaries; the gain is higher near metal boundaries than ceramic ones because of the better cooling. Secondly, there is a contribution to the charge balance of the discharge made by energetic electrons that are generated at the boundary or in the boundary sheath zone [27]. These fast electrons produce secondaries which must supplement the laser pumping near the electrodes.

9.6 CONCLUSION

The dependence of laser power on gas density N, electrode separation L and RF excitation frequency f has been found to be such that the maximum laser ouptut power occurs for lower f and N as the value of L increases. A suggested explanation for this behaviour is that the electron energy ϵ in the gain region has to approach a value that is a compromise between the optimum for laser level pumping and ionisation giving a maximum density of CO_2 molecules in the upper laser level. While the simple alpha type discharge model used allows the calculation of credible variations and values of ϵ, a more complex model is required to explain such features of RF CO_2 amplifiers as the enhanced small signal gain found near the electrode boundaries and the transition of the discharge to the arc like gamma type discharge.

REFERENCES

[1] J.L. Lachambre, J. Macfarlane, G. Otis and P. Lavigne, Appl.Phys.Lett., Vol.32, 652 (1978).

[2] P.P. Chenausky, R.A. Hart, L.A. Newman and N. Hoffman, Proc. CLEO (Phoenix, Arizona, USA), Optical Soc.America., 88 (1982).

[3] D. He and D.R. Hall, Appl.Phys.Lett., Vol.43, 726 (1983).

[4] P. Vidaud, D. He and D.R. Hall, Optics Communications, Vol.56, 185 (1985).

[5] H. Hage, H. Martinen and T. Northmann, SPIE (High Power Lasers) Vol.801, 58 (1987).

[6] D. He and D.R. Hall, IEEE J. Quant. Electronics, Vol. QE-20(5), 509 (1984).

[7] D.R. Hall and C.A. Hill, "Hand book of Molecular Lasers", P.K. Cheo editor, Marcel Dekker USA (1987).

[8] J.G. Xin, G. Allcock and D.R. Hall, J.Phys.E.Sci.Instrum., Vol.19, 210 (1986).

[9] G.A. Griffiths, SPIE (CO_2 Laser Devices and Applications) Vol.227, 6 (1980).

[10] D. He, C.J. Baker and D.R. Hall, J.Appl.Phys., Vol.55, 4120 (1984).

[11] A.A. Kuzovnikov, V.L. Kovalevskii, V.P. Savinov and V.G. Yakunin, Journal De Physique, C7- Vol.40, 7 (1979).

[12] V.A. Godyak and A.S. Khanneh, Sov.J.Plasma.Phys., Vol.6, 372 (1980).

[13] V.A. Godyak, Sov.J.Plasma Phys., Vol.2, 78 (1976).

[14] C.G. Parazzoli and K.R. Chien, IEEE J.Quant.Electronics, Vol.QE-22 (3), 479 (1986).

[15] C.J. Baker, Ph.D. Thesis, University of Hull, Hull, UK (1984).

[16] R.C. Sharp, J.Appl.Phys., Vol.61, 5184 (1987).

[17] P. Vidaud, S.M.A. Durrani and D.R. Hall, J.Phys.D., Vol.21, 57 (1988).

[18] B.E. Cherrington, "Gaseous Electronics and Electronics and Gas Lasers" Pergamon Press, Oxford (1979).

[19] C.J. Baker, D.R. Hall and A.R. Davies, J.Phys.D., Vol.17, 1597 (1984).

[20] G. Francis, "Ionisation Phenomena in Gases", Butterworth, London (1960).

[21] Y. Sakai, S. Kaneko, H. Tagashira and S. Sakamoto, J.Phys.D., Vol.12, 23 (1979).

[22] D. Rapp and P. Englander-Golden, J.Chem.Phys., Vol.43, 1464 (1965).

[23] A. Von Engel "Ionised Gases" O.U.P. Oxford (1965).

[24] J.J. Lowke, A.V. Phelps and B.W. Irwin, J.Appl.Phys., Vol.44, 4664 (1973).

[25] R.L. Taylor and S. Bitterman, Rev.Mod.Phys., Vol.41, 26 (1969).

[26] S.M. Levitskii, Sov.Phys. - Tech.Phys., Vol.2, 887 (1958).

[27] V.A. Godyak and A.S. Khanneh, IEEE Trans.Plasma.Sci., Vol.PS-14, 112 (1986).

[28] N.A. Yatsenko, Sov.Phys.Tech.Phys. Vol.26, 678 (1980).

[29] L.J. Denes and J.J. Lowke, Appl.Phys.Lett., Vol.23, 130 (1973).

CHAPTER 10

SUMMARY AND PROPOSALS FOR FUTURE WORK

10.1 SUMMARY

This thesis has made an experimental and theoretical study of RF capacitative discharges at intermediate pressures with the objective of explaining and improving the performance of the Rf excited CO_2 laser. Because little was known about the internal characteristics of this type of discharge, it was decided for simplicity of analysis to examine it first in a single well documented gas before proceeding to look at the three or four component gas mixtures actually used in CO_2 lasers. In Chapter 2, a theoretical model for the N_2 discharge was given that made the following main predictions. Considerable voltages are developed across the sheath in contact with the instantaneous cathode. The sheath voltage drops with increasing frequency while the displacement current and discharge current rise. The model allowed the calculation of an average electron energy and absolute electron densities in the central volume of the discharge. The model indicated that the discharge would be able to accommodate higher power loadings before a transition occurred to the arc like gamma discharge if the RF frequency was raised. The model did not allow for the heating of the gas or the effect of the secondary electrons generated at the instantaneous cathode.

The results of a detailed experimental study of the alpha and gamma type discharges in N_2 were given in Chapter 4 with pressure, RF frequency and interelectrode separation ranging from respectively 10 to 100 torr, 20 to 60 MHz and 6 to 12 mm. The electrical characteristics showed that the irreversible transition from the alpha to the gamma discharge was accompanied by a drop in

voltage and a rise in current and that the power loading at the transition point was higher the higher the frequency and that coating the electrode surface with insulators inhibited the transition. Again, as predicted, the discharge current rose with RF frequency for constant power loading. Time dependent observations of the visible emissions showed that the light was modulated at the RF frequency near each electrode and twice this value in the volume of the discharge corresponding respectively to oscillation and/or emission of fast electrons at/or from the instantaneous cathodes and the electron energies following the applied field in the centre of the discharge. Time averaged spectroscopic analysis of the visible emission showed strong emission from N_2 in the gamma discharge and was taken as evidence of higher charge densities as compared to the alpha discharge.

In Chapter 5, the development with time of the alpha discharge was studied by examining pulses of RF in pure N_2. For pulse durations of less than a few micro seconds it was found that the pulses were uniform and free of the near electrode "striations". Rough agreement was obtained between measured striation formation times and calculated times which assumed that the onset of striations and space charge effects coincide. Chapter 6 gives results of observations made in pure helium of multiple striations. These interesting results which are probably due to standing wave effects await a theoretical explanation.

Chapter 7 dealt with experimental observations an alpha and gamma discharges in laser gas mixtures. The general characteristics were the same as for N_2 except that the alpha to gamma transition was found to be reversible. The addition of xenon reduced the electron energy and increased the gas temperature and the transition point power loading. Evidence of dissociation of CO_2 was found in the spectra of both alpha and gamma discharges.

In Chapter 8 the electrical and stability properties of pulses in CO_2 laser mixture were examined. The electrical characteristics of the pulses were similar to

the CW ones except that the voltages and powers at the transition point were higher for the pulses. The fact that higher power loadings could be tolerated by the pulses for higher gas pressures and shorter pulse durations and that helium improves the stability of the pulses points to the importance of heating in the alpha to gamma transition.

Chapter 9 is the core of the thesis where the discharge properties were related to the laser performance. First of all, a modification of the discharge theory for N_2 of Chapter 4 for the $3He:1CO_2:1N_2$ laser mixture was presented from which the density in the gain volume of excited CO_2 molecules could be calculated. This was followed by measurements of discharge properties and corresponding laser output power for pressures between 10 and 70 torr, RF frequencies 25 to 88 MHz, electrode separations 4 to 10 mm and power densities 5 to 50 Wcm^{-3}. The optimum laser performance as a function of all these parameters was mapped out and finally an explanation for the observed performance given in terms of the densities of excited CO_2 molecules. It was found that the optimum RF frequency decreased monotonically with increasing electrode separation and noted that the advantages of running diffusively cooled lasers at large electrode separations where the best pressures and RF frequencies are low will be offset by decreased discharge stability and higher gas temperatures.

10.2 PROPOSALS FOR FUTURE WORK

10.2.1 Experimental Work

1. A study of the possible use of gamma discharges to excite lasers. It has been seen that the gamma discharge, which tolerates high power loadings, has high charge densities and gas temperatures and low mean electron energies. If an extended gamma discharge can be produced and its gas temperature lowered, by say transverse flow, it might be possible to make a very compact powerful

CO_2 laser.

2. The method of measuring gas temperature in the discharges with a mercury bulb thermometer is not satisfactory. Possible alternatives to be investigated for their costs and feasibilities are; Doppler shift on the He lines, rotational temperature measurements for CO or CO_2 or an interferometric density measurement. A cheap alternative would be to use fine thermocouples at the mouths of the discharges.

3. Investigate the possibility of using the stark broadening of suitable emission lines from the discharge to measure the internal electric field.

4. Measure the small signal gain profiles for the discharges studied in Chapter 9 and relate these profiles near the discharge boundaries to the striations.

5. It was mentioned in Chapter 7 that other researchers had found that gold plating the electrodes reduced the dissociation of CO_2. Investigate this effect.

6. Repeat in more detail the experiments on the RF pulses. In particular the range of RF frequencies and powers need to be extended.

10.2.2 Theoretical Work

Develop a theory of alpha discharges that makes allowance for the effect of the secondary electrons emitted from the instantaneous cathode and which gives quantitative predictions of the alpha to gamma transition voltages and power loadings.